1990

Photoion-photoelectron coincidence studies of clusters and transient molecules

Kevin Norwood
Iowa State University

Order Number 9110548

Photoion-photoelectron coincidence studies of clusters and transient molecules

Norwood, Kevin, Ph.D.

Iowa State University, 1990

U·M·I
300 N. Zeeb Rd.
Ann Arbor, MI 48106

Photoion-photoelectron coincidence studies of clusters and transient molecules

by

Kevin Norwood

A Dissertation Submitted to the

Graduate Faculty in Partial Fulfillment of the

Requirements for the Degree of

DOCTOR OF PHILOSOPHY

Department: Chemistry
Major: Physical Chemistry

Approved:

Members of the Committee:

Signature was redacted for privacy.

In Charge of Major Work

Signature was redacted for privacy.

Signature was redacted for privacy.

For the Major Department

Signature was redacted for privacy.

For the Graduate College

Iowa State University
Ames, Iowa
1990

TABLE OF CONTENTS

		Page
ACKNOWLEDGEMENTS		v
GENERAL INTRODUCTION		1
EXPLANATION OF THESIS FORMAT		6
PART I.	PHOTOION-PHOTOELECTRON COINCIDENCE STUDIES OF CLUSTERS	7
SECTION I.	A PHOTOION-PHOTOELECTRON COINCIDENCE STUDY OF Ar_n (n = 2 - 4)	8
INTRODUCTION		9
EXPERIMENTAL		12
RESULTS AND DISCUSSION		22
SUMMARY		42
REFERENCES		44
SECTION II.	A PHOTOION-PHOTOELECTRON COINCIDENCE STUDY OF Kr AND Xe DIMERS	47
INTRODUCTION		48
EXPERIMENTAL		50
RESULTS		52
DISCUSSION		68
SUMMARY		79

REFERENCES 80

SECTION III. A PHOTOION-PHOTOELECTRON COINCIDENCE STUDY OF $(CO)_2$ AND $(CO)_3$ 82

INTRODUCTION 83

EXPERIMENTAL 85

RESULTS 87

DISCUSSION 98

CONCLUSIONS 111

REFERENCES 112

SECTION IV. A STUDY OF INTRAMOLECULAR CHARGE TRANSFER IN MIXED Ar/CO DIMER AND TRIMER IONS USING THE PHOTOION-PHOTOELECTRON COINCIDENCE METHOD 114

INTRODUCTION 115

EXPERIMENTAL 119

RESULTS AND DISCUSSION 129

CONCLUSIONS 155

REFERENCES 157

PART II. PHOTOION-PHOTOELECTRON COINCIDENCE SPECTROSCOPY OF THE TRANSIENT MOLECULES SO AND S_2O 161

INTRODUCTION 162

EXPERIMENTAL 164

RESULTS 169

DISCUSSION 176

CONCLUSIONS 181

REFERENCES 182

GENERAL CONCLUSIONS 183

REFERENCES 186

ACKNOWLEDGEMENTS

I express my sincere appreciation to professor Cheuk -Yiu Ng for his understanding, and guidance, and his willingness to share his knowledge of ion-molecule interactions with me. His genuine concern for my academic and personal well-being goes far beyond my expectations of a major professor. The numerous and enlightening conversations we shared, on topics too diverse to mention, will be missed. Jerry Flesch deserves special thanks for his willingness to spend time proof-reading my documents and attempting to teach me the skills of technical writing. His conversation, good spirit, and technical skills made my working environment enjoyable.

I acknowledge Elden Ness and the support staff of the chemistry shop. These people have always been helpful in providing ideas to overcome experimental difficulties. Their good skills and prompt service were beneficial to my research. I am grateful to H. Skank, and D. Jensen for their assistance in solving hardware and software related problems. Many thanks to E. Hendrickson for forcing me into the world of computer interfacing. I owe many thanks to the staff of the electronics shop for fixing and constructing electronic equipment essential to my research.

I also thank my colleagues, G. Guo, G. Luo, and S. Nourbash for their assistance in obtaining some of the data.

There are no words to express my gratefulness to my parents, Joe and Elaine Norwood, and my brother, Derrick Norwood. Their love, support, and guidance have

always been appreciated.

I am very thankful to my fiance Sheri Mertz for her love and support throughout these past four years. My canine-like eating, sleeping, and studying hours are more than any human should be subjected to.

I acknowledge the Iowa State University Chemistry Department and Mr. Catron for Fellowships which payed my stipend and helped make this work possible.

This work was performed at Ames Laboratory under contract no. W-7405-eng-82 with the U. S. Department of Energy. The United States government has assigned the DOE Report number IS-T 1498 to this thesis.

GENERAL INTRODUCTION

Interest in the properties of ionic clusters has increased dramatically in the last ten years. Much of the research in this area has focused on characterizing energetic properties of clusters as a function of size. The reviews by Ng[1], Märk and Castleman[2], and the references cited within, provide numerous examples of such studies. Much of the interest in these studies stems from the desire to bridge the gap between the properties exhibited by isolated gas phase molecules (or atoms) and the properties characteristic of the corresponding bulk condensed state. These studies increase our understanding of solvation effects, nucleation phenomena, and the formation of the condensed phase. Studies on cluster ions have also increased our understanding of ion-molecule interactions by serving as reactants in studies of ion-molecule half-reactions. Photoionization of neutral van der Waals clusters offers a unique opportunity for initiating half reactions under conditions of restricted geometry and angular momentum. References 1 and 2 list some examples of ionic half-reactions which have been studied by using van der Waals clusters as the reactants.

Despite the wealth of information available on cluster ions, little is known about the electronic excited states of these species (dissociation energies, ionization energies (IEs), lifetimes, reactivities, etc.). Photofragment spectroscopy has provided some information in this regard. A few typical examples of these are the photofragmentation study of Ar_2^+ [3], Kr_2^+ [4], Ar_3^+ [5-7], $(CO)_2^+$ [8], $(CO_2)_2^+$ [9] and $(N_2)_2^+$.[10] These experiments provide

information only on states which are accessible via electric dipole allowed transitions from the ground state and which dissociate within the timescale of the experiment.

HeI photoelectron spectroscopy (PES) and threshold photoelectron spectroscopy (TPES) are powerful techniques which are not restricted by selection rules like the photofragment spectroscopic technique, nor do they depend on the fate of the ionic molecule. Photoelectron spectroscopic techniques usually provide energetic and spectroscopic information on all ionic states falling within experimental constraints such as electron energy resolution, photon source energy and intensity, and signal to noise ratio. However, few unambiguous results for van der Waals clusters have been reported from PES studies. Noteworthy exceptions are the HeI PES studies of the rare gas dimers reported by Dehmer and Dehmer. [11,12] These studies provide information on the ground and some excited states of the rare gas dimer ions.

The difficulty in obtaining PE spectra of van der Waals clusters is a consequence of the way in which neutral van der Waals clusters are produced for these experiments. The neutral van der Waals clusters probed in these experiments are formed during the supersonic expansion of precursor monomers into the vacuum chamber. The resulting molecular beam generally contains only a few percent of the neutral van der Waals cluster of interest, along with the monomer used in its preparation. The fact that all photoelectrons produced are indistinguishable means one must assign which electrons are due to the cluster being studied. This is accomplished in two separate experiments. In the first experiment one selects the proper expansion conditions so that only monomer and dimer clusters are present in the molecular beam. The ability to select expansion

conditions such that no van der Waals clusters larger than dimers exist was first shown by van Deursen and Ruess[13] in their studies on the Ne, Ar, H_2, N_2, and O_2 systems. In the second experiment, expansion conditions are chosen such that only monomers exist in the molecular beam. Comparison of the two spectra reveals which structures are due solely to the dimer.

A major drawback of the comparison technique is its inability to measure PE bands of the van der Waals cluster when they are obscured by those of the monomer. One way to overcome this problem is to selectively ionize the van der Waals cluster of interest using resonance enhanced multiphoton ionization (REMPI). The electrons which are solely from the van der Waals cluster of study may now be analyzed using conventional techniques. One example of such a study is the REMPI PES spectrum of Xe_2^* reported by Dehmer, Pratt, and Dehmer.[14] The generality of this technique is limited by several factors. First, spectroscopic information about the neutral van der Waals cluster must be known. There are few van der Waals cluster systems for which the necessary spectroscopic details are known. Secondly, care must be taken to ensure that the observed electron does not arise from unwanted multiphoton events. Finally, it is generally necessary to generate PE spectra from many different resonant intermediate states in order to observe all the ionic states energetically allowed.

Another possible solution to this problem is to use a technique capable of identifying the origins of photoelectrons. The photoion-photoelectron coincidence (PIPECO) technique, which is based on the time correlation of electron-ion pairs formed in photoionization, is capable of this. Brehm and von Puttkamer[15] reported the first

PIPECO study in 1967. Since this time, many reports of PIPECO studies of stable molecules have appeared in the literature. Nearly all of these studies have provided information on the final energy (or state) distribution of product ions resulting from the unimolecular decomposition of energy (or state)-selected ions. The review by Baer[16] discusses the PIPECO technique and its applications as a state selection method for use in probing ion-molecule interactions. The capability of state selection offered by the PIPECO technique is not attainable using the techniques of HeI PES, TPES, or REMPI PES. One feature of the PIPECO spectrum of an ion is that the observation of a PIPECO band of an ion implies that the energy (or state)-selected ion is non-dissociative within the ion flight time from the photoionization region to the ion detector. Thus, the absence of a PIPECO band in a spectral region known to contain an ionic state (from other experiments, or theoretical calculations) provides some information on the dissociative lifetime of this ionic state.

When this research was begun in 1987, only two PIPECO studies of clusters had appeared in the literature. These studies of Kr_2^+ [17], Xe_2^+ and Xe_3^+ [18] extended only to energies below that of the corresponding monomer IEs, and hence provided no information on the excited states of these cluster ions. This lack of experimental data available for excited states of cluster ions motivated us to apply the techniques of PIPECO spectroscopy (utilizing a PIPECO apparatus recently constructed in our laboratory by modifying a molecular beam photoionization mass spectrometer) to study ground and excited ionic states of clusters.

Another important field which could benefit greatly from availability of PES results is the study of free radicals and transient molecules. The problems which arise in attempting to obtain mass-selective PES of clusters also arise here, and for the same reasons. Namely, the radicals or transient molecules are always produced together with their precursor, and usually in relatively low abundance. By incorporating a microwave discharge, effusive beam source (for production of transient molecules) and a pulsed ion extraction source into the PIPECO apparatus used in the cluster studies, we have succeeded in obtaining the PIPECO spectra of the SO and S_2O transient molecules. To our knowledge this is the first reported application of PIPECO to the study of transient molecules.

EXPLANATION OF THESIS FORMAT

The thesis is divided into two parts: Part I is subdivided into four sections according to the specific van der Waals cluster system being studied; Part II, comprised of only one section, is about transient molecules. Each section is an independent article prepared in a format ready for publication. The experimental apparatus is described in detail in Section I of Part I, and a brief experimental description, including any specific operating conditions, is included in each succeeding section. A description of the modifications made for the study of transient molecules is presented in Part II. The figures, tables, and references cited in each section refer only to those contained in that section. The references cited in the General Introduction and General Conclusion are compiled at the end of the thesis, following the General Conclusions.

PART I.

PHOTOION-PHOTOELECTRON COINCIDENCE STUDIES OF CLUSTERS

SECTION I.

A PHOTOION-PHOTOELECTRON COINCIDENCE STUDY OF Ar_n (n = 2 - 4)

INTRODUCTION

The spectroscopy[1-6] and dissociation dynamics[7-11] of Ar dimer and cluster ions have been the subject of much research in the past decade. Part of the interest in small rare gas cluster ions arises from the development of rare gas excimer lasers.[12] The experimental[1-11,13,14] and theoretical[15-21] investigations of Ar_2^+ and Ar_3^+ have been partly motivated by their possible roles as gain inhibitors in excimer laser systems. The relative simplicity of the Ar cluster ion system, along with the wealth of precise energetic, spectroscopic, and dynamical information accumulated, has made it a focus in cluster research for rigorous comparison of experiment and theory.

The ionization energies (IE) for the ground states of Ar_2^+ and Ar_3^+ have been well established by previous photoionization,[1,4,5] photofragmentation,[2] and equilibrium mass spectrometric[13,14] measurements. For ionized van der Waals clusters such as Ar cluster ions, experiments[4] have shown that the binding energy for Ar_2^+ is overwhelmingly greater than those for Ar_n^+-Ar ($n \geq 2$). This observation has been taken as support of a central charge model,[22] which suggests that the structure of an Ar cluster ion consists of an Ar_2^+ dimer core surrounded by weakly bound neutral Ar atoms. Interestingly, the recent theoretical calculations of Hesslich and Kuntz[19] and Kuntz and Valldorf[21] indicates that the most stable configurations for Ar_n^+ clusters up to $n = 13$ are best approximated as a central Ar trimer ion attached to neutral Ar atoms in the outer shell.

An Ar cluster ion initially formed by photoionization or electron impact ionization at energies above the dissociation threshold may contain enough internal energy for it to dissociate into smaller fragments. The effect on the Ar_3^+ photoionization efficiency (PIE) spectrum due to fragmentation of higher Ar cluster ions has been examined.[4] Buck and Meyer[11] have demonstrated that ionization of Ar_3 by electron impact at electron energies of 40 - 100 eV yields no Ar_3^+. In the time scale of their experiment, Ar_3^+ ions are found to dissociate completely forming Ar_2^+ and Ar^+ in the ratio of ~ 7:3. If the excess internal energy initially deposited by the ionization process is redistributed efficiently within internal motions of the cluster ion, statistical theories predict that the dissociation lifetime of the cluster ion increases with increasing cluster size. The work of Märk and co-workers shows that even Ar_2^+ and Ar_3^+ ions display metastable decays in the microsecond time regime.[9] The metastable decay rate of Ar_3^+ formed by electron impact ionization depends very strongly on the internal energy of Ar_3^+. Due to the broad range of internal energies of Ar_3^+ acquired in its formation process, a unique dissociation lifetime cannot be assigned to the cluster ion. These findings illustrate that the metastability of Ar cluster ions is not totally statistical in nature. Recently, Ferguson et al.[10] have suggested that tunneling through a rotational barrier is responsible for the slow decay of Ar_3^+ to form Ar_2^+. Their model calculation predicts that the tunneling lifetime of Ar_3^+ decaying into $Ar_2^+ + Ar$ may range from 10^{-10} to 10 s.

Photoelectron spectroscopic studies of neutral rare gas dimers[3] formed in a supersonic beam have been made by comparing the photoelectron spectrum (PES) of the monomer with that obtained under nozzle expansion conditions which produce mainly dimers and

monomers. Since the concentration of a van der Waals dimer produced in a supersonic beam is substantially lower than that of the monomer, it is difficult to examine the dimer photoelectron bands which overlap with those of the monomer. In spite of this difficulty, the elegant photoelectron spectroscopic experiment of Dehmer and Dehmer[3] has provided values for the IEs of the excited $I(3/2)_g$ and $II(1/2)_u$ states of Ar_2^+.

In this report, we present the photoion-photoelectron coincidence (PIPECO) data for Ar_n^+ (n = 2 - 4) using the PIPECO technique developed recently in our laboratory.[23,24] The information content of the PIPECO spectrum is more specific compared to the PES of a cluster ion. Since a coincidence signal represents the detection of a time correlated electron-ion pair, the observation of a PIPECO band of a cluster ion implies that the state (or energy) - selected cluster ion has a dissociation lifetime longer than, or close to, the ion flight time from the photoionization region to the ion detector. If the dissociation lifetime of the state (or energy) - selected cluster ion is much shorter than the ion flight time, the corresponding PIPECO band would not be observed. Therefore, the PIPECO spectrum of a cluster ion not only contains spectroscopic information but also provides dynamical information concerning the unimolecular decomposition of a state (or energy) - selected cluster ion.

EXPERIMENTAL

A description of the molecular beam PIPECO apparatus and procedures used in this study has been reported.[23,24] The molecular beam PIPECO apparatus is modified from the molecular beam photoionization apparatus which has been described in detail previously.[25,26] Figure 1 shows a cross-sectional view of the differential pumping arrangement of the molecular beam production system, photoionization region, quadrupole mass spectrometer (QMS), and photoelectron energy analyzer. The major modification involves the installation of the photoelectron energy analyzer opposite to the vertical QMS (4).

The Ar molecular beam is produced by supersonic expansion of pure Ar through a 62 μm nozzle at a stagnation pressure (P_o) range of 60 - 210 Torr. The nozzle is cooled by cold N_2 gas and kept at a constant nozzle temperature of 120 $\pm$ 3 K throughout the experiment. The high intensity portion of the supersonic jet is collimated into the ionization chamber by a conical skimmer (2) before intersecting at 90° with the dispersed light beam emitted from the exit slit of the vacuum ultraviolet (VUV) monochromator.

A constant electrostatic field of ~ 1 V/cm is applied at the photoionization region such that electrons and ions are deflected in opposite directions perpendicular to the molecular beam axis. The electrons and ions are guided toward the electron energy analyzer and the vertical QMS, respectively, by electrostatic lenses. Due to the relatively weak repeller field in the photoionization region, the ion transmission (f_i) through the

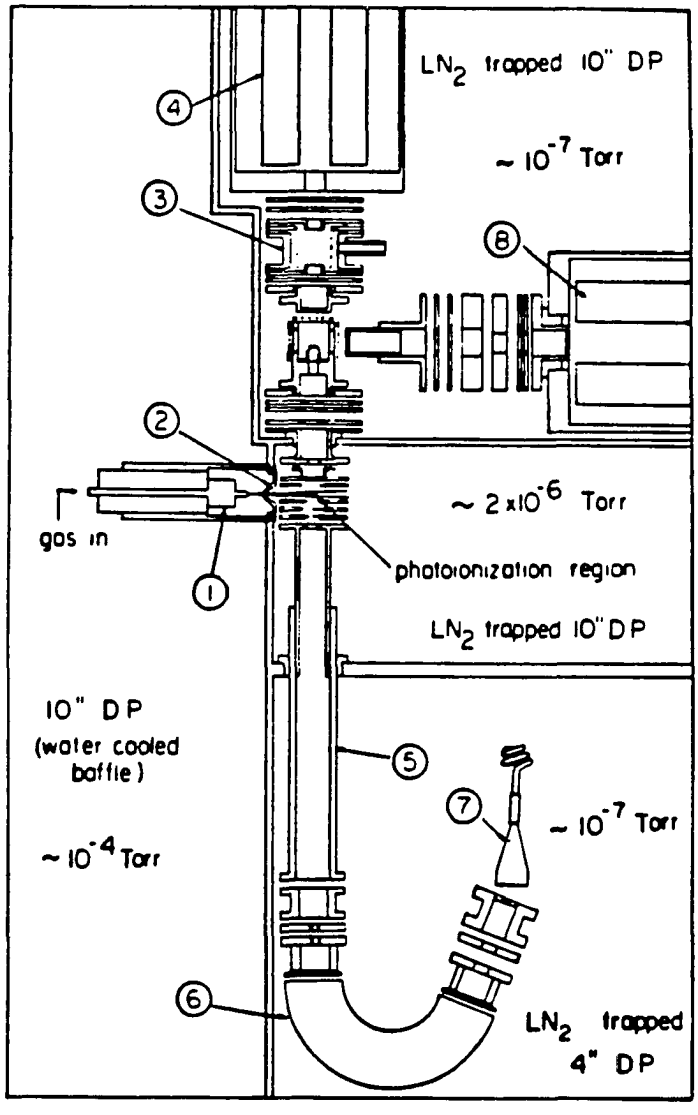

Figure 1. Cross-sectional view of the molecular beam PIPECO apparatus

(1) nozzle; (2) skimmer; (3) reaction gas cell; (4) vertical QMS;

(5) steradiancy analyzer; (6) spherical sector electron energy analyzer;

(7) channeltron electron detector; (8) horizontal QMS

vertical QMS is ~ 0.3.

The electron energy analyzer, optimized for threshold photoelectron detection, consists of a steradiancy analyzer[27,28] and a spherical sector energy analyzer (Comstock model AC-901) (6) arranged in series.[29] At a photon energy coinciding with an ionization threshold, two groups of electrons may be produced, i.e., a group of electrons with near-zero kinetic energies and a group of hot electrons resulting from the formation of ions in lower ionic states. In a conventional steradiancy analyzer, a long tube is connected directly to the repeller plate at the photoionization region. Thus, the long tube functions as a drift tube to eliminate hot electrons moving in directions away from the solid angle sustained by the long tube. In this experiment, the potentials of the long tube (5) and the simple aperture lenses above and below the tube are optimized to transmit preferentially near-zero kinetic energy electrons. Although the potential of the long tube is ~ 80 V higher than the repeller plate, the assembly behaves like a steradiancy analyzer. The advantage of this arrangement is that the electron trajectories through the tube are subject only to minor perturbation by stray magnetic fields because the electrons are moving at velocities corresponding to energies of ~ 80 eV.

The dashed curve shown in Fig. 2(b) is the PES for Ar^+ observed with a channeltron electron multiplier placed at the end of the steradiancy analyzer when the transmission of zero kinetic energy electrons has been maximized. The spherical sector energy analyzer is used to reject hot photoelectrons moving in the direction along the axis of the tube. Figure 2(c) shows the threshold PES for Ar^+ obtained using the steradiancy and spherical sector energy analyzer combination. The hot electron tails of the $^2P_{3/2}$ and $^2P_{1/2}$

Figure 2. Threshold PES of Ar obtained using the spherical sector and/or steradiancy electron energy analyzer

(a) Threshold PES of Ar obtained by taking the difference of the normalized spectra shown in (b); (b) (-o-) PES of Ar observed using only the steradiancy analyzer when the transmission of zero kinetic energy electrons is maximized, (-) PES of Ar recorded using only the steradiancy analyzer in a focusing arrangement which minimizes the transmission of zero kinetic energy electrons, wavelength resolution = 0.3 Å (FWHM); (c) Threshold PES obtained using the steradiancy and spherical sector energy analyzer combination, wavelength resolution = 0.5 Å (FWHM)

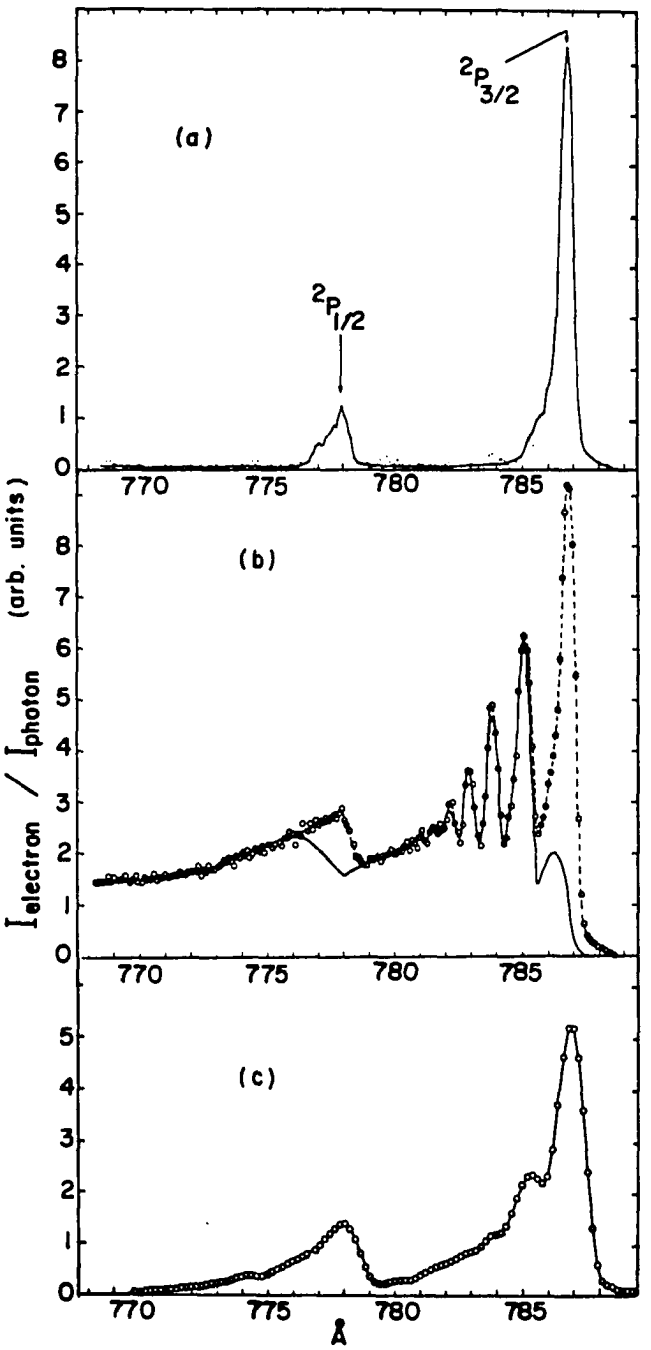
(a)
$^2P_{3/2}$
$^2P_{1/2}$
(b)
(c)
$I_{electron} / I_{photon}$ (arb. units)
770
775
780
785
Å

photoelectron bands observed in Fig. 2(c) are reduced substantially compared to those in Fig. 2(b). At an electron energy resolution of ~ 50 meV (FWHM), the threshold electron transmission (f_e) of the electron energy analyzer assembly is ~ 0.01. Figure 2(b) also shows the PES for Ar^+ (solid curve) recorded using only the steradiancy analyzer in a focusing arrangement which minimizes the transmission of zero kinetic energy electrons. The two PESs depicted in Fig. 2(b) have been normalized in the wavelength range of ~ 750 - 775 Å. Taking the difference of the normalized spectra gives the threshold PES for Ar^+ [Fig. 2(a)] with a resolution of ~ 15 meV, approximately twice the photon bandwidth of 0.3 Å (FWHM) used in measuring the spectra.

In this experiment, we use a multichannel scaler (MCS) to measure the ion time-of-flight (TOF) distribution after the triggering by an electronic pulse signifying the arrival of an electron at the channeltron detector. The active time period (τ_o) of the MCS must be longer than the flight time of the ions of interest. During the active time period of the MCS, the coincidence circuit will not accept other electron pulses. To avoid suppression of the coincidence signal, τ_o should be shorter than the average time interval between two adjacent electron pulses, which is equal to the inverse of the electron counting rate. When the VUV lamp is a continuous light source such as that used in our experiment, the ions which are correlated with the energy-selected electrons appear in a narrow range of channels of the MCS corresponding to the differences in flight times of the correlated electron-ion pairs. The detection of uncorrelated ions will give rise to a uniform background because these ions arrive randomly at the ion detector at a uniform rate.

When the QMS is used to mass select a specific cluster ion, it is straightforward to show that the signal-to-noise (S/N) ratio[30-33] for the coincidence counting of a cluster ion is

$$\frac{S}{N} \sim \sqrt{\frac{N_c g_e f_e f_i}{1 + 2N_T \Delta t}} \qquad (1)$$

where N_c, N_T, and Δt are the ionization rate for the cluster ion of interest, the total ionization rate, and the full width of the cluster ion TOF peak, respectively, and g_e represents the fraction of electrons which falls within the energy band pass of the electron energy analyzer. Equation (1) is derived under the assumption that the background counting rates for the ion and electron detectors are negligible compared to the ion and electron counting rates. By operating the QMS as a radio frequency (rf) ion guide such that all ions are transmitted to the ion detector, the PIPECO TOF spectra for all cluster ions can be measured simultaneously. Following procedures similar to those used in the derivation of Eq. (1), the S/N ratio of such an arrangement can be shown as

$$\frac{S}{N} \sim \sqrt{\frac{N_c g_e f_e f_i}{1 + 2N_T \Delta t (N_T/N_c)}} \; . \qquad (2)$$

In a typical experiment, $N_T \approx 10^5$ - 10^6 counts/s and $N_T \approx 100\ N_c$ at photon energies higher than the IE of the monomer and $\Delta t \sim 5$ - 10 μs, the denominators of Eqs. (1) and (2) are dominated by the terms $2N_T\Delta t$ and $2N_T\Delta t(N_T/N_c)$, respectively. Obviously, based on the expressions shown in Eqs. (1) and (2), the optimization of the experimental S/N

ratio involves maximizing g_e, f_e, f_i, and N_c/N_T and minimizing Δt. Better S/N ratios for coincidence data can be obtained by using the QMS to mass select the cluster ion of interest.

Figures 3(a) - 3(c) show the coincidence TOF spectra recorded for Ar cluster ions at 810 Å and P_o = 60, 90, and 210 Torr, respectively. These spectra are obtained when the vertical QMS is operated as a rf ion guide at an ion entrance energy of ~ 5 V. The flight time differences for e^- -ion pairs are 67 μs for (e^- -Ar^+), 95 μs for (e^- -Ar_2^+), and 116 μs for (e^- -Ar_3^+). The full width of the TOF peak for Ar_2^+ is ~ 8 - 10 μs. The presence of Ar^+ at this photon energy, which is lower than the IE of Ar, is attributed to scattered light arising from imperfections of the grating. The ratio of Ar_3^+ to Ar_2^+ intensities decreases from ~ 1/16 to ~ 0 as the pressure is decreased from 210 to 60 Torr. The intensity of Ar_2^+ measured at 810 Å reaches its maximum value at ~ 90 Torr. At 60 Torr the intensities for Ar_n^+ ($n \geq 3$) are found to be within the noise level. However, a coincidence TOF spectrum with no Ar_n^+ ($n \geq 3$) peaks does not necessarily indicate the absence of Ar_n ($n \geq 3$) in the Ar supersonic beam because fragmentation of Ar_n^+ ($n \geq 3$) parent ions upon ionization may diminish the intensities of the ions. The absence of cluster ions larger than the one of interest in the coincidence TOF spectrum appears to be a necessary, but not a sufficient, condition for the acquisition of PIE or PIPECO data free from the effects of fragmentation from larger clusters.

The PIPECO spectrum of an ion is a plot of the ratio of the ion coincidence intensity to the ionization photon intensity versus photon wavelength. All PIPECO spectra obtained in this experiment are measured using the vertical QMS to select the ion of

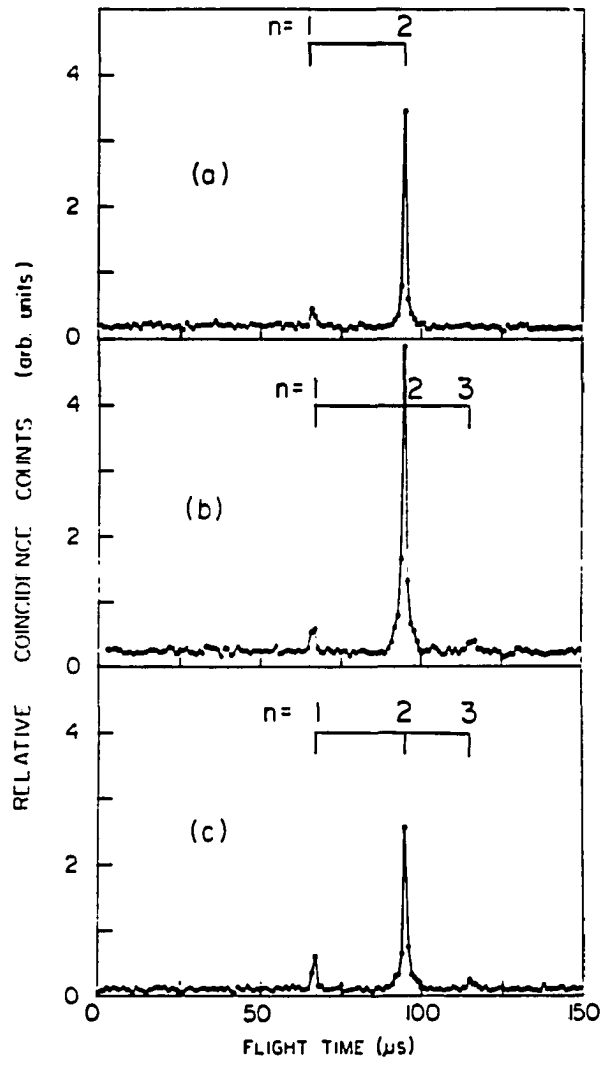

Figure 3. PIPECO TOF mass spectra of Ar_n observed at 810 Å and a nozzle temperature of 120 K

(a) P_o = 60 Torr; (b) P_o = 90 Torr; (c) P_o = 210 Torr

interest. The vertical QMS is floated at a dc potential of ~ 200 V. Under this condition, the flight times of Ar^+, Ar_2^+, Ar_3^+, and Ar_4^+ are ~ 34, 47, 58, and 66 μs, respectively. The value for Δt of the Ar_2^+ TOF peak is found to be ~ 4 - 5 μs.

RESULTS AND DISCUSSION

Spectra for Ar_2^+

Figures 4(a) - 4(c) display the PIE spectra for Ar_2^+ obtained using a wavelength resolution of 1.5 Å (FWHM) at P_o = 60, 90, and 210 Torr, respectively. The PIE spectrum for Ar^+ is included in Fig. 4(a) for comparison. The Ar_2^+ spectrum show in Fig. 4(a) is in good agreement with that recorded by Ng et al.[1] using a similar wavelength resolution. The PIE spectrum for Ar_2^+ is dominated by strong autoionization peaks superimposed on an ionization continuum structure rising slowly from the ionization threshold. The ionization continuum structure arises mostly from direct ionization of Ar_2. When taken at higher wavelength resolutions, the autoionization structure is found to be very complex.[5] The ionization continuum structure appears to rise more rapidly from the ionization threshold and become more significant compared to the autoionization features as P_o is increased from 60 Torr [see Figs. 4(b) and 4(c)]. This observation can be attributed to the production of Ar_2^+ from dissociative ionization processes of higher Ar clusters. The PIE spectra for Ar_2^+ measured at $P_o < 60$ Torr are essentially identical to that shown in Fig. 4(a), indicating a negligible effect of fragmentation of larger clusters on the Ar_2^+ spectrum observed at P_o = 60 Torr.

The PIPECO spectra for Ar_2^+ obtained at P_o = 60, 90, 210 Torr using a wavelength resolution of 1.5 Å (FWHM) and an electron energy resolution of 70 meV are depicted in

Figure 4. PIE spectra for Ar^+ and Ar_2^+ obtained using a wavelength resolution of 1.5 Å (FWHM) and a nozzle temperature of 120 K

(a) P_o = 60 Torr; (b) P_o = 90 Torr; (c) P_o = 210 Torr

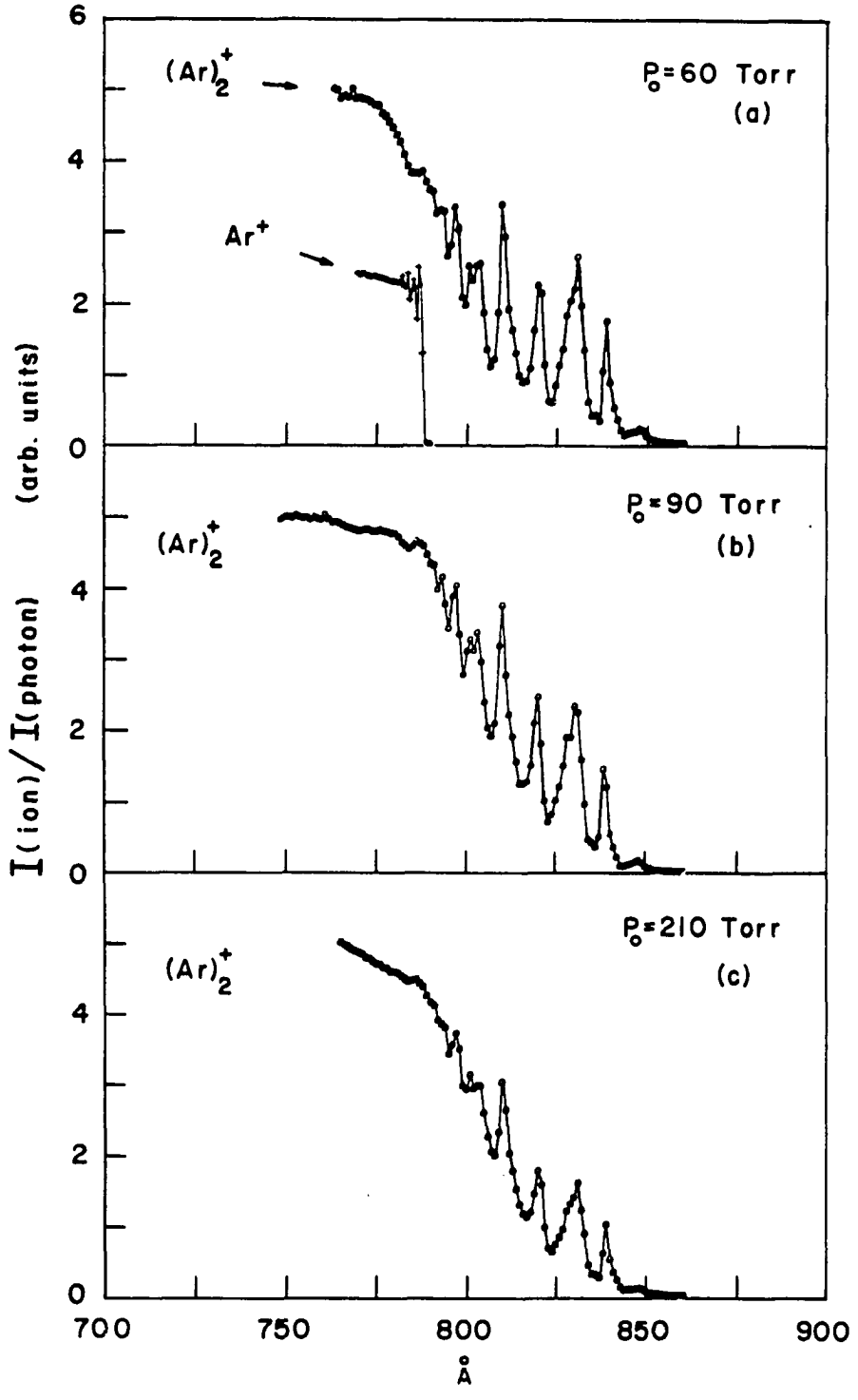
(Ar)$_2^+$
Ar$^+$
P_o=60 Torr
(a)
(Ar)$_2^+$
P_o=90 Torr
(b)
(Ar)$_2^+$
P_o=210 Torr
(c)
I(ion)/I(photon) (arb. units)
0
2
4
6
700
750
800
850
900
Å

Figs. 5(a) - 5(c), respectively. The autoionization features resolved in the Ar_2^+ PIPECO and PIE spectra are similar.

Based on the examination of the PIPECO, TOF, and PIE spectra as a function of P_o, it is logical to conclude that the PIPECO spectrum of Ar_2^+ measured at P_o = 60 Torr represents the "true" PIPECO spectrum of Ar_2. The Ar_2^+ PIPECO spectrum of Fig. 5(a) shows a sharp drop in intensity at photon energies coinciding with the $Ar^+(^2P_{3/2})$ PIPECO band, and observation consistent with the interpretation that Ar_2^+ formed by photoionization at energies above the Ar^+ $(^2P_{3/2})$ + $Ar(^1S_o)$ asymptote is dissociative.

The dashed broad peak shown in the Ar_2^+ PIPECO spectrum in Fig. 5(a) outlines the continuum structure which reveals the Franck-Condon overlap profile between vibrational levels of the Ar_2 ground state and those of the Ar_2^+ ionic states correlating to the $Ar^+(^2P_{3/2})$ + $Ar(^1S_o)$ dissociation limit. The Ar_2^+ potential curves including spin-orbit coupling have been calculated by Wadt.[16] There are four Ar_2^+ potential curves, $I(1/2)_u$, $I(3/2)_g$, $I(1/2)_g$, and $I(3/2)_u$, which correlate to the $Ar^+(^2P_{3/2})$ + $Ar(^1S_o)$ asymptote. The calculation predicts that with the exception of the $I(1/2)_u$ state which is bound by 1.19 eV, the other states are repulsive or only weakly bound. The HeI PES for Ar_2 obtained by Dehmer and Dehmer[3] resolved two electronic bands below the IE for $Ar^+(^2P_{3/2})$ which are assigned to eh $I(1/2)_u$ and $I(3/2)_g$ electronic bands. The peaks of the $I(1/2)_u$ and $I(3/2)_g$ bands are red shifted with respect to the IE for $Ar^+(^2P_{3/2})$ by ~ 0.08 and ~ 0.2 eV, respectively. The peak position of the Franck-Condon profile shown in Fig. 5(a) is consistent with the measured shifts for Ar_2^+ $[I(1/2)_u]$ and Ar_2^+ $[I(3/2)_g]$. It is most likely

Figure 5. PIPECO spectra for Ar_2^+ obtained using a wavelength resolution = 1.5 Å (FWHM), an electron energy resolution of ≈ 70 meV, and a nozzle temperature of 120 K

(a) P_o = 60 Torr; (b) P_o = 90 Torr; (c) P_o = 210 Torr

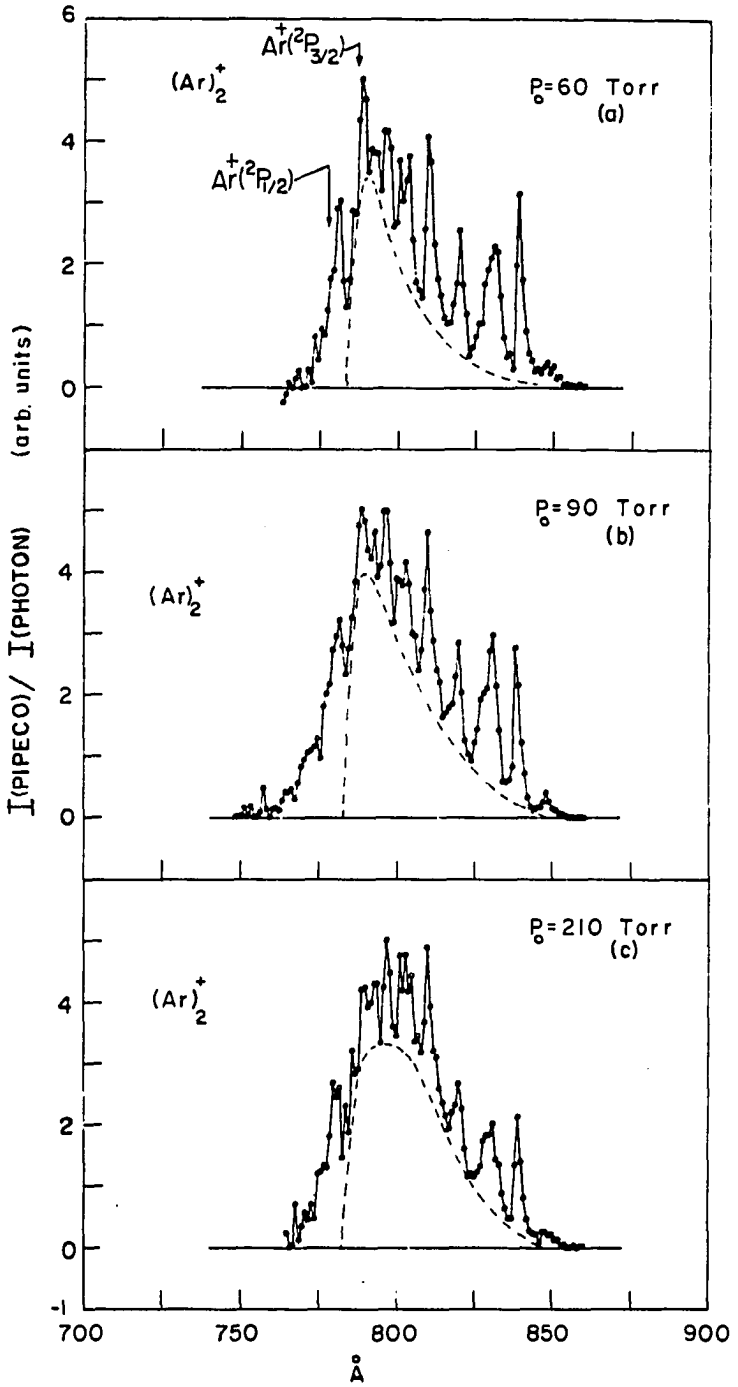
$Ar^+(^2P_{3/2})$
$(Ar)_2^+$
P_o=60 Torr
(a)
$Ar^+(^2P_{1/2})$
P_o=90 Torr
(b)
$(Ar)_2^+$
P_o=210 Torr
(c)
$(Ar)_2^+$
I(PIPECO)/ I(PHOTON) (arb. units)
6
4
2
0
4
2
0
4
2
0
-1
700
750
800
850
900
Å

that the Franck-Condon profile represents the sum of the $I(1/2)_u$ and $I(3/2)_g$ electronic bands. Considering the fact that Ar_2^+ $[I(3/2)_g]$ is only bound by ~ 0.14 eV, the contribution to the observed profile due to the formation of Ar_2^+ $[I(3/2)_g]$ should be minor. Because of the superposition of strong autoionization features on the continuum structure, the Franck-Condon profiles for the Ar_2^+ $[I(1/2)_u]$ and Ar_2^+ $[I(3/2)_g]$ electronic bands are not resolved in Fig. 5(a). The HeI PES of Ar_2 shows no autoionization structure.

The comparison of the PIPECO spectra for Ar_2^+ in Figs. 5(a) - 5(c) indicates that the autoionization peaks become less pronounced relative to the underlying continuum profile as P_o is increased, an observation similar to that found in examining the P_o effect on the PIE spectrum for Ar_2^+. As a result of the production of Ar_2^+ from the dissociative ionization of higher Ar clusters, the widths of the continuum structures shown by the dashed profiles in Fig. 5(b) and 5(c) are broader than the Franck-Condon profile observed in Fig. 5(a). The finding that fragmentation of higher Ar clusters mostly affects the continuum structure implies that the PIPECO spectra for higher Ar cluster ions are relatively smooth and have few autoionization features.

The value of 14.518 ± 0.017 eV (854 ± 1 Å) for the IE for Ar_2^+ $[I(1/2)_u]$ determined from the PIPECO spectra for Ar_2^+ [Figs. 5(a) - 5(c)] is in excellent agreement with that obtained from the PIE curves for Ar_2^+ [Figs. 4(a) - 4(c)]. This value is also in accord with the results of previous photoionization studies.[1,4,5] Using this value and the known values for the IE for $Ar^+(^2P_{3/2})$ and the dissociation energy of Ar_2 (10.4 meV), we calculate a value of 1.24 ± 0.02 eV for the dissociation energy of Ar_2^+. This

value is slightly lower than the value of 1.33 ± 0.02 eV obtained by Moseley et al.[2] using photofragmentation spectroscopic techniques.

The relative peak intensities of the PIPECO bands for Ar_2^+ in the wavelength region of 775 - 783 Å and 783 - 854 Å [Fig. 5(a)] are similar to those observed for the $Ar^+(^2P_{1/2})$ and $Ar^+(^2P_{3/2})$ bands in the threshold PES of Ar [Fig. 2(c)]. The fact that the Ar_2^+ PIPECO intensity diminishes at photon energies above the IE for $Ar^+(^2P_{1/2})$ suggests that the weaker Ar_2^+ PIPECO band in the wavelength region 775 - 783 Å may arise from an excited state of Ar_2^+ correlating to the $Ar^+(^2P_{1/2})$ + $Ar(^1S_o)$ dissociation limit. Of the two states, $II(1/2)_u$ and $II(1/2)_g$, correlating to this limit, only the $II(1/2)_u$ state is predicted to be bound.[16] Thus, we assign the weaker Ar_2^+ PIPECO band to the formation of Ar_2^+ $[II(1/2)_u]$. The Ar_2^+ $[II(1/2)_u]$ PIPECO band is also evident, but less well resolved in the PIPECO spectra measured at P_o = 90 and 210 Torr, possibly due to the fragmentation effect of higher Ar cluster ions. The IE for Ar_2^+ $[II(1/2)_u]$ is difficult to assign because the Ar_2^+ $[II(1/2)_u]$ band overlaps with the lower energy PIPECO bands for Ar_2^+ $[I(3/2)_g]$ and Ar_2^+ $[I(1/2)_u]$.

In an effort to obtain a better estimate for the adiabatic IE for Ar_2^+ $[II(1/2)_u]$, a PIPECO spectrum for Ar_2^+ has been measured at P_o = 60 Torr using a wavelength resolution of 0.5 Å (FWHM) and an electron energy resolution of 50 meV (FWHM). Figures 6(a) and 6(b) show the PIE and PIPECO spectra for Ar_2^+, respectively, recorded under these experimental conditions. The PIPECO spectra for Ar^+ is plotted in Fig. 6(c). The error bars shown in Fig. 6(b) represent one standard deviation. The comparison of the PIPECO spectra of Fig. 6(b) and 5(a) indicates that improving the

Figure 6. PIE and PIPECO spectra for Ar^+ and Ar_2^+ obtained using a wavelength resolution = 0.5 Å (FWHM), P_o = 60 Torr, electron energy resolution ≈ 50 meV (FWHM)

(a) PIE spectrum for Ar_2^+; (b) PIPECO spectrum for Ar_2^+; (c) PIPECO spectrum for Ar^+

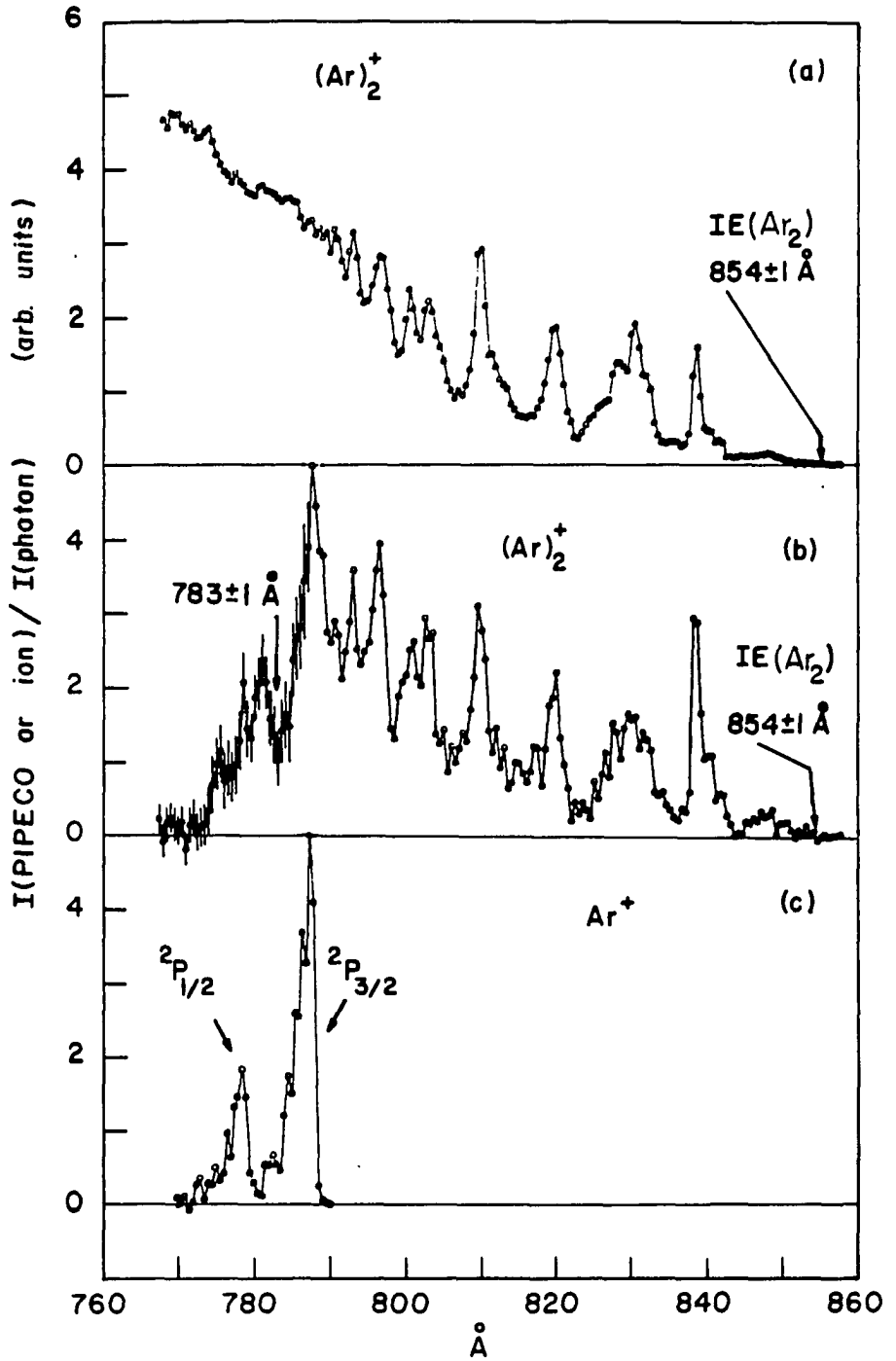
(Ar)$_2^+$
(a)
IE(Ar$_2$)
854±1 Å
(Ar)$_2^+$
(b)
783±1 Å
IE(Ar$_2$)
854±1 Å
Ar$^+$
(c)
$^2P_{1/2}$
$^2P_{3/2}$
I(PIPECO or ion) / I(photon) (arb. units)
0
2
4
6
760
780
800
820
840
860
Å

wavelength and electron energy resolutions does not reveal much new structure and that the PIPECO band for Ar_2^+ [$II(1/2)_u$] remains unresolved from the lower energy PIPECO bands.

The minimum at 15.835 ± 0.010 eV (783 ± 0.5 Å) in the overlapping region between the Ar_2^+ [$II(1/2)_u$] PIPECO band and the lower energy PIPECO bands is taken as an upper bound for the IE for Ar_2^+ [$II(1/2)_u$]. This value leads to a lower limit of 0.11 eV for the dissociation energy of Ar_2^+ [$II(1/2)_u$]. A value of 0.10 ± 0.02 eV for the dissociation energy of Ar_2^+ [$II(1/2)_u$] has been determined previously by photoelectron spectroscopy.[3] The calculation predicts that Ar_2^+ [$II(1/2)_u$] is bound only by 0.04 eV.[16] The Ar_2^+ [$II(1/2)_u$] PIPECO band peaks at 781 ± 0.5 Å, which can be taken as the vertical IE for the $II(1/2)_u$ state. The location of the peak is consistent with the convergence limit (781.2 Å) of an autoionization Rydberg series observed in the high resolution photoionization experiment.[34]

Depending on the coupling of the ionic and autoionizing Rydberg states, electrons produced by autoionization may have a distribution of kinetic energies. The ratios of the peak heights of corresponding autoionization peaks resolved in PIE and PIPECO spectra for Ar_2^+ [Figs. 6(a) and 6(b) or Figs. 4(a) and 5(a)] provide information about the relative efficiencies of the autoionizing Rydberg states in producing near-zero kinetic energy electrons. The comparison of the PIE and PIPECO data for Ar_2^+ shows that the autoionizing states associated with the autoionization peaks at 797 and 838 Å are more efficient relative to other autoionizing states in forming electrons with near-zero kinetic energies. The similarity of the autoionization structures found in the PIE and PIPECO

spectra seems to indicate that a significant fraction of electrons produced by autoionizing states observed in the wavelength region of 790 - 855 Å are slow electrons with near-zero kinetic energies falling in the energy band pass of the electron energy analyzer.

The excited Ar_2^+ [$II(1/2)_u$] ions initially formed by photoionization may undergo radiative decay to the Ar_2^+ [$I(1/2)_g$] and Ar_2^+ [$I(3/2)_g$] states which correlate to the $Ar^+(^2P_{3/2})$ + Ar dissociation limits. Since the Ar_2^+ [$I(1/2)_g$] state is predicted to be purely repulsive, the radiative transition to this state should lead to instantaneous dissociation of the Ar_2^+ ion. The observation of the Ar_2^+ [$II(1/2)_u$] band is consistent with the interpretation that the Ar_2^+ [$II(1/2)_u$] state is metastable with a radiative lifetime longer than the flight time of Ar_2^+ (47 μs) from the photoionization region to the ion detector. The $II(1/2)_u \rightarrow I(1/2)_g$ transition is expected to be significantly stronger than the $II(1/2)_u \rightarrow I(3/2)_g$ transition. The expected weakness of the $II(1/2)_u \rightarrow I(3/2)_g$ transition is in accord with the propensity rule that transitions involving changes of Ω are weak.[35] This interpretation is supported by the theoretical prediction that the radiative lifetimes for the $II(1/2)_u \rightarrow I(1/2)_g$ and $II(1/2)_u \rightarrow I(3/2)_g$ transitions are 90.9 μs and 50.7 s, respectively.[36]

Spectra for Ar_3^+

Figure 7(b) shows the PIPECO spectrum for Ar_3^+ measured at P_o = 105 Torr. The Ar_4^+ intensity is not observable at P_o = 105 Torr. The PIPECO spectra for Ar_3^+ observed at P_o = 105 and 155 Torr are in general agreement, indicating that the effect of

Figure 7. PIPECO spectra for Ar_n^+ (n = 2 - 4) obtained using a wavelength resolution = 1.5 Å (FWHM) and an electron energy resolution ≈ 70 meV (FWHM)

(a) PIPECO spectrum of Ar_4^+; (b) PIPECO spectrum of Ar_3^+; (c) PIPECO spectrum of Ar_2^+

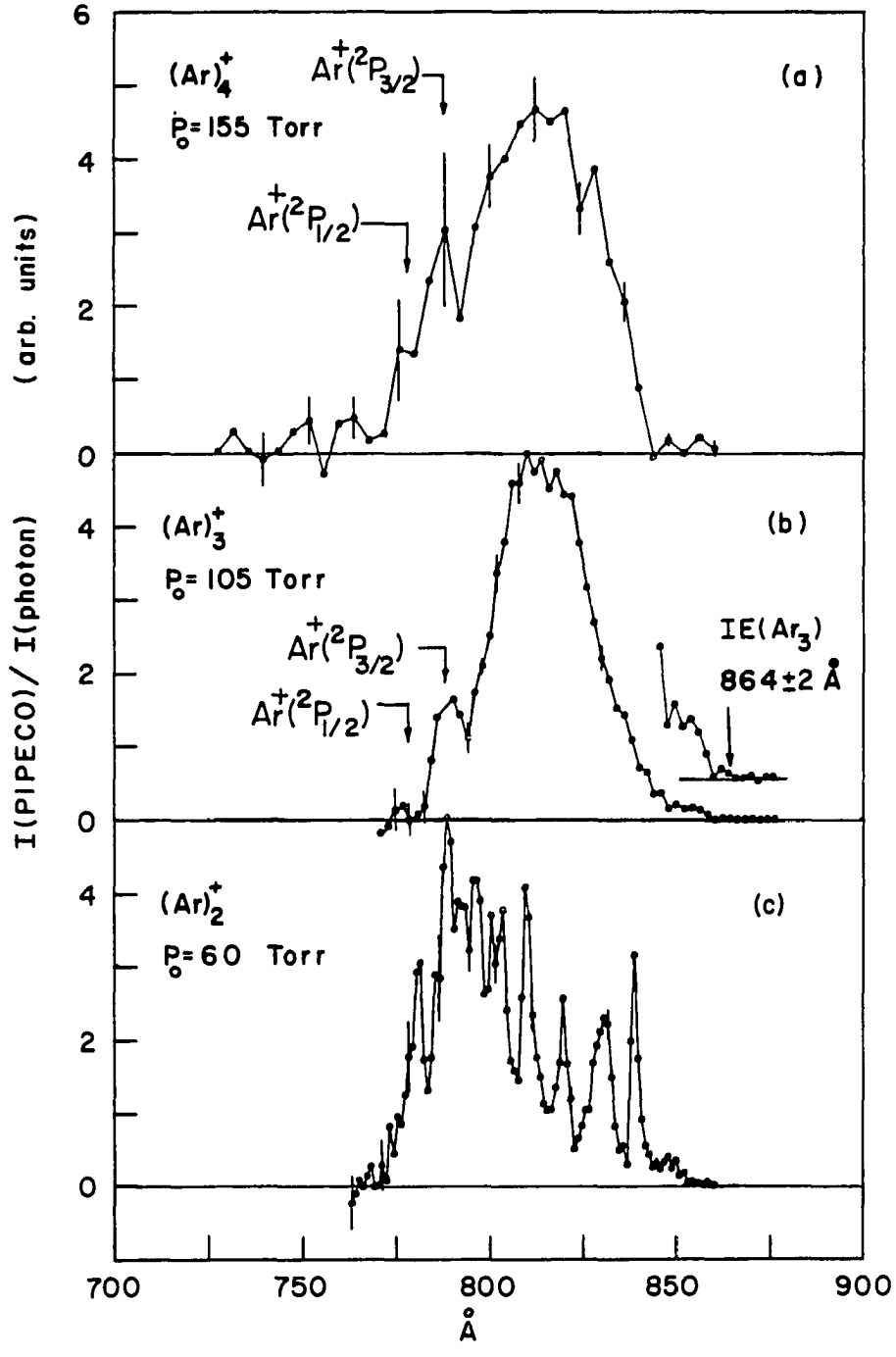
(Ar)$_4^+$
$Ar^+(^2P_{3/2})$
(a)
P_o= 155 Torr
$Ar^+(^2P_{1/2})$
(Ar)$_3^+$
(b)
P_o= 105 Torr
$Ar^+(^2P_{3/2})$
$Ar^+(^2P_{1/2})$
IE(Ar$_3$)
864±2 Å
(Ar)$_2^+$
(c)
P_o= 60 Torr
I(PIPECO)/ I(photon) (arb. units)
0
2
4
6
700
750
800
850
900
Å

fragmentation from higher Ar cluster ions on the PIPECO spectrum for Ar_3^+ is minor under the present experimental conditions. We believe that the spectrum shown in Fig. 7(b) is close to the true PIPECO spectrum of Ar_3. The IE for the ground state of Ar_3^+ is determined to be 14.35 ± 0.04 eV (864 ± 2 Å) from the Ar_3^+ PIPECO spectrum. This value is in accord with that found by the PIE measurements and with that reported by Dehmer and Pratt.[4] Using the IEs for the ground states of Ar_2^+ and Ar_3^+ obtained here, and assuming the dissociation energy for Ar_2-Ar to be equal to that for Ar_2, the dissociation energy for Ar_2^+-Ar is calculated to be 0.16 ± 0.04 eV, a value consistent with values determined by previous photoionization,[4] equilibrium mass spectrometric,[13] and flow tube[14] studies.

The rich autoionization features appearing in the Ar_2^+ PIPECO spectrum are not discernible in the Ar_3^+ PIPECO spectrum which consists simply of a strong and broad band centered at ~ 812 Å and a weak band in the wavelength region of 778 - 791 Å. The peak of the strong band is red shifted with respect to the maximum of the Franck-Condon profile shown in the Ar_2^+ PIPECO spectrum. The PIPECO intensity for Ar_3^+ decreases rapidly in the wavelength region of 791 - 810 Å as compared to the Ar_2^+ PIPECO spectrum which shows a sharp drop at photon energies close to the IE for $Ar^+(^2P_{3/2})$. At photon energies higher than the IE for $Ar^+(^2P_{1/2})$, the PIPECO intensities for Ar_3^+ are found to be within the noise level. The Ar_3^+ PIPECO band in the wavelength region of 778 - 791 Å also appears red shifted relative to the weak Ar_2^+ PIPECO band assigned to the Ar_2^+ $[II(1/2)_u]$ state.

When Ar_3^+ is formed at sufficiently high energies, it may dissociate according to reactions (3) and (4)

$$Ar_3^+ \rightarrow Ar_2^+ [I(1/2)_u, I(3/2)_g, II(1/2)_u] + Ar, \quad (3)$$

$$\rightarrow Ar^+(^2P_{3/2,1/2}) + Ar_2 \text{ (or } 2Ar). \quad (4)$$

Recently, Levinger et al.[8] report observing both dissociation channels for Ar_3^+ in a photofragmentation experiment. In the wavelength region of 6200 - 8200 Å, reaction (4) is observed to be the primary fragment channel. In a similar experiment, Albertoni et al.[7] report no Ar_2^+ forming within their experimental limit of detection. Energetically, Ar_3^+ formed by photoionization of Ar_3 using the PIPECO technique at photon energies above the IE for Ar_2^+ $[I(1/2)_u]$ can dissociate into Ar_2^+ $[I(1/2)_u]$ + Ar.

The observation of the Ar_3^+ PIPECO bands at wavelengths < 864 Å indicates that a significant fraction of Ar_3^+ ions formed at energies higher that the IE for Ar_2^+ $[I(1/2)_u]$ are metastable with lifetimes $\gtrsim 58$ μs. The examination of the PIE and PIPECO spectra for Ar_2^+ as a function of P_o demonstrates that Ar_2^+ ions are formed by dissociative photoionization of higher Ar clusters. If Ar_2^+ ions are formed by fragmentation of Ar_3^+ between the repeller plates at the photoionization region, they can enter the vertical QMS and be detected by the ion detector. Because of the arrangement of potentials for the ion lenses between the repeller plates and the QMS, Ar_2^+ ions resulting from fragmentation along the ion lenses cannot enter the vertical QMS. We conclude that Ar_3^+ ions with dissociative lifetimes $\lesssim 10$ μs, the estimated residence time of Ar_3^+ in the repeller region, may contribute to the observed PIE and PIPECO intensities for Ar_2^+. Thus, this

experiment provides evidence that Ar_3^+ formed by photoionization of Ar_3 in the wavelength range of 777 - 864 Å may have a dissociation lifetime ranging from $\lesssim$ 10 μs to $\gtrsim$ 58 μs. This finding is in accord with the rotational tunneling model proposed by Ferguson et al.[10] Their model calculations show that the lifetime of Ar_3^+ dissociating to form Ar_2^+ depends on the rotational temperatures of Ar_3^+. At Ar_3^+ rotational temperatures of 10 and 150 K, the dissociation lifetimes are predicted to have broad distributions in the range of 10^{-10} to $>$ 10 s.

Stemming from the consideration that Ar_3 is mainly bound by long range dispersion forces, Ar_3 in the ground state should have an equilateral triangular geometry. The Ar_3^+ ion in its ground state is predicted to be linear by recent theoretical calculations. The potential energies of low-lying Ar_3^+ states have been calculated by Wadt[17] as a function of bond angle. Excluding spin-orbit coupling, the $1^2\Sigma_u^+$ ground state of Ar_3^+ correlates with the $^2B_2$ state of Ar_3^+ in C_{2v} geometries. The first excited state of Ar_3^+ in a linear geometry is the $1^2\Pi_u$ state which correlates with the $^2A_1$ and $^2B_1$ states of Ar_3^+ in a C_{2v} symmetry. The $^2B_2$ state dissociates into Ar_2^+ $[I(1/2)_u]$ + Ar, whereas the $^2A_1$ and $^2B_1$ states lead to the $Ar^+(^2P)$ + Ar_2 dissociation limit. Since photoionization is a vertical transition process, the initial Ar_3^+ formed should also have a triangular geometry. By symmetry consideration, radiative decay from the $^2B_1$ state to the $^2B_2$ ground state is not allowed. Thus, the dissociation of $Ar_3^+(^2B_1)$ into Ar_2^+ $[I(1/2)_u]$ + Ar is inefficient. Including spin-orbit coupling will cause some mixings of these states. It is possible that the metastability of Ar_3^+ observed in this experiment is due to Ar_3^+ formed in the $^2B_1$ excited state. The neutral Ar trimer is a van der Waals molecule. The curvature of the

potential surface of Ar_3 with respect to variation of the interatomic distance is expected to be small. Franck-Condon transitions allow Ar_3^+ to be formed in broad regions of excited potential energy surfaces. The lifetime for the excited Ar_3^+ dissociating into Ar_2^+ + Ar depends on the excited state and the location of the excited potential surface where Ar_3^+ is formed because the strength of the coupling between the excited and ground state surfaces depends on the energy separation. Therefore, it seems reasonable to find a distribution of dissociation rates for excited Ar_3^+ formed at a specific photon energy. The instantaneous formation of Ar_2^+ from the dissociative photoionization of Ar_3 may arise from repulsive Ar_3^+ potential surfaces.

The weak Ar_3^+ PIPECO band in the wavelength region of 778 - 791 Å may correlate with the $Ar^+(^2P_{1/2})$ + Ar_2 or Ar_2^+ $[II(1/2)_u]$ + Ar dissociation limits. The position of the minimum between the strong and weak bands at 794 Å (15.615 eV) may be assigned as an upper bound for the adiabatic IE of the weak excited Ar_3^+ PIPECO band. Assuming $Ar^+(^2P_{1/2})$ + Ar_2 to be the dissociation limit, the binding energy for $Ar^+(^2P_{1/2})$ + Ar_2 is estimated to be $\gtrsim$ 0.3 eV. The assumption of Ar_2^+ $[II(1/2)_u]$ + Ar as the dissociation limit leads to a lower limit of 0.22 eV as the binding energy for Ar_2^+ $[II(1/2)_u]$ + Ar.

Spectrum for Ar_4^+

The PIPECO spectrum for Ar_4^+ obtained at P_o = 155 Torr is plotted in Fig. 7(a) to compare with the Ar_3^+ and Ar_2^+ PIPECO spectra in Figs. 7(b) and 7(c). The coincidence counting rate for Ar_4^+ at 810 Å is ~ 0.14 c/s. At P_o lower than 155 Torr,

the measurement of the Ar_4^+ PIPECO spectrum becomes impractical because of the very low coincidence counting rate for Ar_4^+. Although the intensities for Ar_5^+ and higher Ar cluster ions are found to be within the noise level at P_o = 155 Torr, the Ar_4^+ PIPECO spectrum might contain some minor contributions from dissociative photoionization of higher Ar clusters.

The general profiles of the Ar_3^+ and Ar_4^+ PIPECO spectra are similar. The PIPECO spectrum for Ar_4^+ appears to be slightly broadened with respect to that for Ar_3^+. Due to the low signal-to-noise ratio of PIPECO data for Ar_4^+, a reliable estimate of the IE for Ar_4^+ is not possible. It seems that the Ar_4^+ PIPECO spectrum also consists of a strong and a weak band, similar to the finding in the Ar_3^+ PIPECO spectrum.

The Ar_4^+ ions produced by photoionization may dissociate to form Ar_3^+, Ar_2^+, and/or Ar^+ by reactions (5), (6), and (7)

$$Ar_4^+ \rightarrow Ar_3^+ + Ar \tag{5}$$

$$\rightarrow Ar_2^+ + Ar_2 \text{ (or } 2Ar) \tag{6}$$

$$\rightarrow Ar^+ + Ar_3 \text{ (or } Ar_2 + Ar \text{ or } 3Ar). \tag{7}$$

Since the binding energies for Ar_n (n = 2 - 4) are significantly smaller than those for Ar_n^+ (n = 2 - 4), the formations of Ar_3^+, Ar_2^+, and Ar^+ are energetically possible at photon energies slightly higher than the IEs for Ar_3^+ (864 Å), Ar_2^+ (854 Å), and Ar^+ (787 Å). This experiment does not provide information about individual dissociation channels. However, the observation of the Ar_4^+ PIPECO bands shown in Fig. 7(a) supports the conclusion that metastable Ar_4^+ ions with lifetimes $\gtrsim$ 66 μs for dissociation

channels (5) - (7) may be formed by photoionization of Ar_4 in the wavelength region of 775 - 864 Å.

SUMMARY

The photoion-photoelectron coincidence spectra for Ar_n^+ (n = 2 - 4) have been measured using the MCS coincidence technique. The effects on the Ar_2^+ and Ar_3^+ PIPECO spectra due to dissociative photoionization of higher clusters have been examined. The IEs for Ar_2^+ $[I(1/2)_u]$, Ar_2^+ $[II(1/2)_u]$, and Ar_3^+ $[I(1/2)_u]$ determined by the Ar_2^+ and Ar_3^+ PIPECO spectra are in excellent agreement with previous PIE studies. Similar autoionization structures are observed in the PIE and PIPECO spectra for Ar_2^+, indicating that autoionizing states of Ar_2 produce a significant fraction of electrons with near-zero kinetic energies.

The observation of the Ar_2^+ $[II(1/2)_u]$ PIPECO band supports the conclusion that Ar_2^+ $[II(1/2)_u]$ ions are metastable with dissociation lifetimes $\gtrsim$ 47 μs. This conclusion is consistent with the radiative lifetime of 90.9 μs calculated for the $II(1/2)_u \rightarrow I(1/2)_g$ transition.

Metastable Ar_3^+ ions with lifetimes $\gtrsim$ 58 μs for reactions (3) and (4) are also observed. Evidence is found that the lifetimes for metastable Ar_3^+ decaying into Ar_2^+ + Ar may range form $\lesssim$ 10 μs to $\gtrsim$ 58 μs, in agreement with the prediction of the rotational tunneling model. An alternate explanation, which invokes the formation of Ar_3^+ in electronically excited metastable states is proposed for the observation of metastable Ar_3^+ ions.

The appearance of the Ar_4^+ PIPECO spectrum is similar to that of the Ar_3^+ PIPECO spectrum. The observation of Ar_3^+ PIPECO bands in the wavelength region of 775 - 864 Å suggests that the lifetimes for dissociation processes (5) - (7) may be $\gtrsim$ 66 μs.

REFERENCES

1. C. Y. Ng, D. J. Trevor, B. H. Mahan, and Y. T. Lee, J. Chem. Phys. 66, 446 (1977).

2. J. T. Moseley, R. P. Saxon, B. A. Huber, P. C. Cosby, R. Abouaf, and M. Tadjeddine, J. Chem. Phys. 67, 1659 (1977).

3. P. M. Dehmer and J. L. Dehmer, J. Chem. Phys. 69, 125 (1978).

4. P. M. Dehmer and S. T. Pratt, J. Chem. Phys. 76, 843 (1982).

5. P. M. Dehmer, J. Chem. Phys. 76, 1263 (1982).

6. M. G. White and J. R. Grover, J. Chem. Phys. 79, 4124 (1983).

7. C. R. Albertoni, R. Kuhn, H. W. Sarkas, and A. W. Castleman, Jr., J. Chem. Phys. 87, 5043 (1987).

8. N. E. Levinger, D. Ray, K. K. Murray, A. S. Mullin, C. P. Schulz, and W. C. Lineberger, J. Chem. Phys. 89, 71 (1988).

9. P. Scheier and T. D. Märk, Phys. Rev. Lett. 59, 1813 (1987); P. Scheier, A. Stamatovic, and T. D. Märk, J. Chem. Phys. 89, 295 (1988); K. Stephan and T. D. Märk, Chem. Phys. Lett. 90, 51 (1982); K. Stephan and T. D. Märk, Int. J. Mass Spectrom. Ion Phys. 47, 195 (1983); T. D. Märk, P. Scheier, K. Leiter, W. Ritter, K. Stephan, and A. Stamatovic, Int. J. Mass Spectrom. Ion Proc. 74, 281 (1986).

10. E. E. Ferguson, C. R. Albertoni, R. Kuhn, Z. Y. Chen, R. G. Keesee, and A. W. Castleman, Jr., J. Chem. Phys. 88, 6335 (1988).

11. U. Buck and H. Meyer, J. Chem. Phys. 84, 4854 (1986).

12. A. M. Hawryluk, J. A. Mangano, and J. H. Jacob, Appl. Phys. Lett. 31, 164 (1977); C. W. Werner, E. Zamir, and E. V. George, Appl. Phys. Lett. 29, 236 (1976); Y. Nachshon, F. K. Tittel, W. L. Wilson, Jr., and W. L. Nighan, J. Appl. Phys. 56, 36 (1984); W. L. Nighan, R. A. Sauerbrey, Y. Zhu, F. K. Tittel, and W. L. Wilson, Jr., IEEE J. Quantum Electron. 23, 253 (1987).

13. D. L. Turner and D. C. Conway, J. Chem. Phys. 71, 1899 (1979).

14. F. C. Fehsenfeld, T. J. Brown, and D. C. Albriton, Bull. Am. Phys. Soc. 24, 124 (1979).

15. W. J. Stevens, M. Gardner, A. Karo, and Paul Julienne, J. Chem. Phys. 67, 2860 (1977).

16. W. R. Wadt, J. Chem. Phys. 68, 402 (1978).

17. W. R. Wadt, Appl. Phys. Lett. 38, 1030 (1981).

18. H. H. Michels, R. H. Hobbs, and L. A. Wright, Appl. Phys. Lett. 35, 153 (1979).

19. J. Hesslich and P. J. Kuntz, Z. Phys. D2, 251 (1986).

20. H.-U. Bohmer and S. D. Peyerimhoff, Z. Phys. D3, 195 (1986).

21. P. J. Kuntz and J. Valldorf, Z. Phys. D8, 195 (1989).

22. H. Haberland, Surf. Sci. 156, 305 (1985); J. J. Saenz, J. M. Soler, and N. Garcia, Surf. Sci. 156, 121 (1985); E. E. Polymeropoulos and J. Brickmann, Surf. Sci. 156, 563 (1985).

23. K. Norwood, J.-H. Guo, G. Luo, and C. Y. Ng, J. Chem. Phys. 88, 4098 (1988).

24. K. Norwood, J.-H. Guo, G. Luo, and C. Y. Ng, Chem. Phys. 129, 109 (1988).

25. Y. Ono, S. H. Linn, H. F. Prest, M. E. Gress, and C. Y. Ng, J. Chem. Phys. 73, 2523 (1980).

26. C. -L. Liao, J. -D. Shao, R. Xu, G. D. Flesch, Y. -G. Li, and C. Y. Ng, J. Chem. Phys. 85, 3874 (1986).

27. T. Baer, W. B. Peatman, and E. W. Schlag, Chem. Phys. Lett. 4, 243 (1969).

28. R. Spohr, P. M. Guyon, W. A. Chupka, and J. Berkowitz, Rev. Sci. Instrum. 42, 1872 (1971).

29. R. Stockbauer, J. Chem. Phys. 58, 3800 (1973).

30. C. Y. Ng, in "Techniques for the Study of Ion-Molecule Reactions", Eds., J. M. Farrar and W. H. Saunders, Jr. (Wiley, New York, 1988), p. 417.

31. T. Baer, in "Gas Phase Ion Chemistry", Ed., M. T. Bowers (Academic, New York, 1979), Vol. 1, p. 153.

32. M. E. Gellender and A. D. Baker, Int. J. Mass Spectrom. Ion. Phys. 17, 1 (1975); M. E. Gellender and A. D. Baker, in "Electron Spectroscopy", Eds., C. R. Brundle and A. D. Baker (Academic, New York, 1977), Vol. 1, p. 435

33. A. Harvey, M. -del-L. F. Monteiro, And R. I. Reed, Int. J. Mass Spectrom. Ion Phys. 4, 365 (1970).

34. P. M. Dehmer and S. T. Pratt, J. Chem. Phys. 75, 5265 (1981).

35. T. H. Dunning, Jr. and P. J. Hay, Appl. Phys. Lett. 28, 649 (1976); P. J. Hay and T. H. Dunning, Jr., J. Chem. Phys. 66, 1306 (1977).

36. W. R. Wadt, Deputy Division Leader, Chemical and Laser Sciences, Los Alamos National Laboratory, Los Alamos, New Mexico (private communication).

SECTION II.

A PHOTOION-PHOTOELECTRON COINCIDENCE STUDY OF Kr AND Xe DIMERS

INTRODUCTION

Previous photoionization efficiency (PIE) measurements of Kr_2 and Xe_2 provide accurate ionization energies (IE) for Kr_2 and Xe_2 to Kr_2^+ [$I(1/2)_u$] and Xe_2^+ [$I(1/2)_u$].[1-5] The bond dissociation energy for Kr_2^+ calculated using the measured IE for Kr_2^+ is in excellent agreement with that determined by the high resolution photofragmentation study of Kr_2^+.[6] Since the bond distances for Kr_2 and Xe_2 are significantly longer than those for Kr_2^+ and Xe_2^+, the Franck-Condon factors for ionization transitions near the adiabatic IEs of Kr_2 and Xe_2 are poor. The PIE spectra for Kr_2^+ and Xe_2^+ display strong autoionization structures. The ability of PIE measurements to observe the true adiabatic IEs of the rare gas dimers is due partly to autoionization processes.

The IEs for Kr_2 and Xe_2 to Kr_2^+ [$I(3/2)_g$, $II(1/2)_u$] and Xe_2^+ [$I(3/2)_g$, $II(1/2)_u$] states have been obtained from the HeI photoelectron spectra (PES) of Kr_2 and Xe_2.[7,8] The HeI PES of Kr_2 and Xe_2 show no autoionization structure. Furthermore, these photoelectron bands are partially obscured by the more intense atomic $Kr^+(^2P_{3/2,1/2})$ and $Xe^+(^2P_{3/2,1/2})$ peaks. It is possible that the reported values for the IEs of Kr_2 and Xe_2 to Kr_2^+ [$I(3/2)_g$, $II(1/2)_u$] and Xe_2^+ [$I(3/2)_g$, $II(1/2)_u$] are upper limits because of the unfavorable Franck-Condon factors for direct ionization near the adiabatic IEs. Values for the IEs of Kr_2 and Xe_2 to form the ground and excited states of Kr_2^+ and Xe_2^+ have also been obtained from the time-of-flight (TOF) spectra of photoelectrons resulting from resonance-enhanced multiphoton ionization of Kr_2 and Xe_2.[9,10] Recently, the

photoion-photoelectron coincidence spectrum (PIPECO) for Kr_2^+ has been reported by Cordis et al.[5] In this experiment, threshold electrons in coincidence with mass-selected cluster ions are detected as a function of photon energy. Hence, both direct ionization and autoionization are probed. Their PIPECO measurements on Kr_2^+ are limited to photon energies below the IE of Kr and provide no information about excited PIPECO bands correlating to the $Kr^+(^2P_{1/2}) + Kr(^1S_o)$ asymptote.

Hoping to observe the excited Kr_2^+ $[II(1/2)_u]$ and Xe_2^+ $[II(1/2)_u]$ PIPECO bands, we have measured the PIPECO spectra for Kr_2^+ and Xe_2^+ covering wavelength regions above the IEs for $Kr^+(^2P_{1/2})$ and $Xe^+(^2P_{1/2})$. In a similar study on Ar_2, the Ar_2^+ $[II(1/2)_u]$ PIPECO band is identified, indicating that Ar_2^+ $[II(1/2)_u]$ has a dissociation lifetime > 47 μs.[11] The analysis of the Kr_2^+ and Xe_2^+ PIPECO spectra, which yields information about the dissociation lifetimes for Kr_2^+ $[II(1/2)_u]$ and Xe_2^+ $[II(1/2)_u]$, is presented in this report.

EXPERIMENTAL

The experimental arrangement and procedures used in this study have been reported previously.[11-13] Briefly, the apparatus consists of a 3 m near normal incidence vacuum ultraviolet (VUV) monochromator (McPherson 2253 M), a supersonic molecular beam production system, a capillary discharge lamp, a VUV light detector, a quadrupole mass spectrometer (QMS) for ion detection, and an electron energy analyzer for threshold electron detection.

The grating employed in this study is a Bausch and Lomb 1200 lines/mm Os coated aluminum grating blazed at 1360 Å. Either the hydrogen many-lined pseudocontinuum or the helium Hopfield continuum is used as the light source depending on the wavelength region desired. All data are obtained with an optical resolution of 1.5 Å (FWHM).

The Kr and Xe beam are produced by supersonic expansion of pure Kr and Xe through a 62 μm nozzle at a stagnation pressure (P_o) range of 200 - 500 Torr. The nozzle temperature (T) is kept at room temperature ($\sim$ 298 K) for the Xe beam production. In case of the Kr beam formation, T is maintained at either room temperature or 185 K. The high intensity central portion of the Kr or Xe jet is collimated into the ionization chamber by a conical skimmer before intersecting at 90° with the dispersed light beam emitted from the exit slit of the VUV monochromator.

A constant electrostatic field of $<$ 1 V/cm is applied at the photoionization region such that electrons and ions are deflected in opposite directions perpendicular to the

molecular beam axis. The electrons and ions are guided toward the electron energy analyzer and the QMS, respectively, by electrostatic lenses. The electron energy analyzer is optimized to transmit threshold electrons produced by photoionization of the Kr and Xe beams. The electron energy resolution used is in the range of 60-80 meV. In this coincidence experiment, we use a multichannel scaler (MCS) to measure the ion TOF distribution after the triggering by an electronic pulse signifying the arrival of an electron at the electron detector. When the VUV lamp is a continuous light source, such as that used here, the ions which are correlated with the energy-selected electrons appear in a narrow range of channels of the MCS corresponding to the differences in flight times of the correlated electron-ion pairs. The detection of uncorrelated ions will give rise to a uniform background because these ions arrive randomly at the ion detector at a uniform rate.

The PIPECO spectrum of an ion is a plot of the ratio of the electron-ion coincidence intensity to the ionization photon intensity versus photon wavelength (λ). All PIPECO spectra obtained in this experiment are measured using the QMS to select the ion of interest. The QMS is floated at a dc potential of $\sim$ 200 V. Under these conditions, the flight times for Kr_2^+ and Xe_2^+ are 68 and 85 μs, respectively. The full widths of the TOF peaks for Kr_2^+ and Xe_2^+ are < 10 μs.

RESULTS

Spectra for Kr_2^+

The coincidence TOF spectra for Kr_n^+ (n = 1 - 3) measured at λ = 906 Å, T = 185 K, and P_o = 250, 300, and 400 torr are shown in Figs. 1(a), 1(b), and 1(c), respectively. The accumulation time for each spectrum is 1200 s. The spectra are obtained when the QMS is operated as a radio frequency (rf) ion guide at an ion entrance energy of 5.5 V such that all ions are transmitted to the ion detector. The helium Hopfield continuum is used as the light source. The presence of Kr^+ at λ = 906 Å, which is lower than the IE of Kr, is due mostly to scattered light arising from imperfections of the grating. These coincidence TOF spectra illustrate that the ratio of Kr_3^+ to Kr_2^+ intensities decreases as P_o is decreased. At P_o = 250 Torr, the Kr_3^+ peak is not discernible in the spectrum. The coincidence TOF spectrum for the Kr cluster ions has also been examined as a function of P_o at T = 298 K. We find that no Kr_n^+ ($n \geq 3$) ions are observable at $P_o \leq$ 700 Torr and T = 298 K.

In order to measure the "true" PIPECO spectrum for Kr_2^+, it is necessary to minimize the formation of Kr_n ($n \geq 3$) in the Kr supersonic beam. The PIPECO spectra for Kr^+ and Kr_2^+ obtained at T = 298 K and P_o = 500 Torr are plotted in Figs. 2(a) and 2(b). The PIPECO spectrum for Kr^+ consists of the $^2P_{3/2}$ and $^2P_{1/2}$ bands. The stronger peak appearing in the $Kr^+(^2P_{3/2})$ PIPECO band is due to the $9d'[3/2]_1^o$

Figure 1. PIPECO TOF mass spectra for Kr_n^+ (n = 1 - 3) observed at λ = 906 Å and T = 185 K

(a) P_o = 250 Torr; (b) P_o = 300 Torr; (c) P_o = 400 Torr

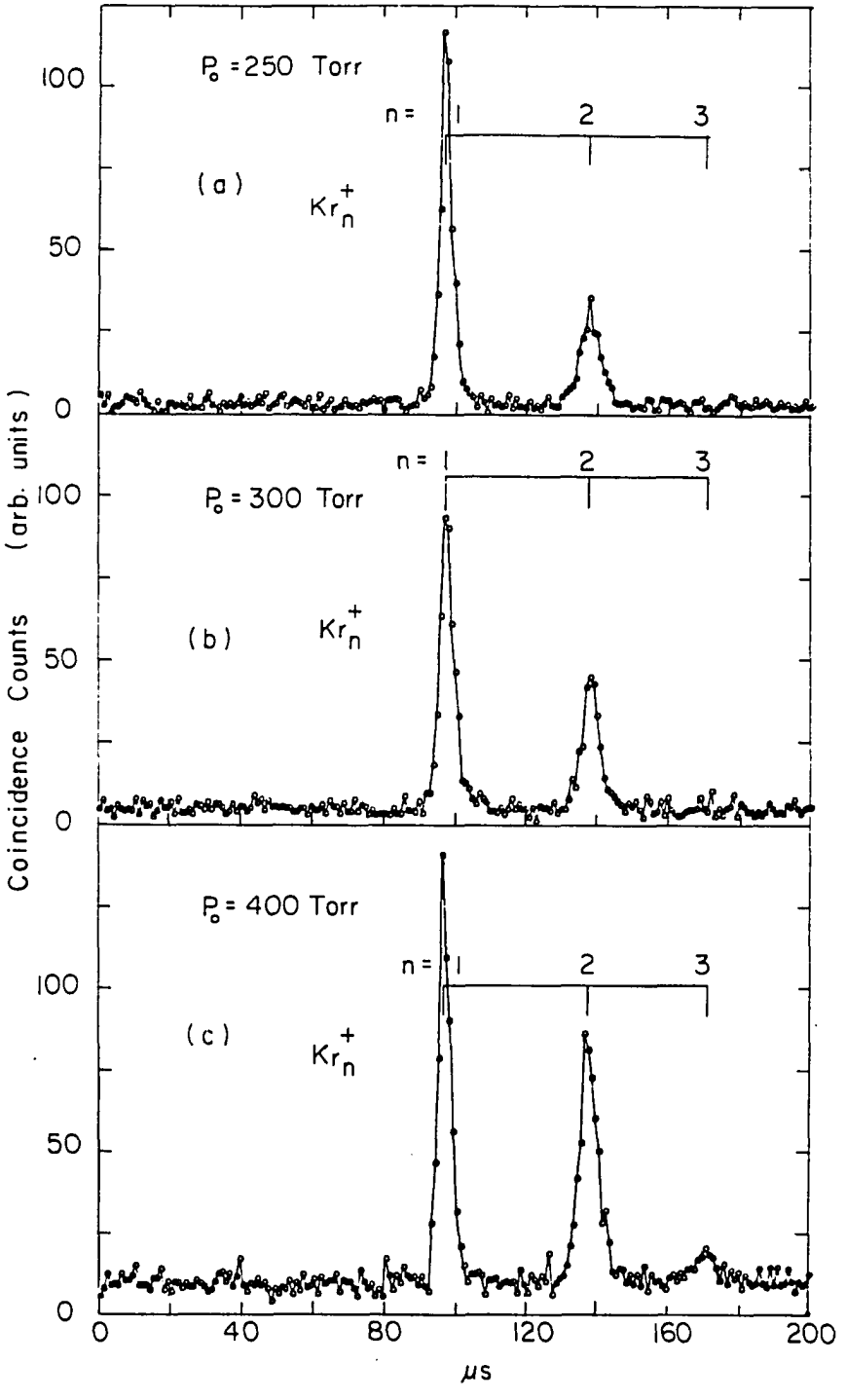
P₀ = 250 Torr
n = 1 2 3
(a)
Kr⁺n
P₀ = 300 Torr
(b)
P₀ = 400 Torr
(c)
Coincidence Counts (arb. units)
100
50
0
0 40 80 120 160 200
μs

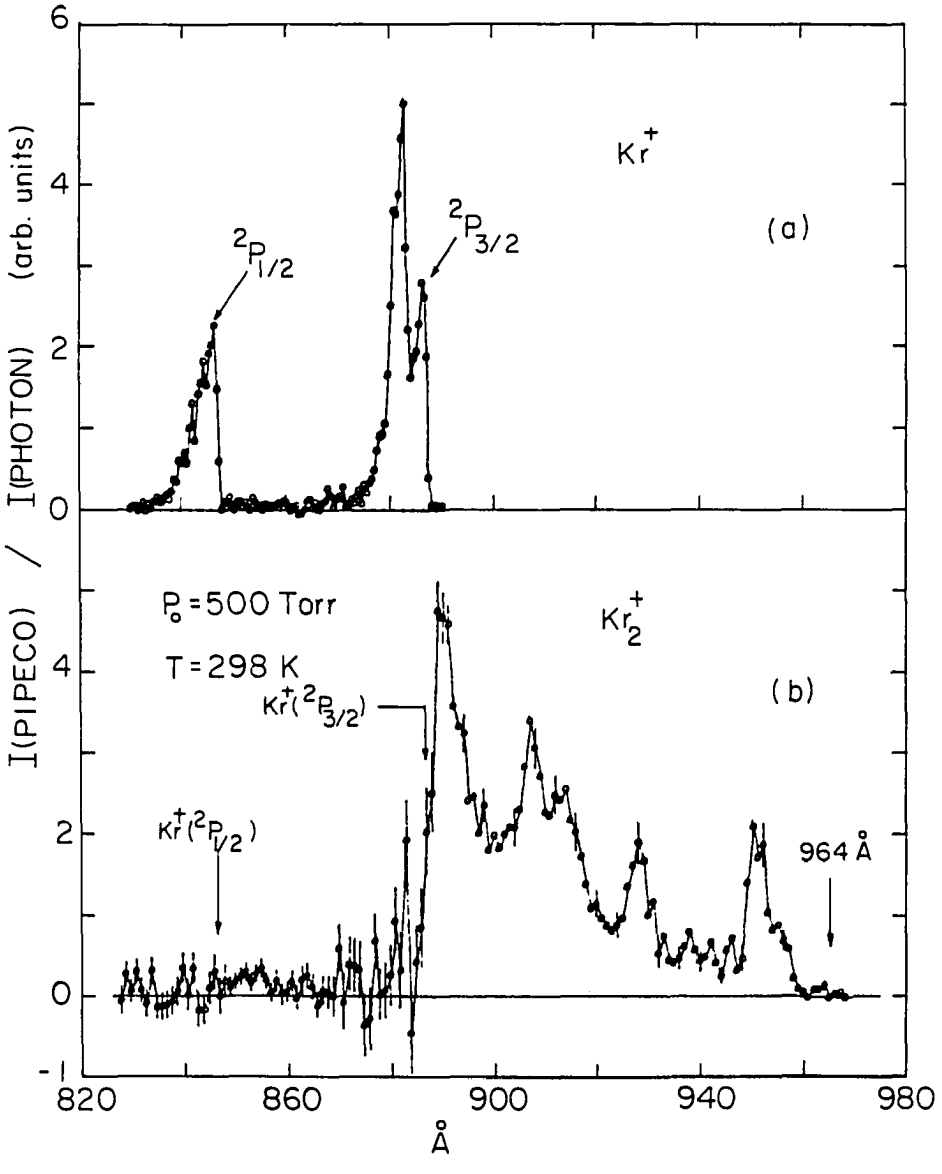

Figure 2. PIPECO spectra for Kr^+ and Kr_2^+ obtained using a wavelength resolution = 1.5 Å (FWHM), P_o = 500 Torr, T = 298 K, and an electron energy resolution ≈ 80 meV (FWHM)

(a) PIPECO spectrum for Kr^+; (b) PIPECO spectra for Kr_2^+

autoionizing state which converges to the $Kr^+(^2P_{1/2})$ ionization threshold. The error bars shown in Fig. 2(b) represent one standard deviation. The corresponding PIE spectra for Kr^+ and Kr_2^+ observed under the same experimental conditions are depicted in Figs. 3(a) and 3(b), respectively. The PIPECO spectrum for Kr_2^+ at $\lambda \geq 895$ Å is consistent with that measured by Cordis et al.[5] The PIE spectrum for Kr_2^+ is also in agreement with results of previous photoionization studies.[1,3,4]

The most interesting observation of the Kr_2^+ PIPECO spectrum is that the PIPECO intensity for Kr_2^+ drops abruptly to zero as the photon energy is increased to the IE for $Kr^+(^2P_{3/2})$. Similarly, the PIPECO intensities for Kr_2^+ at photon energies higher than the IE for $Kr^+(^2P_{1/2})$ are found to be zero. A very weak PIPECO band in the wavelength region of 845 - 856 Å is evident. In order to reduce the standard deviations and to positively identify this band, a counting time of 800 s per data point is used in the wavelength region of 840 - 865 Å.

The PIPECO spectrum for Kr_2^+ in the wavelength region of ~ 840 - 900 Å has been examined as a function P_o. Figures 4(b), 4(c), and 4(d) show the PIPECO spectra for Kr_2^+ observed at T = 185 K and P_o = 200, 250, and 300 Torr, respectively. The PIPECO spectrum for Kr_2^+ shown in Fig. 4(a) is identical to that of Fig. 2(b) except that the PIPECO data of Fig. 4(a) has been smoothed using a three-point averaging routine. The error bars for PIPECO data shown in the figures represent one standard deviation. Figures 4(b)-4(d) clearly demonstrate that the intensity of the weak PIPECO band centered at ~ 855 Å relative to the strong peak at ~ 890 Å increases when the intensities of Kr_n ($n \geq 3$) in the Kr supersonic beam are increased at higher P_o. The

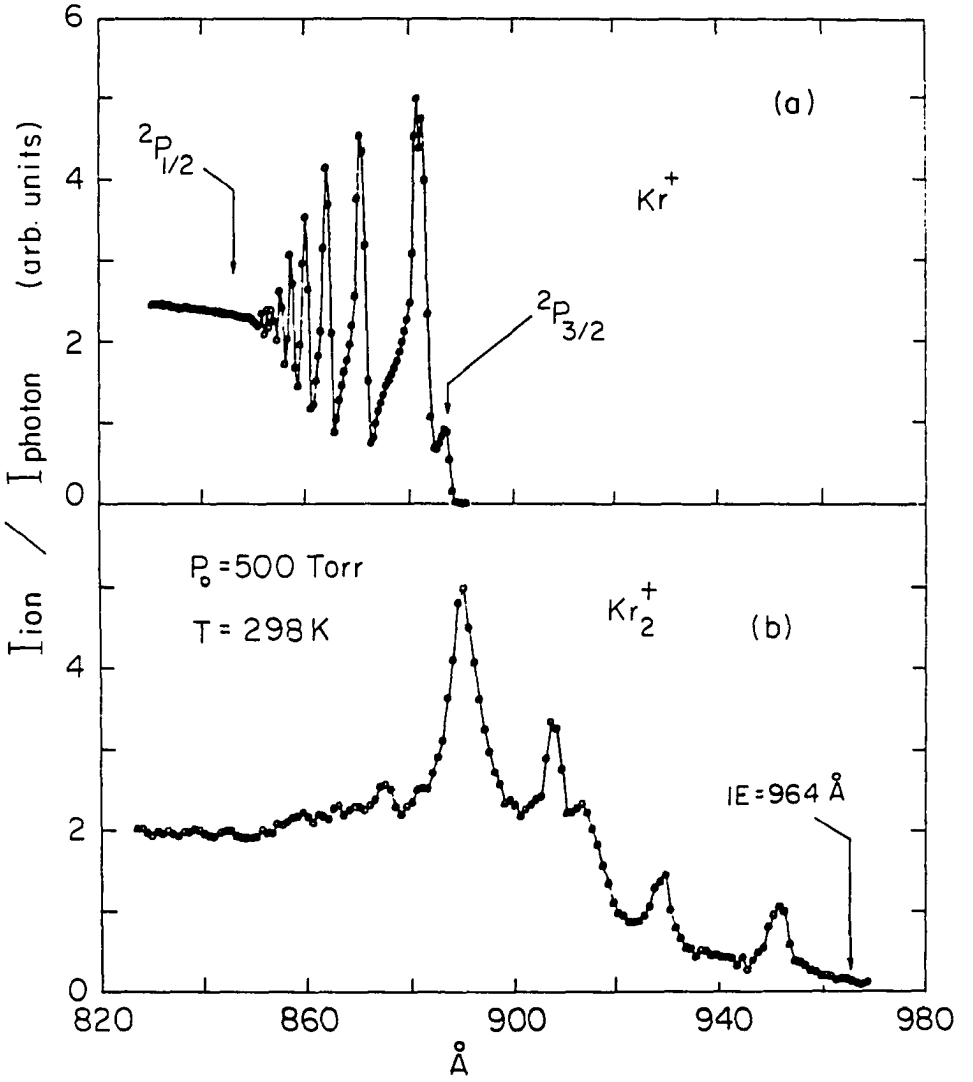

Figure 3. PIE spectra for Kr^+ and Kr_2^+ obtained using a wavelength resolution = 1.5 Å (FWHM), P_o = 500 Torr, and T = 298 K

(a) PIE spectrum for Kr^+; (b) PIE spectrum for Kr_2^+

Figure 4. PIPECO spectra of Kr_2^+ obtained using a wavelength resolution = 1.5 Å (FWHM) and an electron energy resolution ≈ 80 meV (FWHM) (a) P_o = 500 Torr, T = 298 K; (b) P_o = 200 Torr, T = 185 K; (c) P_o = 250 Torr, T = 185 K; (d) P_o = 300 Torr, T = 185 K

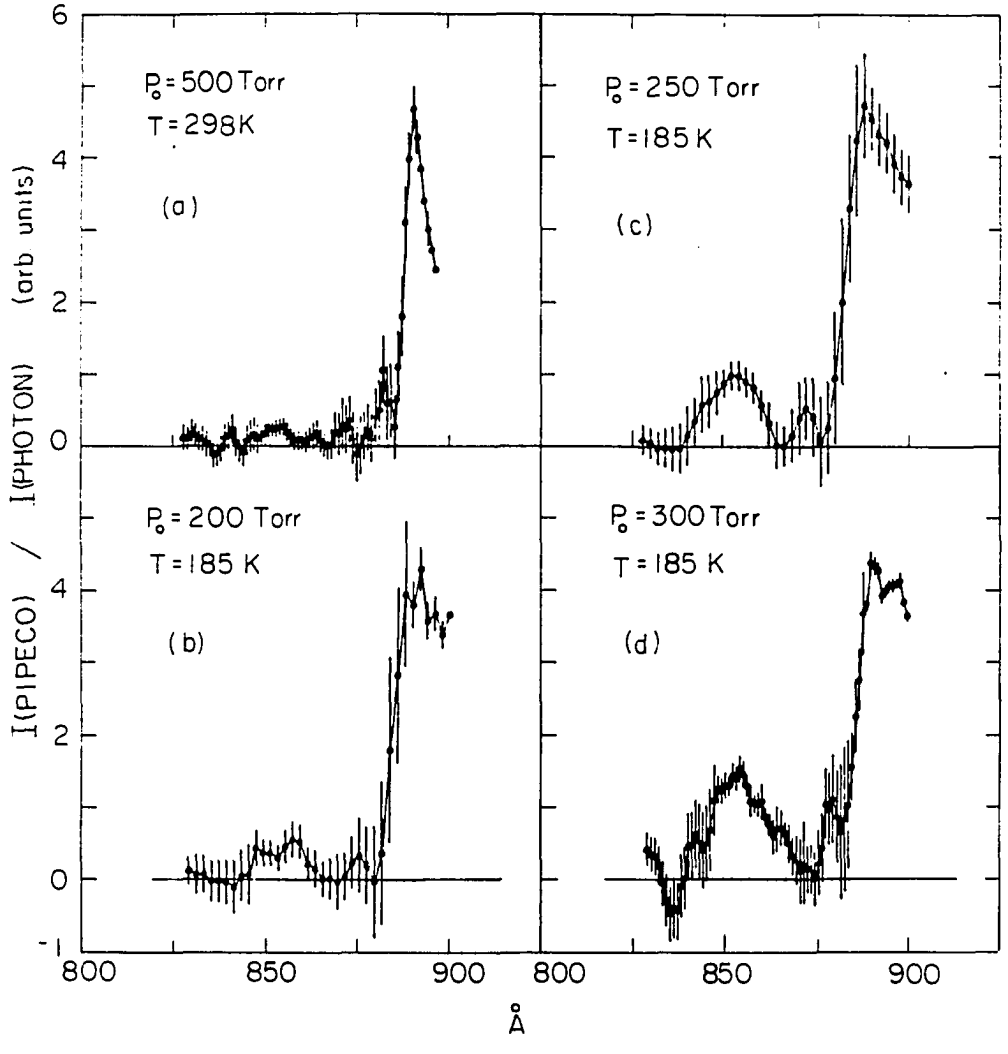
P₀ = 500 Torr
T = 298K
(a)
P₀ = 250 Torr
T = 185 K
(c)
P₀ = 200 Torr
T = 185 K
(b)
P₀ = 300 Torr
T = 185 K
(d)
I(PIPECO) / I(PHOTON) (arb units)
6
4
2
0
-1
800
850
900
Å

appearance energy (AE) of the weak PIPECO band is found to shift to a lower energy as P_o is increased. Furthermore, the widths of the strong peaks at 890 Å observed in Figs. 4(b) - 4(d) are greater than that resolved in Fig. 4(a). If the gradual change illustrated in Figs. 4(a) - 4(d) can be attributed to the formation of Kr_2^+ by dissociative photoionization of Kr_n ($n \geq 3$), the Kr beam formed at T = 298 K and P_o = 500 Torr contains the least amount of Kr_n ($n \geq 3$) compared to those formed at T = 185 K. We note that the intensities for the Kr_n^+ ($n \geq 3$) TOF peaks observed at T = 185 K and $P_o \leq 250$ Torr (Fig. 1(a)) are within the noise level. The comparison of the Kr_2^+ PIPECO spectra in Figs. 4(a) - 4(d) shows that the absence of a cluster ion in the coincidence TOF spectrum is not a sufficient condition for excluding the existence of the corresponding neutral cluster in the supersonic beam. Efficient fragmentation of the parent cluster ions upon ionization may diminish the intensity of the parent cluster ion to the noise level.

Spectra of Xe_2^+

Figures 5(a), 5(b), and 5(c) display the coincidence TOF spectra for Xe cluster ions observed at λ = 1060 Å, T = 298 K, and P_o = 300, 400, and 500 Torr, respectively. The spectra are measured using the QMS as an rf ion guide at an ion entrance energy of 5.5 V. Under these experimental conditions, Xe_2^+ is the predominant ion. The Xe_3^+ TOF peaks are discernible in Figs. 5(b) and 5(c), whereas it is not observed in Fig. 5(a). Contrary to the observation in Figs. 1(a)-1(c) where the TOF peak for Kr^+ has the strongest intensity in comparison to those for Kr_2^+ and Kr_3^+, the TOF peak for Xe^+ is

Figure 5. PIPECO TOF mass spectra for Xe_n^+ (n = 1 - 3) observed at λ = 1060 Å and T = 298 K

(a) P_o = 300 Torr; (b) P_o = 400 Torr; (c) P_o = 500 Torr

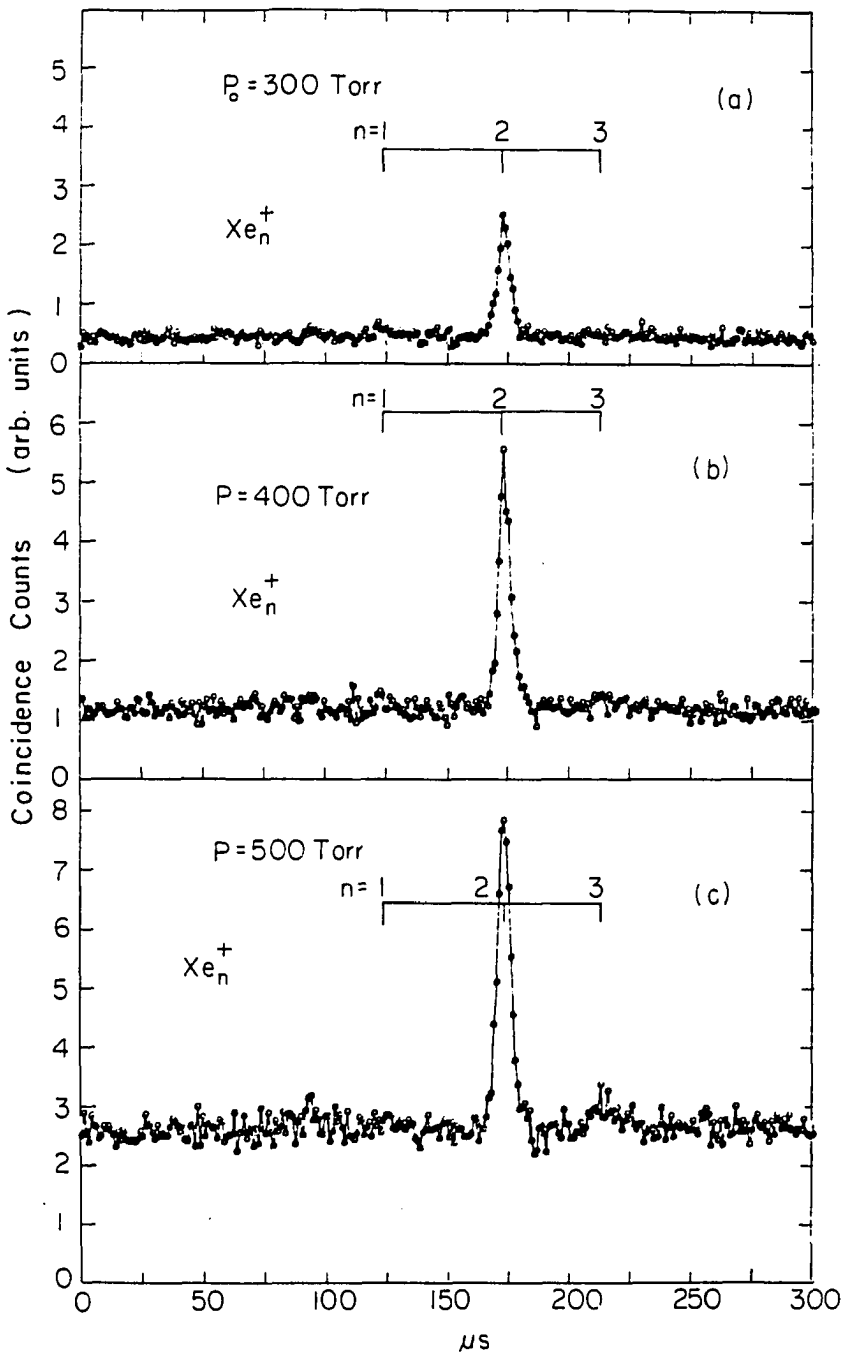
P = 300 Torr
(a)
n=1 2 3
Xe_n^+
n=1 2 3
P = 400 Torr
(b)
Xe_n^+
P = 500 Torr
n= 1 2 3
(c)
Xe_n^+
Coincidence Counts (arb. units)
0 50 100 150 200 250 300
μs

barely visible in Figs. 5(a) - 5(c). The coincidence TOF spectra for Xe cluster ions are recorded using the hydrogen many-lined pseudocontinuum as the light source. This light source has the high energy limit at ~ 850 Å and produces relatively weak VUV radiation in the wavelength range above the IE for $Xe^+(^2P_{3/2})$ (1022 Å). The very low coincidence intensity for Xe^+ observed at λ = 1060 Å is consistent with the conclusion that the intensity of scattered light with λ < 1022 Å is negligible when the grating is adjusted to emit radiation at λ = 1060 Å from the exit slit of the monochromator.

The coincidence TOF spectra shown in Figs. 5(a), 5(b), and 5(c) are measured using the same accumulation time (600 s). When P_o is changed from 300 to 500 Torr, the coincidence intensity for Xe_2^+ increases by ~ 2.5 times, while the false coincidence level rises approximately by a factor of 5. Since the coincidence intensity for Xe_2^+ is proportional to the ionization rate of Xe_2 and the false coincidence level is proportional to the square of the total ionization rate (i.e., the total ionization rate for all Xe clusters at λ = 1060 Å), the observation indicates that the ratio of the intensity for Xe_2 to the total intensity for Xe clusters increases roughly by a factor of 1.12 as P_o is increased from 300 to 500 Torr.

The PIPECO spectra for Xe_2^+ measured at T = 298 K and P_o = 300, 400, and 500 Torr are depicted in Figs. 6(b) - 6(d), respectively. The PIPECO spectrum for Xe^+, which consists of the $^2P_{3/2}$ and $^2P_{1/2}$ bands, is shown in Fig. 6(a) to compare with the Xe_2^+ PIPECO spectra. The PIPECO spectra for Xe_2^+ of Figs. 6(b) - 6(d) are in general agreement. The error bars in the figures indicate one standard deviation. According to the coincidence TOF spectra for Xe cluster ions shown in Figs. 5(a) - 5(c), the spectrum

Figure 6. PIPECO spectra for Xe^+ and Xe_2^+ obtained using a wavelength resolution = 1.5 Å (FWHM) and an electron energy resolution ≈ 80 meV (FWHM) (a) PIPECO spectrum for Xe^+ obtained at T = 298 K and P_o = 300 Torr; (b) PIPECO spectrum for Xe_2^+ obtained at T = 298 K and P_o = 300 Torr; (c) PIPECO spectrum for Xe_2^+ obtained at T = 298 K and P_o = 400 Torr; (d) PIPECO spectrum for Xe_2^+ obtained at T = 298 K and P_o = 500 Torr

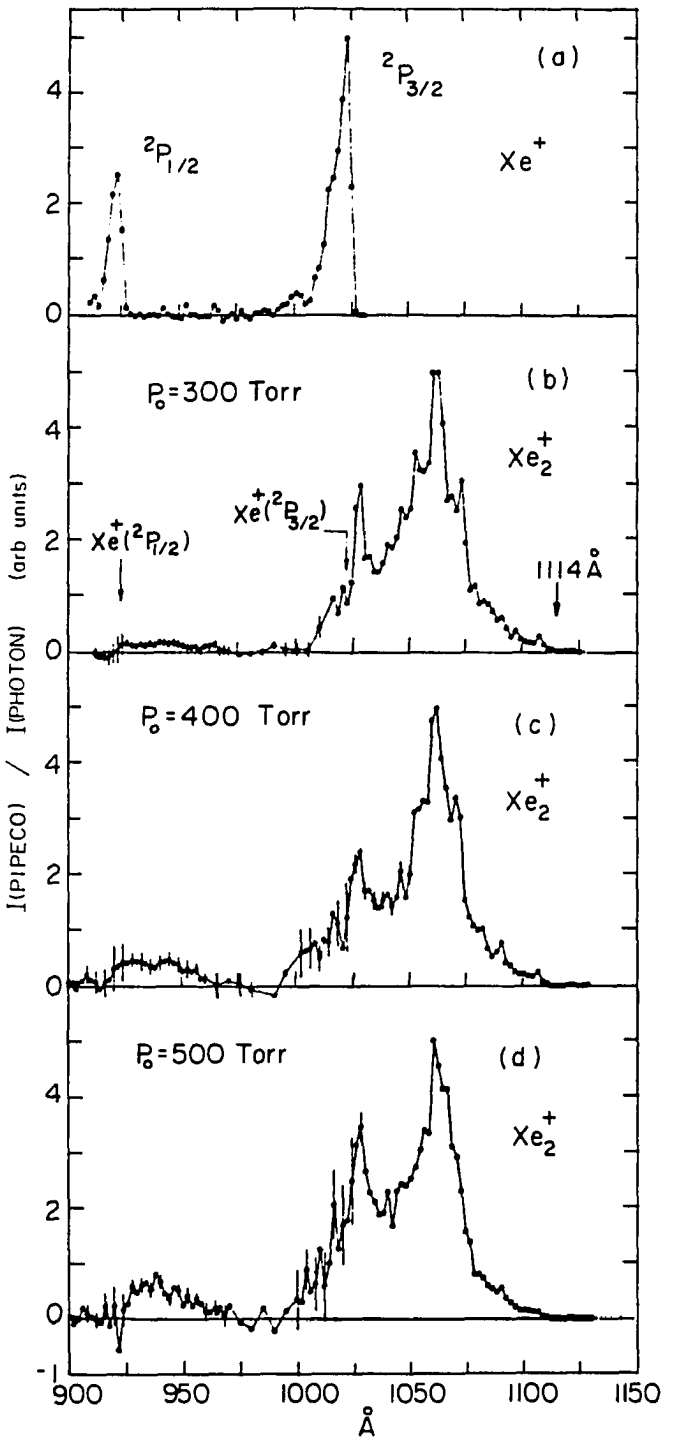
(a)
$^2P_{3/2}$
$^2P_{1/2}$
Xe^+
P_o=300 Torr
(b)
Xe_2^+
$Xe^+(^2P_{3/2})$
$Xe^+(^2P_{1/2})$
1114 Å
P_o=400 Torr
(c)
Xe_2^+
P_o=500 Torr
(d)
Xe_2^+
I(PIPECO) / I(PHOTON) (arb units)
Å
900
950
1000
1050
1100
1150

of Fig. 6(b) should be close to the "true" PIPECO spectrum of Xe_2. Similar to the observation in the Kr_2^+ PIPECO spectrum, the coincidence intensity for Xe_2^+ in Fig. 6(b) is found to decrease sharply at the IE for $Xe^+(^2P_{3/2})$ and drop to the noise level within the energy band pass of the electron energy analyzer. At photon energies higher than the IE for $Xe^+(^2P_{1/2})$ (923 Å), the Xe_2^+ coincidence intensities are zero. Using the accumulation time of 600 s per data point, we identify a very weak PIPECO band in the wavelength region of 923 - 952 Å. The intensity for this band increases as P_o is increased from 300 to 400 or 500 Torr. The AEs for the weak PIPECO bands observed at P_o = 400 and 500 Torr are lower than that measured at P_o = 300 Torr.

Figures 7(a) and 7(b) show the PIE spectra for Xe^+ and Xe_2^+ obtained at T = 298 K and P_o = 300 Torr. The autoionizing Rydberg structure resolved in the PIE spectrum for Xe_2^+ has been analyzed in detail in previous photoionization experiments.[2-4] The PIE spectrum for Xe_2^+ observed here is in agreement with the results of previous PIE studies.

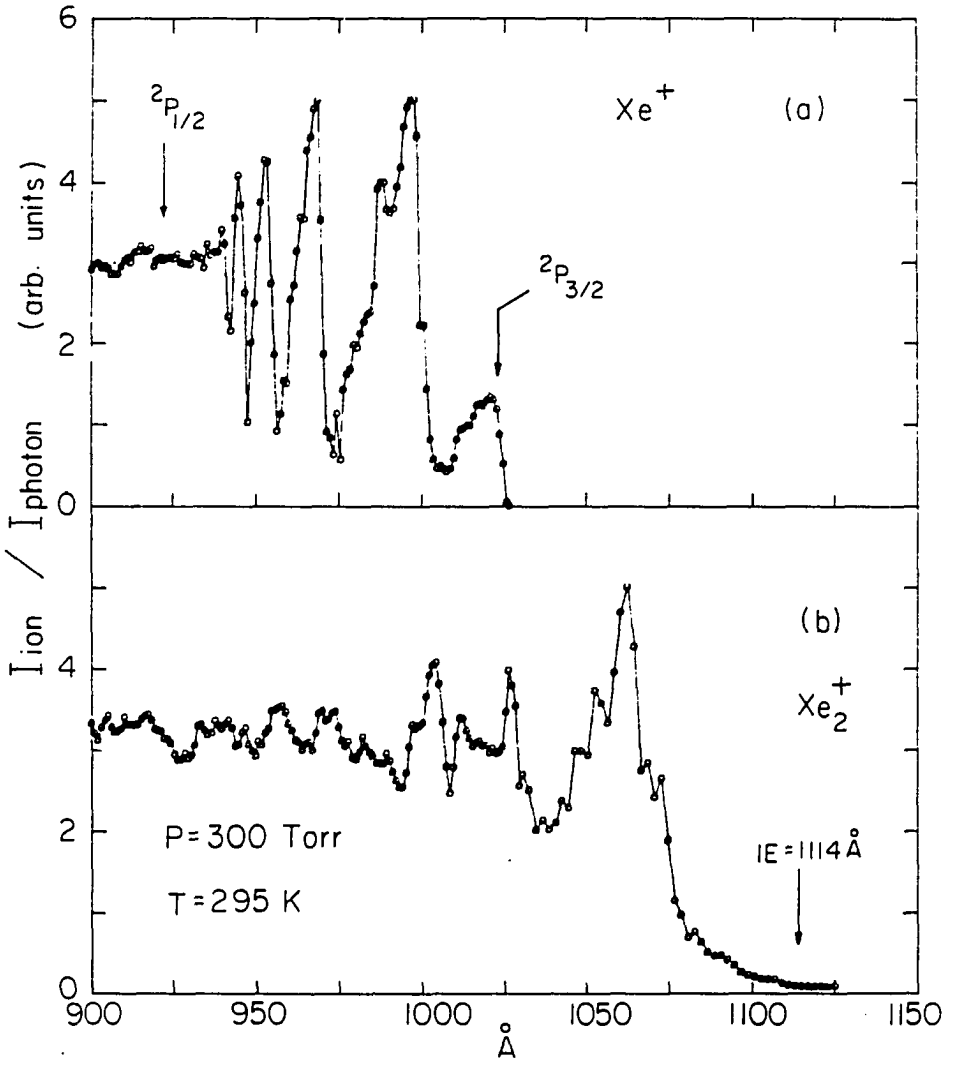

Figure 7. PIE spectra for Xe^+ and Xe_2^+ obtained using a wavelength resolution = 1.5 Å (FWHM), P_o = 300 Torr, and T = 298 K

(a) PIE spectrum for Xe^+; (b) PIE spectrum for Xe_2^+

DISCUSSION

Dissociation Mechanism for Kr_2^+ [$II(1/2)_u$] and Xe_2^+ [$II(1/2)_u$]

Figures 8(a) - 8(c) compare the PIPECO spectra for Ar_2^+, Kr_2^+, and Xe_2^+. As pointed out previously, these spectra are observed at nozzle expansion conditions which minimize the formation of trimers and higher clusters. Thus, they may be viewed as the "true" PIPECO spectra of Ar_2, Kr_2, and Xe_2.

In the discussion below, Rg will be used to represent Ar, Kr, and Xe. The sharp drops in PIPECO intensities of the dimer ions observed at photon energies coinciding with the $Rg^+(^2P_{3/2})$ ionization thresholds are consistent with the interpretation that dimer ions formed with internal energies higher than their dissociation limits are dissociative. The PIPECO bands at photon energy ranges lower than the $Rg^+(^2P_{3/2})$ ionization thresholds can be assigned to electronic states correlating to the $Rg^+(^2P_{3/2})$ + $Rg(^1S_o)$ asymptotes. Four electronic states, $I(1/2)_u$, $I(3/2)_g$, $I(1/2)_g$, and $I(3/2)_u$, result from the interaction of $Rg^+(^2P_{3/2})$ and $Rg(^1S_o)$. The ground Rg_2^+ [$I(1/2)_u$] states are bound by more than 1 eV.[1-10,14,15] The binding energies for the first excited Rg_2^+ [$I(3/2)_g$] states are found to be < 0.2 eV.[7-10,14,15] The theoretical calculation of Wadt[14] predicts that the second excited Rg_2^+ [$I(3/2)_u$] states are bound by $\lesssim 0.03$ eV and the third excited Rg_2^+ [$I(1/2)_g$] states are purely repulsive. The density function calculation of Michels et al.[15] is in general agreement with the results of Wadt except that Ar_2^+ [$I(1/2)_g$] is predicted by

Figure 8. PIPECO spectra for Rg_2^+ (Rg = Ar, Kr, Xe)

(a) PIPECO spectrum for Ar_2^+ obtained at T = 120 K, P_o = 60 Torr, wavelength resolution = 0.5 Å (FWHM), and electron energy resolution $\approx$ 50 meV (FWHM); (b) PIPECO spectrum for Kr_2^+ obtained at T = 298 K, P_o = 500 Torr, wavelength resolution = 1.5 Å (FWHM), and electron energy resolution $\approx$ 80 meV (FWHM); (c) PIPECO spectrum for Xe_2^+ obtained at T = 298 K, P_o = 300 Torr, wavelength resolution = 1.5 Å (FWHM), and electron energy resolution $\approx$ 80 meV (FWHM)

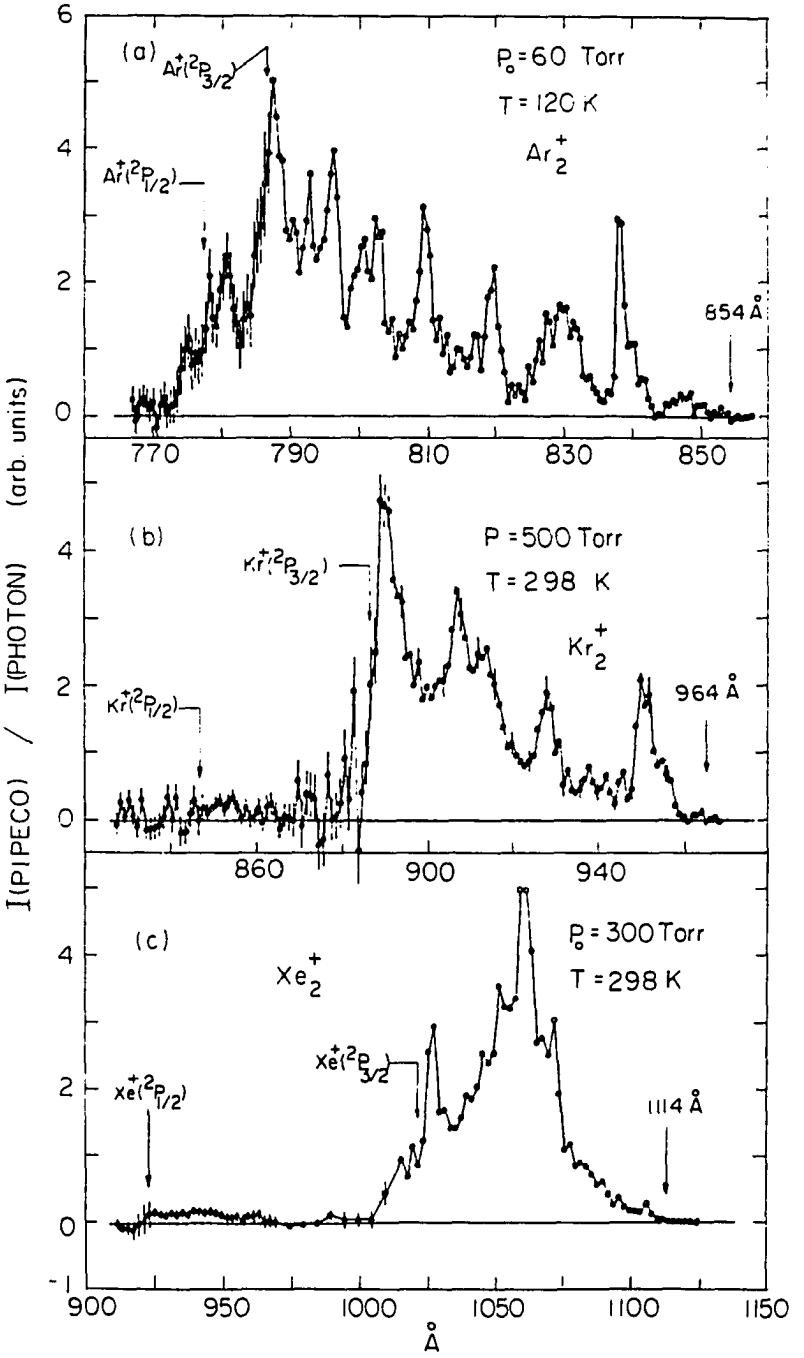
(a)
$Ar^+(^2P_{3/2})$
$Ar^+(^2P_{1/2})$
P_o=60 Torr
T = 120 K
Ar_2^+
854 Å
(b)
$Kr^+(^2P_{3/2})$
$Kr^+(^2P_{1/2})$
P = 500 Torr
T = 298 K
Kr_2^+
964 Å
(c)
Xe_2^+
$Xe^+(^2P_{3/2})$
$Xe^+(^2P_{1/2})$
P_o = 300 Torr
T = 298 K
1114 Å
I(PIPECO) / I(PHOTON) (arb. units)
Å

the former calculation to have a dissociation energy of 0.05 eV. The results of the HeI photoelectron spectroscopic study[7] indicate that the Ar_2^+ $[I(1/2)_g]$ state is repulsive. Two peaks are observed at energies below the $Rg^+(^2P_{3/2})$ ionization threshold in the HeI PESs of Rg_2. These peaks are assigned to the Rg_2^+ $[I(1/2)_u]$ and Rg_2^+ $[I(3/2)_g]$ electronic bands. The PIPECO electronic bands observed at photon energies lower than the $Rg^+(^2P_{3/2})$ ionization thresholds are most likely due to the formation of Rg_2^+ $[I(1/2)_u, I(3/2)_g]$. Because of the existence of strong autoionizing features, the Rg_2^+ $[I(1/2)_u]$ and Rg_2^+ $[I(3/2)_g]$ electronic bands are not resolved in the Rg_2^+ PIPECO spectra. Using arguments similar to those presented above, the weak PIPECO bands in wavelength regions between the $Rg^+(^2P_{3/2})$ and $Rg^+(^2P_{1/2})$ may be attributed to the formation of Rg_2^+ in electronic states correlating to the $Rg^+(^2P_{1/2})$ + $Rg(^1S_o)$ dissociation limits. The combination of $Rg^+(^2P_{1/2})$ + $Rg(^1S_o)$ gives rise to the fourth $[I(1/2)_u]$ and fifth $[I(1/2)_g]$ excited states of Rg_2^+. The dissociation energies for Rg_2^+ $[II(1/2)_u]$ are reported to be in the range of 0.1-0.2 eV.[7-10,14,15] Experimental[9,10] and theoretical[14,15] results show that the $II(1/2)_g$ state is bound by less than 0.04 eV in Xe_2^+ and Kr_2^+ and is purely repulsive in Ar_2^+. Hence, the weak PIPECO bands for Rg_2^+ may be assigned to the formation of Rg_2^+ $[II(1/2)_u]$. Considering that the intensities for the Kr_2^+ $[II(1/2)_u]$ and Xe_2^+ $[II(1/2)_u]$ PIPECO bands decrease gradually as P_o is reduced we cannot exclude the possibility that the intensities of these bands may decrease to zero at P_o lower than those used to measure the Kr_2^+ and Xe_2^+ PIPECO spectra shown in Figs. 8(b) and 8(c). At P_o lower than those used to measure the spectra of Figs. 8(b) and 8(c), the coincidence signals for Kr_2^+ and Xe_2^+ become too weak for a positive identification of these bands.

Whether or not the very weak PIPECO bands observed in Figs. 8(b) and 8(c) are the "true" Kr_2^+ [$II(1/2)_u$] and Xe_2^+ [$II(1/2)_u$] PIPECO bands remains to be determined.

The observation of the Ar_2^+ [$II(1/2)_u$] PIPECO band[11] indicates that Ar_2^+ [$II(1/2)_u$] is metastable with a dissociation lifetime longer than 47 μs, the flight time of Ar_2^+ from the photoionization region to the ion detector. The extreme weakness of the Kr_2^+ [$II(1/2)_u$] and Xe_2^+ [$II(1/2)_u$] PIPECO bands compared to the PIPECO bands for Kr_2^+ [$I(1/2)_u$,$I(3/2)_g$] and Xe_2^+ [$I(1/2)_u$,$I(3/2)_g$] supports the conclusion that Kr_2^+ [$II(1/2)_u$] and Xe_2^+ [$II(1/2)_u$] ions are dissociative with dissociation lifetimes shorter than 68 and 85 μs, respectively. A plausible mechanism for the dissociation of Rg_2^+ [$II(1/2)_u$] is summarized in processes 1(a) and 1(b).

$$\begin{aligned} &\text{(a)} \\ Rg_2^+\,[II(1/2)_u] &\rightarrow Rg_2^+\,[I(1/2)_g, I(3/2)_g] + h\nu \\ &\text{(b)} \\ &\rightarrow Rg^+(^2P_{3/2}) + Rg(^1S_o). \end{aligned} \qquad (1)$$

Process 1(a) involves dipole-allowed radiative decay transitions. In accordance with the propensity rule which favors transitions with no change in Ω[16], the $II(1/2)_u \rightarrow I(1/2)_g$ transition should be significantly stronger than the $II(1/2)_u \rightarrow I(3/2)_g$ transition. The radiative lifetimes for these transitions calculated at the equilibrium distances of Rg_2^+ are listed in Table I.[17]

Table I. Radiative Lifetimes for the Rg_2^+ $[II(1/2)_u]$ (Rg = Ar, Kr, and Xe)

Transitions	Theory[a]	Present Work
Ar_2^+ $II(1/2)_u \rightarrow I(1/2)_g$	90.9 μs	> 47 μs[b]
$\rightarrow I(3/2)_g$	50.7 s	
Kr_2^+ $II(1/2)_u \rightarrow I(1/2)_g$	2.78 μs	< 68 μs
$\rightarrow I(3/2)_g$	90.2 ms	
Xe_2^+ $II(1/2)_u \rightarrow I(1/2)_g$	0.64 μs	< 85 μs
$\rightarrow I(3/2)_g$	4.19 ms	

[a]Reference 17. Values calculated at the equilibrium distances of Rg_2^+ $[II(1/2)_u]$ (Rg=Ar,Kr,and Xe).

[b]Reference 11.

The radiative lifetimes for the $II(1/2)_u \rightarrow I(1/2)_g$ transitions are more than three orders of magnitude smaller than those for the corresponding $II(1/2)_u \rightarrow I(3/2)_g$ transitions. Namely, the decay of the population in the Rg_2^+ $[II(1/2)_u]$ state is overwhelmingly governed by the transition to the lower $I(1/2)_g$ state. Since the $I(1/2)_g$ states for Rg_2^+ are purely repulsive, Rg_2^+ $[I(1/2)_g]$ formed by process 1(a) is expected to dissociate instantaneously according to process 1(b). Thus, the dissociation lifetime for Rg_2^+ $[II(1/2)_u]$ is solely determined by its radiative lifetime to the $I(1/2)_g$ state. The observation of the Ar_2^+ $[II(1/2)_u]$ PIPECO band is consistent with the longer radiative lifetime for Ar_2^+ $[II(1/2)_u]$ compared to the Ar_2^+ flight time. In the cases of Kr_2^+ and Xe_2^+, the calculated radiative lifetimes for the $II(1/2)_u \rightarrow I(1/2)_g$ transitions are more than 20 times shorter than the flight times of the dimer ions, predicting that the PIPECO

intensities for Kr_2^+ [$II(1/2)_u$] and Xe_2^+ [$II(1/2)_u$] are negligibly small. This prediction is in accord with the experimental findings. This experiment implies that the radiative lifetimes for the $II(1/2)_u \rightarrow I(1/2)_g$ transitions in Ar_2^+, Kr_2^+, and Xe_2^+ are > 47, < 68, and < 85 μs, respectively.

Effect of Cluster Fragmentation on the IE Measurements of Rg_2

It has been pointed out previously by Ng[18] that the IE measurement for a van der Waals dimer should not be affected by dissociative ionization processes of higher clusters. For example, the threshold energy for the dissociative ionization process,

$$Rg_3 + h\nu \rightarrow Rg_2^+ [I(1/2)_u] + Rg(^1S_o) \qquad (2)$$

is expected to be higher than the IE of Rg_2 (i.e., the energy required for process (3)) by the dissociation energy for Rg_2-Rg

$$Rg_2 + h\nu \rightarrow Rg_2^+ [I(1/2)_u]. \qquad (3)$$

The conclusion is based on the assumption that the dissociation energies for Rg_2 and Rg_2-Rg are approximately equal, a valid assumption for van der Waals molecules. As shown in Figs. 6(b) - 6(c), the IE for Xe_2 to Xe_2^+ [$I(1/2)_u$] (1114 $\pm$ 2 Å) determined from the spectra measured at P_o = 300, 400, and 500 Torr are identical, a finding consistent with the above reasoning. Experimental results show that the AEs for the excited Kr_2^+ [$II(1/2)_u$] and Xe_2^+ [$II(1/2)_u$] PIPECO bands are strongly affected by higher cluster fragmentation, shifting them to lower photon energies as the intensities of higher clusters become more significant. To a first approximation, an excited $Rg^+(^2P_{1/2})\cdot Rg_{n-1}$ (n

$\geq$ 3) ion formed by photoionization of Rg_n ($n \geq 3$) may dissociate into product channels such as

$$Rg_n(n \geq 3) + h\nu \rightarrow Rg^+(^2P_{1/2})\cdot Rg_{n-1}$$

$$\rightarrow Rg_2^+ [II(1/2)_u] + Rg_{n-2}, \quad (4)$$

$$\rightarrow Rg_2^+ [I(1/2)_u] + Rg_{n-2}. \quad (5)$$

For the same reasons given above, the threshold for process (4) is expected to be higher than the IE for $Rg_2^+ [II(1/2)_u]$. However, process (5) is energetically allowed as soon as $Rg^+(^2P_{1/2})\cdot Rg_{n-1}$ ($n \geq 3$) is formed. Since the IE for Rg_n to $Rg^+(^2P_{1/2})\cdot Rg_{n-1}$ ($n \geq 3$) decreases as n increases, cluster fragmentation processes such as process (5) have the effect of lowering the AEs for the $Rg_2^+ [II(1/2)_u]$ bands. This expectation is in accord with the experimental observation.

Dissociation Energies of $Rg_2^+ [I(1/2)_u, II(1/2)_u]$

The IEs of 14.518 $\pm$ 0.026 eV (854 $\pm$ 1.5 Å) and 11.130 $\pm$ 0.015 eV (1114 $\pm$ 1.5 Å) for $Kr_2^+ [I(1/2)_u]$ and $Xe_2^+ [I(1/2)_u]$, respectively, determined by the PIPECO measurements are consistent with those obtained from the PIE spectra for Kr_2^+ (Fig. 3(b)) and Xe_2^+ (Fig. 7(b)). These values are also in excellent agreement with those measured in previous PIE studies.[1-4]

As pointed out above, if the calculated lifetimes for the $II(1/2)_u \rightarrow I(1/2)_g$ transitions in Kr_2^+ and Xe_2^+ are accurate, the coincidence intensities for Kr_2^+ and $Xe_2^+ [II(1/2)_u]$ should be negligibly small in the time scale of this experiment. The weak $Kr_2^+ [II(1/2)_u]$

and Xe_2^+ [$II(1/2)_u$] PIPECO bands observed in Figs. 8(b) and 8(c) might be the results of fragmentation of excited $Kr^+(^2P_{1/2})\cdot Kr_{n-1}$ and $Xe^+(^2P_{1/2})\cdot Xe_{n-1}$ ($n > 2$) ions. Judging from the nozzle expansion conditions used in measuring the PIPECO spectra, the formation of Kr_2^+ and Xe_2^+ by fragmentation of excited $Kr^+(^2P_{1/2})\cdot Kr_2$ and $Xe^+(^2P_{1/2})\cdot Xe_2$ produced in the photoionization of Kr_3 and Xe_3 is most likely responsible for the finite intensities observed for the Kr_2^+ [$II(1/2)_u$] and Xe_2^+ [$II(1/2)_u$] PIPECO bands. Assuming that the IEs for the excited $Rg^+(^2P_{1/2})\cdot Rg_{n-1}$ ($n \geq 3$) ions are lower than that for Rg_2^+ [$II(1/2)_u$] and that there are no potential barriers for fragmentation processes such as process (5), we may take the AEs of 14.445 eV (858 Å) and 13.024 eV (952 Å) for the Kr_2^+ [$II(1/2)_u$] and Xe_2^+ [$II(1/2)_u$] PIPECO bands observed in Figs. 8(b) and 8(c), as lower limits for the IEs for Kr_2 and Xe_2 to Kr_2^+ [$II(1/2)_u$] and Xe_2^+ [$II(1/2)_u$], respectively. These values are lower than the IE values of 14.54 eV for Kr_2 to Kr_2^+ [$II(1/2)_u$] and 13.27 eV for Xe_2 to Xe_2^+ [$II(1/2)_u$] reported previously.[7,8] Using the lower limits for the IEs for Kr_2 and Xe_2 to Kr_2^+ [$II(1/2)_u$] and Xe_2^+ [$II(1/2)_u$] and the known dissociation energies for Kr_2 (16 meV)[19] and Xe_2 (23 meV)[20], we have calculated upper limits for the dissociation energies of Kr_2^+ [II(1/2)] and Xe_2^+ [$II(1/2)_u$]. These values and the lower limit for the dissociation energy of Ar_2^+ [$II(1/2)_u$][11] are compared to previous theoretical[14,15] and experimental[7-11] results in Table II. The upper limits for the Kr_2^+ [$II(1/2)_u$] and Xe_2^+ [$II(1/2)_u$] dissociation energies obtained in this study are approximately twice the experimental values[7-10] reported previously.

Table II. Dissociation energies(eV) of Rg_2^+ [$II(1/2)_u$] (Rg = Ar, Kr, and Xe)

	Experiment	Theory
Ar_2^+ $II(1/2)_u$	0.10 ± 0.02[a] > 0.11[c]	0.04[b] 0.084[d]
Kr_2^+ $II(1/2)_u$	0.14 ± 0.02[a] < 0.24[e] 0.11[f]	0.10[b] 0.175[d]
Xe_2^+ $II(1/2)_u$	0.19 ± 0.02[g] < 0.43[e] 0.17[h]	0.12[b] 0.206[d]

[a]Reference 7.

[b]Reference 14.

[c]Reference 11.

[d]Reference 15.

[e]This work.

[f]Reference 9.

[g]Reference 8.

[h]Reference 10.

Comparison of Autoionization Features in the PIPECO and PIE Spectra for Rg_2^+

The ratios of the peak heights of corresponding autoionization peaks resolved in the PIPECO and PIE spectra for Rg_2^+ provide information about the relative efficiencies of autoionizing Rydberg states in producing near-zero kinetic energy electrons. At photon

energies below the IE for $Kr^+(^2P_{3/2})$, five major autoionization peaks at λ = 890, 907, 913, 928, and 941 Å are resolved in the PIPECO and PIE spectra for Kr_2^+. The ratios of the heights of these autoionization peaks observed in the PIPECO spectrum to those of the corresponding peaks resolved in the PIE spectrum are found to increase in the order of increasing λ. This observation indicates that the fraction of autoionizing electrons produced with near-zero kinetic energies decreases as the difference in energy between the autoionization peak and the IE for Kr_2^+ $[I(1/2)_u]$ (964 Å) becomes greater. The higher in energy is the autoionization state above the IE for Kr_2^+ $[I(1/2)_u]$, the wider is the energy distribution of autoionizing electrons. It is logical to expect that the fraction of near-zero kinetic energy electrons produced in autoionization from a higher energy autoionizing state is lower than that from an autoionizing state at a lower energy.

With the exception of minor differences, the autoionization structures resolved in the PIPECO and PIE spectra for Rg_2^+ are similar. This finding can be taken as support for the conclusion that a significant fraction of electrons produced by the autoionizing states are slow electrons with near-zero kinetic energies.

SUMMARY

The PIPECO spectra of Kr_2^+ and Xe_2^+ have been measured in wavelength ranges covering the Kr_2^+ $[II(1/2)_u]$ and Xe_2^+ $[II(1/2)_u]$ photoelectron bands. The Kr_2^+ $[II(1/2)_u]$ and Xe_2^+ $[II(1/2)_u]$ ions are found to have dissociation lifetimes shorter than 68 and 85 μs, respectively. The dissociation of Kr_2^+ $[II(1/2)_u]$ and Xe_2^+ $[II(1/2)_u]$ is rationalized by a radiative decay mechanism which involves radiative transitions of Rg_2^+ $[II(1/2)_u]$ to the repulsive Rg_2^+ $[I(1/2)_g]$ states. The calculated radiative lifetimes for the transitions Rg_2^+ $[II(1/2)_u] \rightarrow Rg_2^+$ $[I(1/2)_g]$ are consistent with this rationalization. The production of Kr_2^+ and Xe_2^+ from fragmentation of excited $Kr^+(^2P_{1/2})\cdot Kr_{n-1}$ and $Xe^+(^2P_{1/2})\cdot Xe_{n-1}$ ions formed in the photoionization of Kr_n and Xe_n ($n \geq 3$) are found to be efficient. These fragmentation processes have the effect of lowering the appearance energies for the Kr_2^+ $[II(1/2)_u]$ and Xe_2^+ $[II(1/2)_u]$ PIPECO bands.

REFERENCES

1. C. Y. Ng, D. J. Trevor, B. H. Mahan, and Y. T. Lee, J. Chem. Phys. 66, 446 (1977).

2. C. Y. Ng, D. J. Trevor, B. H. Mahan, and Y. T. Lee, J. Chem. Phys. 65, 4 (1976).

3. S. T. Pratt and P. M. Dehmer, Chem. Phys. Lett. 87, 533 (1982).

4. P. M. Dehmer and S. T. Pratt, J. Chem. Phys. 75, 5265 (1981).

5. L. Cordis, G. Ganteför, J. Heßlich, and A. Ding, Z. Phys. D3, 323 (1986).

6. R. Abouaf, B. A. Huber, P. C. Cosby, R. P. Saxon, and J. T. Moseley, J. Chem. Phys. 68, 2406 (1978).

7. P. M. Dehmer and J. L. Dehmer, J. Chem. Phys. 68, 3462 (1978).

8. P. M. Dehmer and J. L. Dehmer, J. Chem. Phys. 69, 125 (1978).

9. P. M. Dehmer and S. T. Pratt, J. Chem. Phys. 88, 4139 (1988).

10. P. M. Dehmer, S. T. Pratt, and J. L. Dehmer, J. Phys. Chem. 91, 2593 (1987).

11. K. Norwood, J.-H. Guo, and C. Y. Ng, J. Chem. Phys. 90, 2995 (1989).

12. K. Norwood, J.-H. Guo, G. Luo, and C. Y. Ng, J. Chem. Phys. 88, 4098 (1988).

13. K. Norwood, J.-H. Guo, G. Luo, and C. Y. Ng, Chem. Phys. 129, 109 (1989).

14. W. R. Wadt, J. Chem. Phys. 68, 402 (1978).

15. H. H. Michels, R. H. Hobbs, and L. A. Wright, J. Chem. Phys. 69, 5151 (1978).

16. P. J. Hay and T. H. Dunning, Jr., J. Chem. Phys. 66, 1306 (1977).

17. W. R. Wadt, Deputy Division Leader, Chemical and Laser Sciences, Los Alamos National Laboratory, Los Alamos, New Mexico (private communication).

18. C. Y. Ng, Adv. Chem. Phys. 52, 263 (1983).

19. Y. Tanaka, K. Yoshino, and D. E. Freeman, J. Chem. Phys. 59, 5160 (1973).

20. D. E. Freeman, K. Yoshino, and Y. Tanaka, J. Chem. Phys. 61, 4880 (1974).

SECTION III.

A PHOTOION-PHOTOELECTRON COINCIDENCE STUDY OF $(CO)_2$ AND $(CO)_3$

INTRODUCTION

Equilibrium mass spectrometric studies[1] and molecular beam photoionization efficiency (PIE) measurements[2] provide energetic information about dimer and cluster ions in their ground states. Among all the ionized diatomic and polyatomic van der Waals dimers studied today,[1-3] $(CO)_2^+$ is shown to have the greatest binding energy. Partly due to the strong bonding between CO^+ and CO, $(CO)_2^+$ is an important atmospheric species.[4]

With the exception of rare gas dimer ions, little is known about the excited states of ionized van der Waals dimers. Laser photodissociation techniques have been used to probe the ground as well as excited states of many dimer ions. The photodissociation spectra of dimer ions, such as $(O_2)_2^+$, $(NO)_2^+$, $(N_2)_2^+$, and $(CO_2)_2^+$, at visible wavelengths are found to be broad and featureless,[5-10] an observation consistent with a direct dissociation mechanism involving repulsive excited states. Unlike these dimer ions, $(CO)_2^+$ does not photodissociate at visible wavelengths.[9] Recently, Weisshaar and coworkers[11] have obtained the photodissociation spectrum of $(CO)_2^+$ in the wavelength range of 270-330 nm which exhibits a long progression of vibronic bands, inferring the existence of a bound excited state.

High level quantum chemical calculations on $(CO)_2^+$ [12-14] predict a symmetric, trans planar (C_{2h}) O-C-C-O structure for the ground ($\tilde{X}^2B_u$) state of $(CO)_2^+$. The calculation of Blair et al.[13] shows that the $\tilde{X}^2B_u$ state potential has a well of ~ 60 kcal/mol at a C-C

distance (r_{cc}) of 1.3 Å. The latter calculation also suggests that an excited ^2B_g state, which correlate to the $CO^+(\tilde{A})$ + CO asymptote, is the most plausible candidate responsible for the vibrational progression observed in the near - UV photodissociation spectrum of $(CO)_2^+$. The excited ^2B_g and ^2A_g states of $(CO)_2^+$ are also found to have a C_{2h} symmetry and a potential well at r_{cc} = 1.3-1.4 Å.

Stimulated by the theoretical calculations on $(CO)_2^+$, we have performed a photoion-photoelectron coincidence (PIPECO) experiment on $(CO)_2$ formed in a CO supersonic beam. The primary motivation of this experiment is to obtain energetic and dynamical information about the excited states of $(CO)_2^+$ for the comparison with theoretical predictions. Preliminary results based on the PIPECO spectrum for $(CO)_2^+$ measured at a nozzle stagnation pressure (P_o) of 350 Torr and a nozzle temperature (T) of 120 K have been reported.[15] The finding of the effects due to dissociative photoionization of trimers and higher clusters on the PIPECO spectra for $ArCO^+$,[16] Ar_2^+,[17] Kr_2^+, and Xe_2^+[18] has prompted us to reexamine the PIPECO spectrum for $(CO)_2^+$ as a function of P_o.

EXPERIMENTAL

The experimental arrangement and procedures used in this study has been reported previously.[16,17] Briefly, the apparatus consists of a 3 m near normal incidence vacuum ultraviolet (VUV) monochromator (McPherson 2253M), a supersonic molecular beam production system, a capillary discharge lamp, a VUV light detector, a quadrupole mass spectrometer (QMS) for ion detection, and an electron energy analyzer for threshold electron detection.

The grating employed in this study is a Bausch and Lomb 1200 lines/mm Os coated aluminum grating blazed at 1360 Å. The helium Hopfield continuum is used as the light source. All data are obtained with an optical resolution of 1.5 Å (FWHM).

The CO beam is produced by supersonic expansion of pure CO through a 62 μm nozzle at T = 120 K and a P_o range of 150 - 450 Torr. The CO supersonic jet is collimated into the ionization chamber by a conical skimmer before intersecting at 90° with the dispersed light beam emitted from the exit slit of the VUV monochromator.

A constant electrostatic field of $\lesssim$ 1 V/cm is applied at the photoionization region such that electrons and ions are deflected in opposite direction perpendicular to the molecular beam axis. The electrons and ions are guided toward the electron energy analyzer and the QMS,respectively, by electrostatic lenses. The electron energy analyzer is optimized to transmit threshold electrons produced by photoionization of the CO supersonic beam. The electron energy resolution used is in the range of 50 - 80 meV.

In this coincidence experiment, we use a multichannel scaler (MCS) to measure the ion time-of-flight (TOF) distribution after the triggering by an electronic pulse signifying the arrival of an electron at the electron detector. When the VUV lamp is a continuous light source, such as that used here, the ions which are correlated with the energy-selected electrons appear in a narrow range of channels of the MCS corresponding to the differences in flight times of the correlated electron-ion pairs. The detection of uncorrelated ions will give rise to a uniform background because these ions arrive randomly at the ion detector at a uniform rate.

The PIPECO spectrum of an ion is a plot of the ratio of the electron-ion coincidence intensity to the ionization photon intensity versus photon wavelength. All PIPECO spectra obtained in this experiment are measured using the QMS to select the ion of interest. The QMS is floated at a dc potential of $\sim$ 200 V. Under these conditions, the flight time for $(CO)_2^+$ is 42 μs. At 900 Å, P_o = 350 torr, and T = 120 K, the coincidence counting rate for $(CO)_2^+$ is $\sim$ 8 counts/s.

RESULTS

Figure 1(a) and 1(b) show the coincidence TOF spectra for $(CO)_n^+$ (n = 1 - 5) observed at T = 120 K and P_o = 350 and 200 Torr, respectively. The spectra are measured at 910 Å which corresponds to a photon energy (13.62 eV) below the ionization energy (IE) of CO. The presence of CO^+ at this photon energy is attributed to scattered light arising from imperfections of the grating. At P_o = 350 Torr, the spectrum show that the relative intensities of CO^+, $(CO)_2^+$, $(CO)_3^+$, $(CO)_4^+$, and $(CO)_5^+$ are 0.19:1.00:0.13:0.03:0.01. The TOF peaks for $(CO)_n^+$, n >3, are indiscernible in the spectrum shown in Fig. 1(b), indicating that the concentrations of $(CO)_n$, n > 3, formed in the CO supersonic beam at P_o = 200 Torr are negligible compared to that of $(CO)_2$.

Relative PIEs for $(CO)_n^+$, n = 1 - 5, measured at 900 Å, T = 120 K, and P_o = 150, 200, 350, and 450 Torr are listed in Table I. The PIE values are given in comparison with the PIE for $(CO)_2^+$ measured at P_o = 450 Torr, which is assigned arbitrarily to have a value of 100. Relative PIEs with values (< 0.02) within the noise level are not shown in the table.

Figure 1. PIPECO TOF mass spectra of $(CO)_n^+$ observed at 910 Å and a nozzle temperature of 120 K

(a) P_o = 350 Torr; (b) P_o = 200 Torr

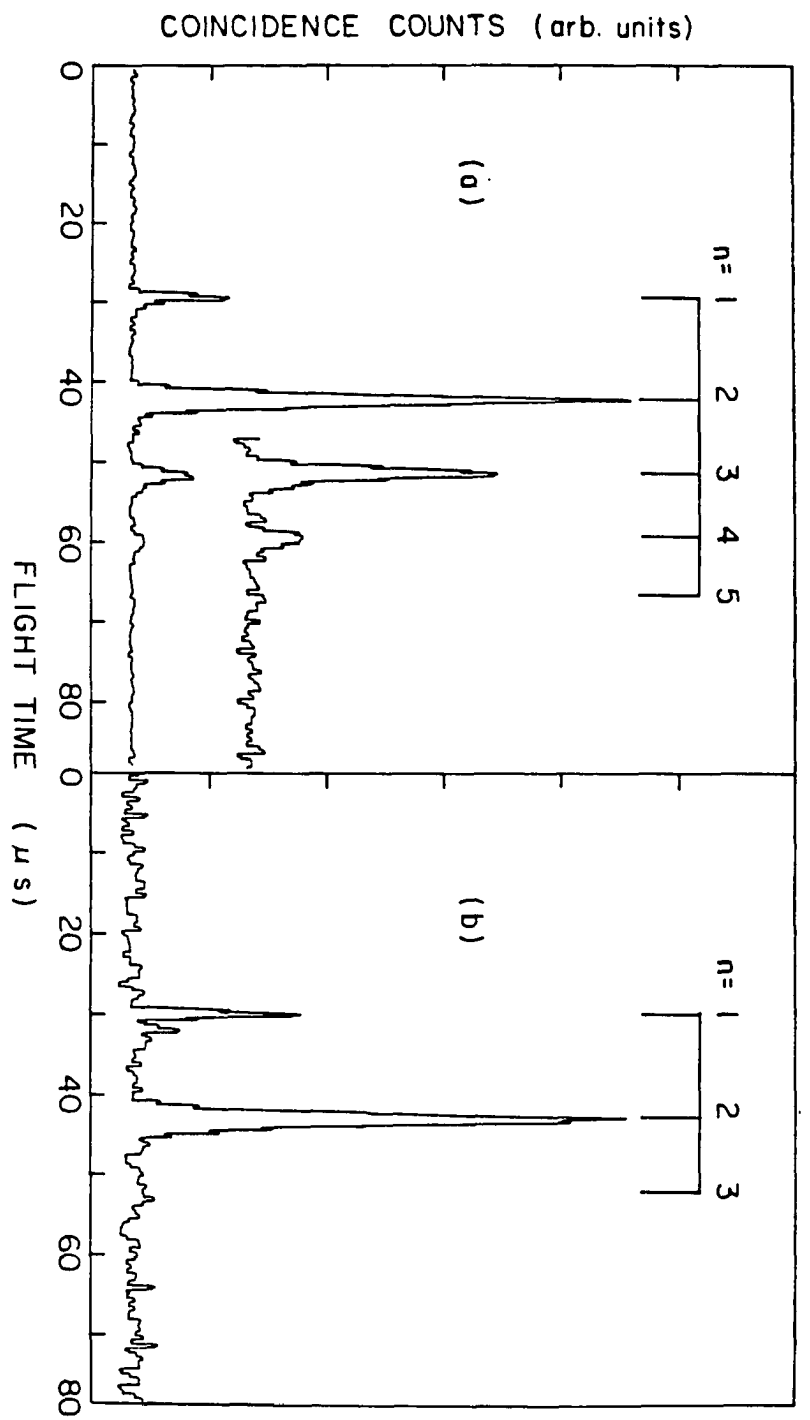
COINCIDENCE COUNTS (arb. units)
(a)
n= 1 2 3 4 5
(b)
n= 1 2 3
0 20 40 60 80
0 20 40 60 80
FLIGHT TIME (μs)

Table I. Relative PIEs for $(CO)_n^+$, n = 1 - 5, measured at 900 Å, T = 120 K and P_o = 150, 200, 350, and 450 Torr

	Relative PIE[a,b]				
P_o (Torr)	CO^+	$(CO)_2^+$	$(CO)_3^+$	$(CO)_4^+$	$(CO)_5^+$
150	8	6	...	...	...
200	9	13	0.1	...	...
350	17	65	2.5	0.3	...
450	28	100	15	3	0.3

[a]PIE for $(CO)_2^+$ measured at P_o = 450 Torr is assigned arbitrarily a value of 100.

[b]Relative PIEs with values (< 0.02) within the noise level are not listed in the table.

Although the relative PIEs for $(CO)_n^+$ measured at P_o = 200 and 350 Torr are different from the relative intensities for $(CO)_n^+$, n = 1 - 5, found in the coincidence TOF spectra, both the PIE and coincidence TOF measurements agree that the intensities for $(CO)_{n>3}^+$ and $(CO)_{n>5}^+$ are not observable at P_o = 200 and 350 Torr, respectively. At P_o = 150 torr, only CO^+ and $(CO)_2^+$ are observed. The ratio of the intensity of $(CO)_2^+$ to that of CO^+ measured at 750 Å is found to decrease from 0.03 at P_o = 450 Torr to 0.004 at P_o = 150 Torr.

The PIPECO spectra for $(CO)_2^+$ in wavelength region of 625 - 990 Å obtained at P_o = 150, 200, and 350 Torr are compared to the PIPECO spectrum for CO^+ in Figs. 2(a) - 2(d). The CO^+ PIPECO spectrum is in general agreement with the HeI photoelectron

Figure 2. PIPECO spectra for $(CO)_2^+$ and $(CO)_3^+$ obtained using a wavelength resolution = 1.5 Å (FWHM) and an electron energy resolution ≈ 80 meV

(a) Comparison of the PIPECO spectrum for $(CO)_3^+$ obtained at P_o = 450 Torr and T = 120 K and that for $(CO)_2^+$ obtained at P_o = 350 Torr and T = 120 K in the wavelength region of 800 - 990 Å; (b) PIPECO spectrum for $(CO)_3^+$ in the wavelength region of 620 - 990 Å

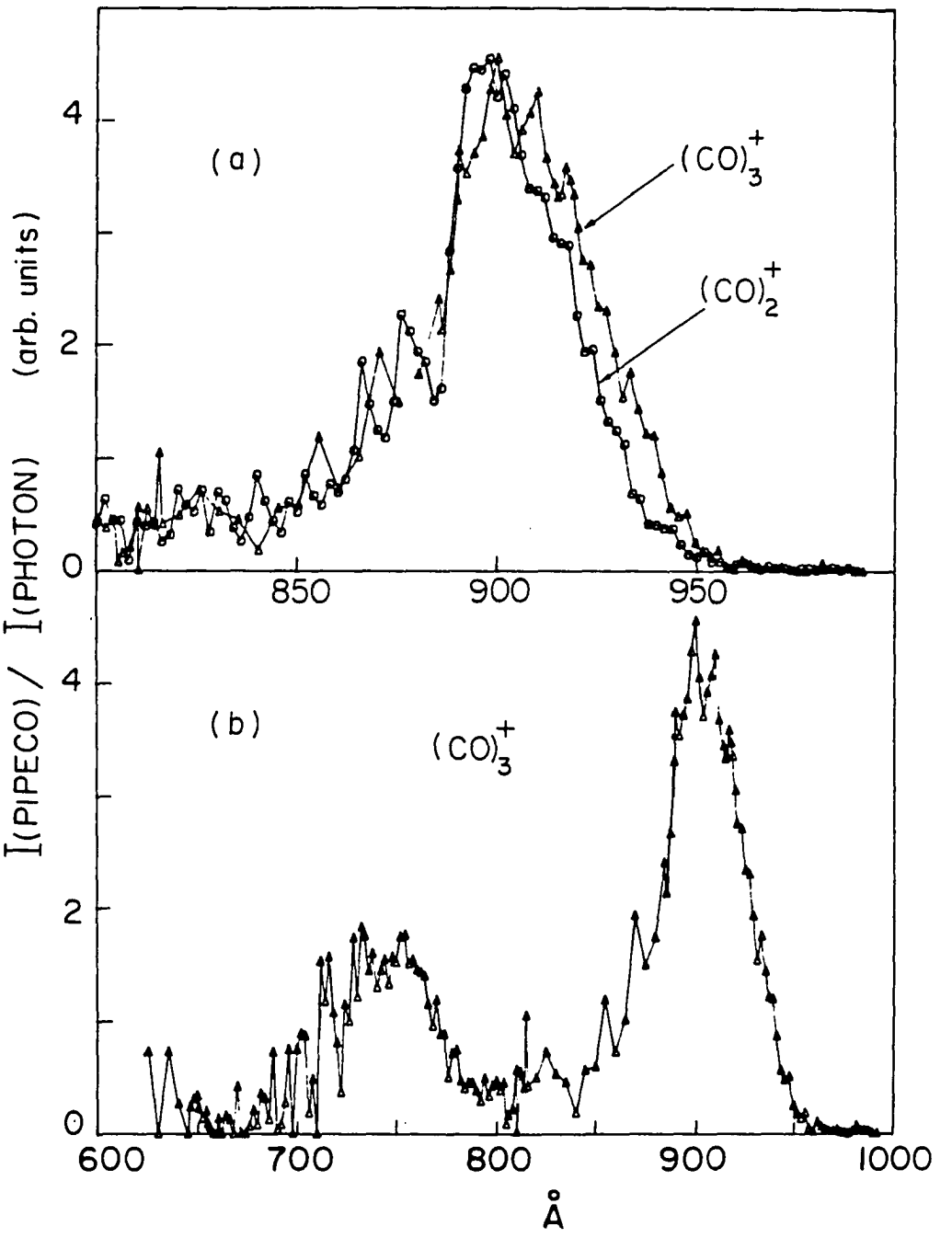
(a)
$(CO)_3^+$
$(CO)_2^+$
(b)
$(CO)_3^+$
I(PIPECO) / I(PHOTON) (arb. units)
0
2
4
850
900
950
600
700
800
900
1000
Å

spectrum (PES) of CO.[19] The three electronic bands resolved in the CO^+ PIPECO spectrum have been assigned to the $\tilde{X}^2\Sigma^+$, $\tilde{A}^2\Pi$, and $\tilde{B}^2\Sigma^+$ states of CO^+. The positions of the vibronic states observed in the HeI PES of CO are indicated by tic marks in Fig. 2(d). Weak vibronic bands attributable to the formation of $CO^+(\tilde{X},v = 3 - 9)$ are also found in the CO^+ PIPECO spectrum. These features arise from autoionization and are not observed in the HeI PES of CO.

The PIE spectra for $(CO)_2^+$ in the wavelength range of 650 - 975 Å measured at P_o = 350, 200, and 150 Torr are depicted in Figs. 3(a), 3(b), and 3(c), respectively. The PIE spectrum for CO^+ in the wavelength range of 700 - 910 Å, which exhibits rich autoionization features, are shown in Fig. 3(d) for comparison.

Figure 4(b) shows the PIPECO spectrum for $(CO)_3^+$ in the wavelength range of 620 - 990 Å obtained at P_o = 450 Torr. At P_o below 450 Torr, the PIPECO intensity for $(CO)_3^+$ becomes too low for the spectrum to be measured. The PIPECO spectrum for $(CO)_3^+$ in the wavelength range of 800 - 990 Å is compared to that for $(CO)_2^+$ measured at P_o = 350 Torr in Fig. 4(a).

Figure 3. PIE spectra for CO^+ and $(CO)_2^+$ obtained using a wavelength resolution = 1.5 Å (FWHM)

(a) PIE spectrum for $(CO)_2^+$ obtained at P_o = 350 Torr and T = 120 K;

(b) PIE spectrum for $(CO)_2^+$ obtained at P_o = 200 Torr and T = 120 K;

(c) PIE spectrum for $(CO)_2^+$ obtained at P_o = 150 Torr and T = 120 K;

(d) PIE spectrum for CO^+ obtained at P_o = 150 Torr and T = 298 K

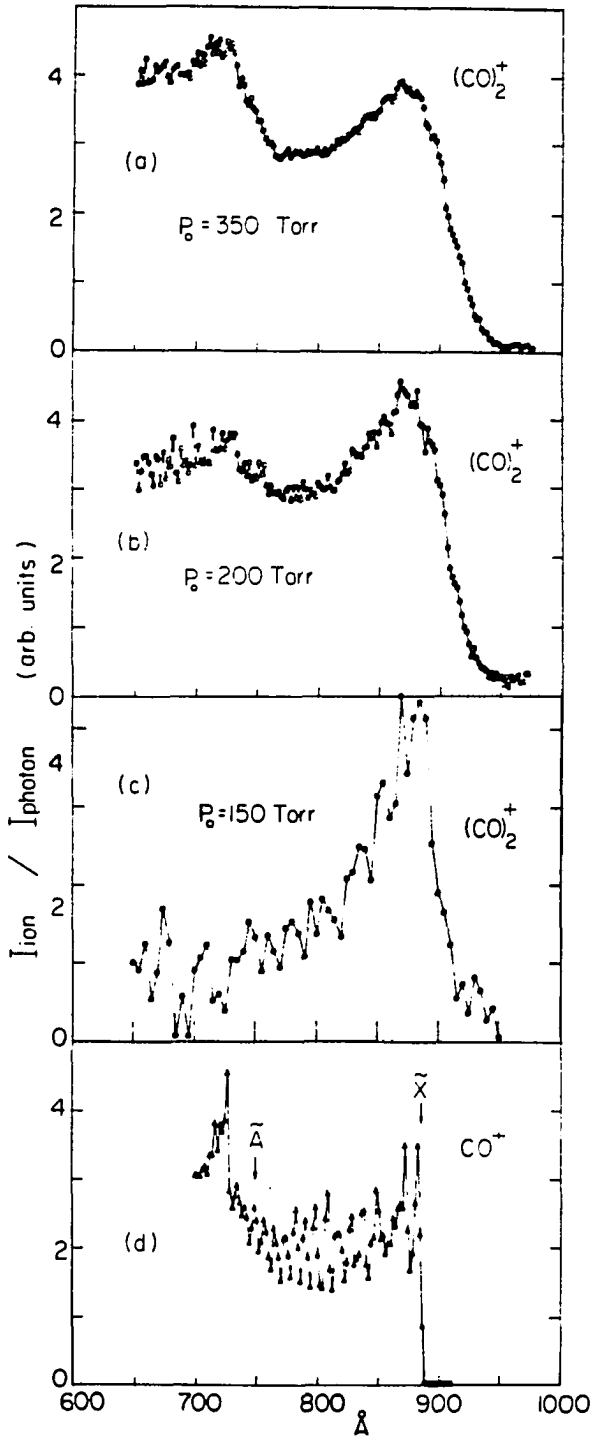
(CO)$_2^+$
(a)
P_o = 350 Torr
(CO)$_2^+$
(b)
P_o = 200 Torr
(c)
P_o = 150 Torr
(CO)$_2^+$
$\tilde{A}$
$\tilde{X}$
CO^+
(d)
I_{ion} / I_{photon} (arb. units)
0
2
4
600
700
800
900
1000
Å

Figure 4. PIPECO spectra for CO^+ and $(CO)_2^+$ obtained using a wavelength resolution = 1.5 Å (FWHM), and an electron energy resolution ≈ 80 meV (FWHM)

(a) PIPECO spectrum for $(CO)_2^+$ obtained at P_o = 150 Torr and T = 120 K; (b) PIPECO spectrum for $(CO)_2^+$ obtained at P_o = 200 Torr and T = 120 K; (c) PIPECO spectrum for $(CO)_2^+$ obtained at P_o = 350 Torr and T = 120 K; (d) PIPECO spectrum for CO^+ obtained at P_o = 150 Torr and T = 298 K

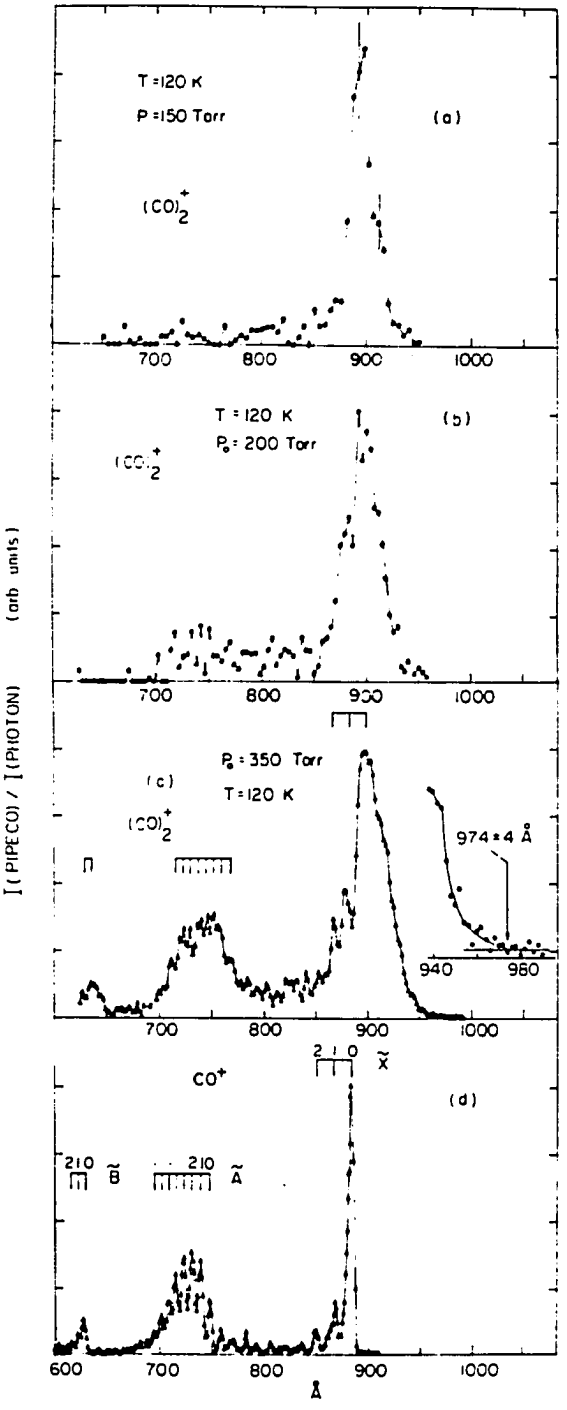
T = 120 K
P = 150 Torr
(a)
$(CO)_2^+$
700
800
900
1000
T = 120 K
P_o = 200 Torr
(b)
$(CO)_2^+$
700
800
900
1000
P_o = 350 Torr
T = 120 K
(c)
$(CO)_2^+$
974 ± 4 Å
940
980
700
800
900
1000
2 1 0 $\tilde{X}$
CO^+
(d)
210 $\tilde{B}$
210 $\tilde{A}$
600
700
800
900
1000
Å
[(PIPECO) / ∫(PHOTON)] (arb units)

DISCUSSION

Dissociation mechanism and lifetimes for electronic Excited $CO^+(\tilde{A},\tilde{B})\cdot CO$ Complexes

Since $(CO)_{n>2}^+$ ions are not observed at P_o = 150 Torr, the PIPECO spectrum shown in Fig. 2(a) may be attributed mainly to the photoionization of $(CO)_2$. The spectrum exhibits a broad band at photon energies below the IE for CO to $CO^+(\tilde{X},v'=0)$. The $(CO)_2^+$ coincidence intensity drops abruptly as the photon energy is increased to the $CO^+(\tilde{X},v=0)$ ionization threshold. The observation is consistent with the interpretation that $(CO)_2^+$ ions formed with internal energies above the $CO^+(\tilde{X},v'=0)$ + CO asymptote are dissociative. The broad PIPECO band can be assigned to the formation of $(CO)_2^+$ in a bonding electronic state arising from the interaction of $CO^+(\tilde{X})$ and CO. The equilibrium intermolecular distance in $(CO)_2$ is expected to be significantly longer than that in $(CO)_2^+$. Thus, the major fraction of $(CO)_2^+$ formed by vertical ionization of $(CO)_2$ may be viewed as $CO^+(\tilde{X})\cdot CO$ which is held together mainly by long-range ion-dipole and ion-induced dipole interactions. The peak of the $CO^+(\tilde{X})\cdot CO$ PIPECO band at 900 Å may be taken as the vertical IE for $(CO)_2$ to $CO^+(\tilde{X},v'=0)\cdot CO$.

In addition to the $CO^+(\tilde{X})\cdot CO$ PIPECO band, we anticipate to find the $CO^+(\tilde{A})\cdot CO$ and $CO^+(\tilde{B})\cdot CO$ PIPECO bands at photon energies below the IEs for CO to $CO^+(\tilde{A},v'=0)$ and $CO^+(\tilde{B},v'=0)$, respectively, provided that the excited dimer ions, $CO^+(\tilde{A},\tilde{B})\cdot CO$, are stable. The $(CO)_2^+$ PIPECO spectrum depicted in Fig. 2(a) shows

that at photon energies above the $CO^+(\tilde{X},v' = 0)$ ionization threshold, the $(CO)_2^+$ PIPECO intensities are negligibly small compared to the intensity of the $CO^+(\tilde{X})\cdot CO$ band. The observation supports the conclusion that $CO^+(\tilde{A},\tilde{B})\cdot CO$ are dissociative in temporal ranges shorter than 42 μs, the flight time of $(CO)_2^+$. The $\tilde{A}$ and $\tilde{B}$ states of CO^+ are radiative states with radiative lifetimes of $\sim$ 4 μs[20,21] and 50 ns,[22] respectively. The excited $CO^+(\tilde{A},\tilde{B})\cdot CO$ dimer ions may be stabilized by radiative decay. Assuming that the radiative lifetimes of $CO^+(\tilde{A},\tilde{B})$ and $CO^+(\tilde{A},\tilde{B})\cdot CO$ are identical, we estimate that the dissociation lifetimes of $CO^+(\tilde{A})\cdot CO$ and $CO^+(\tilde{B})\cdot CO$ are shorter than 4 μs and 50 ns, respectively.

The rapid dissociation of $CO^+(\tilde{A},v' = 0)\cdot CO(X,v = 0)$ may be rationalized by the stepwise mechanism:

(1)

$$CO^+(\tilde{A},v' = 0)\cdot CO(X,v = 0) \xrightarrow{(a)} CO(X,v)\cdot CO^+(\tilde{X},v') \xrightarrow{(c)} CO^+(\tilde{X},v') + CO(X,v).$$

$$CO^+(\tilde{A},v' = 0)\cdot CO(X,v = 0) \xrightarrow{(b)} CO^+(\tilde{X},v')\cdot CO(X,v = 0) \xrightarrow{(c)} CO^+(\tilde{X},v') + CO(X,v).$$

Step 1(a) involves a near-resonance intramolecular charge transfer to produce a highly vibrationally excited complex, $CO(X,v)\cdot CO^+(\tilde{X},v')$. The $\tilde{A}$ state is 2.5 eV above the $\tilde{X}$ state and the vibrationally quanta for $CO^+(\tilde{X})$ and CO(X) are $\sim$ 0.27 eV.[19] The sum of v' and v for $CO(X,v)\cdot CO^+(\tilde{X},v')$ formed by Step 1(a) should be $\lesssim$ 9. Vibrationally excited dimer ions $CO^+(\tilde{X},v' \sim 9)\cdot CO(X,v = 0)$, which are in close energy resonance with $CO^+(\tilde{A},v' = 0)\cdot CO(X,v = 0)$, may result from the intramolecular quenching

process 1(b). The fact that the vibrational quantum of $CO^+(\tilde{X})$ is only slightly higher than that for CO(X) may facilitate the conversion of $CO^+(\tilde{X},v')\cdot CO(X,v = 0)$ into $CO(X,v)\cdot CO^+(\tilde{X},v')$ via near-resonance intramolecular charge transfer processes. The vibrationally excited complexes, $CO(X,v)\cdot CO^+(\tilde{X},v')$ and $CO^+(\tilde{X},v' \sim 9)\cdot CO(X,v = 0)$, are expected to fall apart rapidly via vibrational predissociation processes 1(c) because their internal energy contents are greater than the dissociation energy of $CO^+(\tilde{X},v' = 0)\cdot CO(X,v = 0)$. The vibrational predissociation lifetimes for dimer ions such as $CO(X,v)\cdot CO^+(\tilde{X},v')$ are predicted to be shorter than 10^{-9} s.[23] The dissociation mechanism for $CO^+(\tilde{B},v' = 0)\cdot CO(X,v = 0)$ is likely to be more complicated than that for $CO^+(\tilde{A},v' = 0)\cdot CO(X,v = 0)$. However, a scheme similar to that summarized by processes 2(a)-2(c) may be devised to account for the rapid dissociation of $CO^+(\tilde{B},v' = 0)\cdot CO(X,v = 0)$.

Formation of Stable $(CO)_2^+$ From Fragmentation of Electronic and Vibrationally Excited CO Cluster Ions

The $(CO)_2^+$ PIPECO spectrum measured at P_o = 200 Torr (Fig. 2(b)) reveals the $CO^+(\tilde{X})\cdot CO$ band as well as a weak band centered at ~ 750 Å. The intensity of the weak band in the wavelength region of ~ 700 - 790 Å relative to that of the $CO^+(\tilde{X})\cdot CO$ band observed at P_o = 350 Torr (Fig. 2(c)) is higher than that found in Fig. 2(b). A third PIPECO band peaked at 637 Å also becomes evident in Fig. 2(c). The appearance of the second and third bands in the $(CO)_2^+$ PIPECO spectra measured at P_o = 200 and

350 Torr is consistent with the observation that the PIE spectrum in the wavelength region < 850 Å shown in Fig. 3(c) is lower than that in Fig. 3(b) which is in turn lower than that in Fig. 3(a). It is interesting to note that the relative intensities of the three PIPECO bands observed in the $(CO)_2^+$ spectrum shown in Fig. 2(c) are similar to those of the $CO^+(\tilde{X},\tilde{A},\tilde{B})$ bands found in the CO^+ PIPECO spectrum. The second and third bands, peaked at 750 and 637 Å, respectively, necessarily arise from fragmentation of higher CO cluster ions. Based on the coincidence TOF spectrum observed at 350 Torr, it is logical to conclude that $(CO)_2^+$ ions detected at the second and third bands observed in the $(CO)_2^+$ PIPECO spectrum of Fig. 2(c) are predominantly produced by fragmentation of $CO^+(\tilde{A}$ or $\tilde{B},v')\cdot(CO)_{n-1}$ initially formed by photoionization of $(CO)_n$, n = 3 - 5. Rapid intramolecular charge transfer and quenching processes followed by ejection of vibrationally excited CO molecules can be a very effective mechanism in disposing the excess internal energy of an excited CO cluster ion. For example, a stable $CO^+(\tilde{X},v' = 0)\cdot CO(X,v = 0)$ dimer may be formed by the decomposition of a $CO^+(\tilde{A},v')\cdot(CO)_3$ ion via the stepwise charge transfer mechanism:

$$\text{(a)} \qquad\qquad (2)$$

$$CO^+(\tilde{A},v')\cdot(CO)_3 \rightarrow CO(X,v)\cdot CO^+(\tilde{X},v')\cdot(CO)_2$$

$$\text{(b)}$$

$$\rightarrow CO(X,v) + CO^+(\tilde{X},v')\cdot(CO)_2,$$

$$CO^+(\tilde{X},v')\cdot(CO)_2 \xrightarrow{(a)} CO(X,v)\cdot CO^+(\tilde{X},v' = 0)\cdot CO \qquad (3)$$

$$\xrightarrow{(b)} CO(X,v) + CO^+(\tilde{X},v' = 0)\cdot CO.$$

Steps 2(a) and 2(b) are similar to Steps 1(a) and 1(c). If $CO^+(\tilde{X},v')\cdot(CO)_2$ produced in Step 2(b) is unstable, it may further eject a vibrationally excited CO(X,v) molecule to form a stable $CO^+(\tilde{X},v' = 0)\cdot CO(X,v = 0)$ dimer ion by similar processes as summarized in Steps 3(a) and 3(b). The conversion of $CO^+(\tilde{X},v')\cdot(CO)_2$ to $CO(X,v)\cdot CO^+(\tilde{X},v' = 0)\cdot CO$ by a near-resonance charge transfer process should be highly efficient. The formation of $CO^+(\tilde{X},v' = 0)\cdot CO(X,v = 0)$ from the unimolecular decomposition of $CO^+(\tilde{B},v')\cdot(CO)_3$ may also be rationalized by using a scheme similar to that shown in processes (2) and (3).

The $(CO)_2^+$ PIPECO intensities observed at P_o = 200 Torr and 350 Torr in the wavelength region between the $CO^+(\tilde{X},v' = 0)$ ionization threshold and the second PIPECO band may be attributed to fragmentation of vibrationally excited cluster ions, $CO^+(\tilde{X},v' > 0)\cdot(CO)_n$, n = 2 - 4. The formation of stable $CO^+(\tilde{X},v' = 0)\cdot CO(X,v = 0)$ from $CO^+(\tilde{X},v' > 0)\cdot(CO)_n$, n = 2 - 4, may follow processes 3(a) and 3(b).

Dissociation Energies For $CO^+(\tilde{X},\tilde{A},\tilde{B})\cdot CO$

The threshold energy for dissociative photoionization processes involving $(CO)_{n>3}$ clusters, such as

$$(CO)_3 + h\nu \rightarrow (CO)_2^+ + CO, \quad (4)$$

is expected to be higher than the IE of $(CO)_2$ (i.e., energy required for process (5)) by the dissociation energy of $(CO)_2$-CO

$$(CO)_2 + h\nu \rightarrow (CO)_2^+. \quad (5)$$

This conclusion is based on the assumption that the dissociation energies for $(CO)_2$ and $(CO)_2$-CO are approximately equal, a valid assumption for van der Waals molecules. Thus, the determination of the IE for $CO^+(\tilde{X},v' = 0)\cdot CO$ by PIE and PIPECO measurements should not be affected by fragmentation of higher CO cluster ions.[2]

As pointed out previously, the Franck-Condon factors for direct ionization near the adiabatic IE of a van der Waals dimer such as $(CO)_2$ are poor. If ionization only involves direct ionization, it is likely that appearance energies (AE) for $(CO)_2^+$ observed in the $(CO)_2^+$ PIE and PIPECO spectra represent upper limits for the adiabatic IE of $(CO)_2$. Since tunable VUV radiation is used in the PIE and PIPECO measurements described here, both direct ionization and autoionization are probed. To a first approximation, autoionization of a dimer in an excited Rydberg state may be viewed as an associative ionization process.[2] Autoionization has the effect of enhancing the dimer ion yield near the IE of the van der Waals dimer. The ability of PIE and PIPECO measurements to observe the true adiabatic IEs of the rare gas dimers is mostly due to

autoionization processes.[17,18,24,25] The curvature of the ground state potential curve of a van der Waals dimer with respect to variation of the intermolecular distance is expected to be small. The diffuseness of the vibrational ground state wavefunction of a neutral van der Waals dimer may provide finite overlap between the neutral and ion ground vibrational state wavefunctions and allow the observation of the true adiabatic IE. The dissociation energies for many ionized van der Waals dimers calculated using the IEs determined by PIE measurements are in agreement with values obtained by equilibrium mass spectrometric studies, indicating that PIE and PIPECO measurements are capable of providing accurate IEs for van der Waals dimers.[2,3] The ability to observe the true adiabatic IE certainly depends on the sensitivity of the photoionization experiment.

The large uncertainties of $(CO)_2^+$ PIPECO data measured at P_o = 200 and 150 Torr account for part of the differences of the first $(CO)_2^+$ PIPECO bands in the wavelength region of ~ 850 - 990 Å shown in Figs. 2(a), 2(b), and 2(c). The PIE spectrum for $(CO)_2^+$ observed at P_o = 150 Torr (Fig. 3(c)) reveals autoionization features in close resemblance with those found in the CO^+ PIE spectrum (Fig. 3(d)), showing that $(CO)_2^+$ are formed efficiently by autoionization of $(CO)_2$ in high Rydberg states. Considering the fact that only the $CO^+(\tilde{X})\cdot CO$ PIPECO band is observed at P_o = 150 Torr, we conclude that $(CO)_2^+$ ions observed in the PIE spectrum of Fig. 3(c) are all in the ground $CO^+(\tilde{X})\cdot CO$ states. Steplike features are discernible near the onset of the first PIPECO band of the $(CO)_2^+$ PIPECO spectrum shown in Fig. 2(c). The resolution of the electron energy analyzer used in this experiment is probably insufficient to resolve the vibrational structure for $(CO)_2^+$. The steplike features found near the onset of the first PIPECO

band in the wavelength region of ~ 900 - 975 Å most likely arise from autoionization.

The AE of 12.73 ± 0.05 eV (974 ± 4 Å) for $(CO)_2^+$ determined by the $(CO)_2^+$ PIPECO spectrum in Fig. 2(c) may be taken as an upper bound for the adiabatic IE of $(CO)_2$. This value is lower by 0.32 eV compared to the AE for $(CO)_2^+$ obtained in previous PIE measurement.[26] We find that the PIPECO technique is more sensitive than photoion and photoelectron measurements in determining IE because background ionization events due to scattered light are greatly reduced in coincidence studies. Using the IE for $CO^+(\tilde{X},v' = 0)$,[19] the AE of 12.73 ± 0.05 eV for $(CO)_2^+$, and the estimated binding energy for $(CO)_2$,[27] we calculate a lower limit of 29.8 ± 1.0 kcal/mol for the dissociation energy of $CO^+(\tilde{X},v' = 0)\cdot CO(X,v = 0)$. The latter value is consistent with the estimates of > 21.2[28] and 26 ± 7 kcal/mol[29] for the dissociation energy of $(CO)_2^+$ determined by equilibrium mass spectrometric studies. The lower limit of 29.8 ± 1.0 kcal/mol determined in this experiment is a factor of 2 lower than the theoretical value of ~ 60 kcal/mol obtained by the ab initio calculation of Blair et al.[13] The structures for $(CO)_2^+$ and $(CO)_2$ are probably different. The estimated equilibrium intermolecular distance of ~ 3.5 Å[30] for $(CO)_2$ is substantially greater than the calculated equilibrium r_{cc} distance of 1.3 Å for $(CO)_2^+$ in the ground $\tilde{X}^2B_u$ state. Based on the Franck-Condon consideration the production of $(CO)_2^+$ near the adiabatic IE of $(CO)_2$ should be highly inefficient. It appears that the formation of $(CO)_2^+$ by autoionization at photon energies below the IE for $CO^+(\tilde{X},v' = 0)$ is also inefficient. The weakness of autoionization processes is probably due to the strong competition of neutral predissociation channels.

The sensitivity of this experiment may not allow the observation of the true adiabatic IE of $(CO)_2$.

In the recent PIPECO study of rare gas dimers,[18] we have shown that fragmentation of electronically excited cluster ions has the effect of lowering the AEs for electronically excited PIPECO bands for the dimer ions. The AEs of the second and third $(CO)_2^+$ PIPECO bands observed at P_o = 350 Torr are determined to be 15.79 eV (785 Å) and 18.99 eV (653 Å), respectively. These values can be taken as upper limits for the IEs for $CO^+(\tilde{A})\cdot(CO)_n$ and $CO^+(\tilde{B})\cdot(CO)_n$, n = 4, because CO cluster ions heavier than $(CO)_5^+$ are not observed at P_o = 350 Torr. Assuming that the dissociation energies of $(CO)_2$ and $(CO)_n$-CO, n = 2 - 4 , are identical, we estimate that the binding energies for $CO^+(\tilde{A})\cdot(CO)_4$ and $CO^+(\tilde{B})\cdot(CO)_4$ are > 17.5 and 17.0 kcal/mol with respect to the dissociation limits, $CO^+(\tilde{A})$ + 4CO and $CO^+(\tilde{B})$ + 4CO, respectively. Previous measurements on the energetics of ionized van der Waals clusters[2,3] shows that the stabilization of a cluster ion such as $(CO)_5^+$ is dominated by the dimeric interaction between CO^+ and a CO in the cluster. The observation of a bound CO cluster ion strongly supports the conclusion that $CO^+(\tilde{A})\cdot CO$ and $CO^+(\tilde{B})\cdot CO$ are bound.

The $CO^+(\tilde{A}^2\Pi)$ and $CO^+(\tilde{B}^2\Sigma^+)$ states correspond to the removal of an electron from the π2p and σ2s orbitals, respectively. Based on a simple molecular orbital picture, sigma bonding can be formed between the half filled π2p orbital of $CO^+(\tilde{A}^2\Pi)$ and that of CO, if $CO^+(\tilde{A})\cdot CO$ has a rectangular geometry. The calculation at the self-consistent-field level on the isoelectronic $(N_2)_2^+$ system[31] indicates that a $^2B_{2u}$ state for the rectangular shape $(N_2)_2^+$ ion, which dissociates into $N_2^+(\tilde{A})$ + N_2, is bound by 1.56

eV. Similarly, a linear configuration for $CO^+(\tilde{B})\cdot CO$ is expected to be bound by half of a sigma bond. This expectation is consistent with experimental evidence obtained in this study which supports the view that $CO^+(\tilde{A},\tilde{B})\cdot CO$ are bound. The ^2B_g and ^2A_g excited potential energy surfaces for $(CO)_2^+$ in a constrained C_{2h} geometry calculated by Blair et al.[13,14] exhibit local minima at r_{cc} = 1.3 - 1.4 Å. These local minima are at energies above the $CO^+(\tilde{A})$ + CO asymptote. Based on the Franck-Condon consideration, it is unlikely that the experiment can sample these potential wells. The calculation shows that as r_{cc} increases from 1.3 Å, the ^2B_g potential surface rises to a barrier at $r_{cc} \sim$ 1.7 Å and descends repulsively in the r_{cc} range of 1.7 - 2.8 Å. Potential energies for the ^2B_g state at $r_{cc} >$ 2.8 Å are not reported. The result of this experiment is in favor of a potential well between $r_{cc} \sim$ 1.7 Å and the $CO^+(\tilde{A})$ + CO dissociation limit.

Model for the Photoionization of a van der Waals Cluster

The widths of the three $(CO)_2^+$ PIPECO electronic bands observed at P_o = 350 Torr are greater than the respective $CO^+(\tilde{X},\tilde{A},\tilde{B})$ bands. The broadening is mostly the result of the broad Franck-Condon profile of ionization transitions between vibrational levels of the neutral van der Waals CO dimer and CO dimer ion states. It is interesting to note that vibronic structures similar to those resolved in the CO^+ PIPECO spectrum are discernible in the $(CO)_2^+$ PIPECO spectrum shown in Fig. 2(c) except that the vibronic structures in the $(CO)_2^+$ spectrum are red-shifted with respect to the corresponding structures in the CO^+ spectrum. This, together with the finding that the relative

intensities of the $(CO)_2^+$ PIPECO electronic bands observed in Fig. 2(c) and those of the $CO^+(\tilde{X},\tilde{A},\tilde{B})$ PIPECO bands are essentially identical, supports the perturbed monomer ion model for the photoionization of a van der Waals cluster. Namely, the formation of $CO^+\cdot(CO)_{n-1}$ by photoionization of $(CO)_n$, $n > 2$ can be considered as a photoionization process of CO perturbed by the presence of other CO molecules in the clusters. This model is consistent with the results of the PIPECO study on N_2 clusters.[32] Previous studies on the stability of ionized van der Waals clusters show that the interaction energy of the dimer ion constitutes overwhelmingly the stabilization energy of a cluster ion. These results have led Haberland[33] to suggest that a rare gas cluster ion $(Rg)_n^+$ should be viewed as $(Rg)_2^+\cdot R_{n-2}$, $n > 2$. The vertical IE of the first PIPECO band (900 Å) remains nearly the same as P_o is increased from 150 to 350 Torr, suggesting that the $CO^+(\tilde{X})$ in $CO^+(\tilde{X})\cdot(CO)_{n-1}$ initially formed by photoionization of $(CO)_n$, $n = 2 - 5$ mostly experiences the influence of the $CO^+(\tilde{X})\cdot CO$ dimer ion potential. Table II compares the vertical IEs for CO and those for $(CO)_n$, $2 < n < 5$ determined by the PIPECO spectrum shown in Fig. 2(c). The differences between the vertical IEs of CO to $CO^+(\tilde{X},\tilde{A},\tilde{B})$ and the corresponding vertical IEs for $(CO)_n$ to $CO^+(\tilde{X},\tilde{A},\tilde{B})$ are in the range of 0.23 - 0.31 eV. Assuming the validity of the model proposed here for the photoionization of a van der Waals cluster, we estimated that the dissociation energies for $CO^+(\tilde{A})\cdot CO$ and $CO^+(\tilde{B})\cdot CO$ are greater than 0.39 and 0.31 eV, respectively.

Table II. Comparison of the vertical IEs of CO to $CO^+(\tilde{X},\tilde{A},\tilde{B}, v' = 0)$ and $(CO)_n$ to $CO^+(\tilde{X},\tilde{A},\tilde{B}, v' = 0)\cdot(CO)_{n-1}$, $2 \leq n \leq 5$

State	Vertical IE (eV)		ΔE (eV)[c]
	CO^+ [a]	$CO^+\cdot(CO)_n$ $(2 \leq n \leq 5)$[b]	
$\tilde{X}^2\Sigma^+, v' = 0$	14.01	13.78	0.23
$\tilde{A}^2\Pi, v' = 0$	16.55	16.16	0.39
$\tilde{B}^2\Sigma^+, v' = 0$	19.71	19.40	0.31

[a]References 19 and 34.

[b]Values determined by the PIPECO spectrum shown in Fig. 2(c).

[c]Differences of the vertical IEs for CO to $CO^+(\tilde{X},\tilde{A},\tilde{B}, v' = 0)$ and $(CO)_n$ to $CO^+(\tilde{X},\tilde{A},\tilde{B}, v' = 0)\cdot(CO)_{n-1}$, $2 \leq n \leq 5$.

PIPECO Spectrum for $(CO)_3^+$

The PIPECO spectrum for $(CO)_3^+$ shown in Fig. 4(b) closely resembles that for $(CO)_2^+$ measured at $P_o = 350$ Torr. The corresponding PIE spectrum for $(CO)_3^+$, which is not shown here, is also found to be nearly identical to that depicted in Fig. 3(b). It is most likely that the second and third $(CO)_3^+$ PIPECO bands are due to fragmentation of higher cluster ions $(CO)_n^+$, $n > 3$. The comparison of the PIPECO spectrum for $(CO)_3^+$ and that for $(CO)_2^+$ measured at $P_o = 350$ Torr in Fig. 4(a) reveals that the width of the first PIPECO band for $(CO)_3^+$ is slightly greater than that for $(CO)_2^+$. The second $(CO)_3^+$ band centered at $\sim$ 750 Å also seems to be slightly broader than the second $(CO)_2^+$ bands shown in Fig. 3(b). Nevertheless, the peak positions of the first and

second PIPECO bands for $(CO)_2^+$ and $(CO)_3^+$ are essentially identical. Furthermore, the relative intensities for the three PIPECO bands for $(CO)_3^+$ agrees with those for $(CO)_2^+$ of Fig. 3(b). These observations can be taken as additional support for the model for the photoionization of a van der Waals cluster.

CONCLUSIONS

The PIPECO spectrum for $(CO)_2^+$ has been examined as a function of P_o. The formation of $(CO)_2^+$ from fragmentation of higher excited cluster ions $CO^+(\tilde{A},\tilde{B})\cdot(CO)_{n-1}$ initially produced by photoionization of $(CO)_n$, $n > 3$ are found to be efficient. The experiment provides evidence that the dissociation lifetimes for $CO^+(\tilde{A})\cdot CO$ and $CO^+(\tilde{B})\cdot CO$ are $\lesssim 4\ \mu s$ and $\lesssim 50$ ns, respectively. Using the upper limit of 12.73 ± 0.05 eV for the IE of $(CO)_2$ determined by the$(CO)_2^+$ PIPECO spectrum, the dissociation energy for $CO^+(\tilde{X})\cdot CO$ is estimated to be $\gtrsim 1.29$ eV. The PIPECO spectrum for $(CO)_2^+$ observed at $P_o = 350$ Torr also suggests that $CO^+(\tilde{A},\tilde{B})\cdot CO$ are bound. The comparison of the PIPECO spectrum for $(CO)_3^+$ and those for $(CO)_2^+$ measured at different P_o indicates that the formation of $CO^+\cdot(CO)_{n-1}$ from the photoionization of $(CO)_n$ can be considered as a perturbed monomer photoionization process and that CO^+ in $CO^+\cdot(CO)_{n-1}$, $n > 2$ initially formed by photoionization mostly experiences the influence of the $CO^+\cdot CO$ dimer ion potential.

REFERENCES

1. P. Kebarle, Ann. Rev. Phys. Chem. 28, 445 (1977).

2. C. Y. Ng, Adv. Chem. Phys. 52, 263 (1983).

3. T. D. Märk and A. W. Castleman, Adv. At. Mol. Phys. 20, 65 (1985).

4. E. E. Ferguson, in "Kinetics of Ion-Molecule Reactions", Ed. by P. Ausloos (Plenum Press, New York, 1979).

5. J. T. Moseley, R. P. Saxon, B. A. Huber, P. C. Cosby, R. Abouaf, and M.Tadjeddine, J. Chem. Phys. 67, 1659 (1977).

6. R. Abouaf, B. A. Huber, P. C. Cosby, R. P. Saxon, and J. T. Moseley, J. Chem. Phys. 68, 2406 (1978).

7. J. A. Vanderhoff, J. Chem. Phys. 67, 2332 (1977).

8. G. P. Smith, P. C. Cosby, and J. T. Moseley, J. Chem. Phys. 67, 3818 (1977).

9. G. P. Smith and L. C. Lee, J. Chem. Phys. 69, 5393 (1978).

10. J. P. Flamme, T. Mark, and J. Los, Chem. Phys. Lett. 75, 419 (1980).

11. S. C. Ostrander, L. A. Sanders, and J. C. Weisshaar, J. Chem. Phys. 84, 529 (1986).

12. L. B. Knight, J. Steadman, P. K. Miller, D. E. Bowman, E. R. Davidson, and D. Feller, J. Chem. Phys. 80, 4593 (1984).

13. J. T. Blair, J. C. Weisshaar, J. E. Carpenter, and F. Weinhold, J. Chem. Phys. 87, 392 (1987).

14. J. T. Blair, J. C. Weisshaar, and F. Weinhold, J. Chem. Phys. 88, 1467 (1988).

15. K. Norwood, J.-H. Guo, G. Luo, and C. Y. Ng, J. Chem. Phys. 88, 4098 (1988).

16. K. Norwood, J.-H. Guo, G. Luo, and C. Y. Ng, Chem. Phys. 129, 109 (1989).

17. K. Norwood, J.-H. Guo, and C. Y. Ng, J. Chem. Phys. 90, 2995 (1989).

18. K. Norwood, G. Luo, and C. Y. Ng, J. Chem. Phys., 90, 4689 (1989).

19. D. W. Turner, C. Baker, A. D. Baker, and C. R. Brundle, "Molecular Photoelectron Spectroscopy" (Wiley, New York, 1970).

20. J. Danon, G. Mauclaire, T. R. Govers, and R. Marx, J. Chem. Phys. 76, 1255 (1982).

21. V. E. Bondybey and T. A. Miller, J. Chem. Phys. 69, 3597 (1978).

22. M. Bloch and D. W. Turner, Chem. Phys. Lett. 30, 344 (1975).

23. E. E. Ferguson, J. Phys. Chem. 90, 731 (1986).

24. C. Y. Ng, D. J. Trevor, B. H. Mahan, and Y. T. Lee, J. Chem. Phys. 66, 446 (1977); 65, 4327 (1976).

25. P. M. Dehmer and S. T. Pratt, J. Chem. Phys. 76, 843 (1982); 75, 5265 (1981); P. M. Dehmer, J. Chem. Phys. 76, 1263 (1982).

26. S. H. Linn, Y. Ono, and C. Y. Ng, J. Chem. Phys. 74, 3342 (1981).

27. J. O. Hirschfelder, C. P. Curtiss, and R. B. Bird, "Molecular Theory of Gases and Liquids" (Wiley, New York, 1964), p. 111.

28. M. Meot-Ner and F. H. Field, J. Chem. Phys. 61, 3742 (1974).

29. S. L. Chong and J. L. Franklin, J. Chem. Phys. 54, 1487 (1971).

30. R. M. Berns and A. van der Avoird, J. Chem. Phys. 72, 6107 (1980).

31. S. C. deCastro and H. F. Schaefer, and R. M. Pitzer, J. Chem. Phys. 74, 550 (1981).

32. K. Norwood, G. Luo, and C. Y. Ng, J. Chem. Phys. 91, 849 (1989).

33. H. Haberland, Surface Sciences 156, 305 (1985).

34. A. Katrib, T. P. Debies, R. J. Cotton, T. H. Lee, and J. W. Rabalais, Chem. Phys. Lett. 22, 196 (1973).

SECTION IV.

A STUDY OF INTRAMOLECULAR CHARGE TRANSFER IN MIXED Ar/CO DIMER AND TRIMER IONS USING THE PHOTOION-PHOTOELECTRON COINCIDENCE METHOD

INTRODUCTION

A "superexcited" state in general represents a state with energy well above that of the ground state such that it may readily decay into various product channels by dissociation and/or radiation. In this sense, superexcited states of a dimer ion such as $ArCO^+$ can be formed by the interactions of $Ar^+(^2P_{3/2,1/2}) + CO$, $CO^+(\tilde{A}) + Ar$, and $CO^+(\tilde{B}) + Ar$. To a first approximation, the ion-neutral complexes, $CO^+(\tilde{X})\cdot Ar$, $Ar^+(^2P_{3/2,1/2})\cdot CO$, $CO^+(\tilde{A})\cdot Ar$, and $CO^+(\tilde{B})\cdot Ar$, can be prepared by the photoionization of van der Waals $Ar\cdot CO$ dimers formed in a supersonic expansion,[1]

$$Ar\cdot CO + h\nu \rightarrow CO^+(\tilde{X})\cdot Ar + e^-, \quad (1)$$

$$\rightarrow Ar^+(^2P_{3/2,1/2})\cdot CO + e^-, \quad (2)$$

$$\rightarrow CO^+(\tilde{A},\tilde{B})\cdot Ar + e^-. \quad (3)$$

Since the excited ion-neutral complexes, $Ar^+(^2P_{3/2,1/2})\cdot CO$ and $CO^+(\tilde{A},\tilde{B})\cdot Ar$, are in energy levels substantially higher than the $Ar + CO^+(\tilde{X},v' = 0)$ asymptote, they may eventually decompose to give $Ar + CO^+(\tilde{X},v')$ via a stepwise mechanism involving intramolecular charge transfer and vibrational predissociation. In the time scale ($> 10^{-5}$ sec) of a mass spectrometry experiment, the $CO^+(\tilde{A},\tilde{B})\cdot Ar$ may also be stabilized by a radiative process.

It has been shown in previous molecular beam photoionization experiments[1] that the studies of the unimolecular decomposition processes of energized ion-neutral complexes, also referred to as ion-neutral half collision processes, provide valuable energetic and

dynamical information for specific ion-molecule reactions which is difficult to measure by other means. The information obtainable from such studies includes binding energies of ion-neutral reaction complexes, upper limits of reaction barriers, and relative reactivities of excited reactant ion states.[2-7] Nevertheless, dimer ions formed by photoionization often have an unknown distribution of internal energy. In such cases, information concerning the relative reactivities of excited reactant ion states in a half reaction cannot be obtained solely from photoionization efficiency (PIE) measurements. A more ideal experimental approach is to incorporate a state or energy selection method into the molecular beam photoionization experiment such that the dissociation of ion-neutral complexes in well defined internal states can be examined.

The photoion-photoelectron coincidence (PIPECO) techniques, which utilize the flight time correlation of an ion-electron pair, have been used extensively in the study of the dissociation dynamics of state or energy-selected molecular ions.[8-12] The application of the PIPECO method to dimers and clusters has been hindered by a sensitivity problem partly due to the low concentrations of dimers and clusters formed in a supersonic beam. As a result of the high false coincidence rate stemmed from the overwhelming monomer photoelectron signal at photon energies above the IE of the monomer, PIPECO studies of electronically excited dimer and cluster ions have not been carried out previously. The PIPECO spectra for Kr_2^+, Xe_2^+, and Xe_3^+ at photon energies below the IEs of the corresponding atoms have been reported.[13,14] Recently, we have overcome some of the experimental difficulties and obtained the PIPECO spectra for $(CO)_2^+$ and $(CO)_3^+$ over a wavelength region covering the $\tilde{X}^2\Sigma^+$, $\tilde{A}^2\Pi$, and $\tilde{B}^2\Sigma^+$ electronic bands of CO^+.[15]

The Ar^+ + CO charge transfer reaction at low collision energies has been investigated extensively using flow tube,[16] ion cyclotron resonance,[17,18] laser-induced fluorescence (LIF),[19-21] and threshold electron-secondary ion coincidence techniques.[22] The LIF experiments of Leone and co-workers[19,20] show that at near thermal energies all accessible vibrational states, v = 0 - 7, of product $CO^+(\tilde{X})$ are populated and the vibrational distribution is peaked at v = 5. The observed wide distribution of $CO^+(\tilde{X})$ vibrational states and the small rate constants measured in the flow tube experiment[16] suggest that the Ar^+ + CO charge transfer reaction may take place at relatively short distances via a bent configuration. At collision energies below 1 eV, the rate constant increases as the collision energy decreases,[16] an observation supporting a mechanism which involves the formation of a long-lived $CO^+ \cdot Ar$ complex. Recently, state-to-state inelastic and charge transfer cross sections for collisions of $Ar^+(^2P_{3/2,1/2})$ + CO at a collision energy of 2 eV have been calculated by the vibronic semiclassical method.[23-25] The theoretical study reveals that the vibrational distribution of product CO^+ appears to represent a compromise between energy resonance and Franck-Condon factors. The inclusion of the $CO^+(\tilde{A})$ state in the calculation is shown to be important. Hoping to learn about the interaction energies and the dissociation mechanisms of the $CO^+(\tilde{X}) \cdot Ar$, $Ar^+(^2P_{3/2,1/2}) \cdot CO$, and $CO^+(\tilde{A},\tilde{B}) \cdot Ar$ ion-neutral complexes, we have performed a PIPECO study on ArCO and mixed Ar/CO trimers. The ArCO van der Waals dimer has a near T-shape geometry.[26,27] Therefore, a near T-shape $Ar^+(^2P_{3/2,1/2}) \cdot CO$ ion-neutral complex, resembling a collisional complex formed in a side-on attack, can be formed by process (2). The study of the unimolecular decomposition of $Ar^+(^2P_{3/2,1/2}) \cdot CO$ is expected

to shed light on the collision complex mechanism for the $Ar^+ + CO$ charge transfer reaction.

EXPERIMENTAL

A brief description of the experimental arrangement and procedures used in this study has been reported.[15] The PIPECO apparatus is modified from the molecular beam photoionization apparatus which has been described in detail previously.[28,29] Figure 1 shows a cross-sectional view of the differential pumping arrangement of the molecular beam production system, photoionization region, quadrupole mass spectrometer (QMS), and photoelectron energy analyzer.

The ArCO molecules are prepared by supersonic expansion of the premixed Ar and CO gases through a 62 μm diameter nozzle (1) with a nozzle stagnation pressure (P_o) in the range of 76 - 350 Torr. The nozzle is cooled by cold N_2 gas and kept at temperature (T) of 120 $\pm$ 3 K throughout the experiment. The mixing ratio of Ar to CO is approximately 3. The high-intensity central portion of the supersonic jet is collimated into the ionization chamber by a conical skimmer (2) before intersecting at 90° with the dispersed vacuum ultraviolet (VUV) light beam emitted from the exit slit of the VUV monochromator (McPherson Model 2253M). The wavelength resolution used in this study is 1.5 Å (FWHM). The beam source chamber is evacuated by a 10 in. water-baffled diffusion pump (DP) and maintained a pressure of $< 2 \times 10^{-4}$ Torr, while the ionization chamber is pumped by a liquid nitrogen (LN_2)-trapped 10 in. DP and has a pressure of $< 2 \times 10^{-6}$ Torr. In order to minimize secondary reactions involving primary photoions, it is necessary to have the differential pumping arrangement.

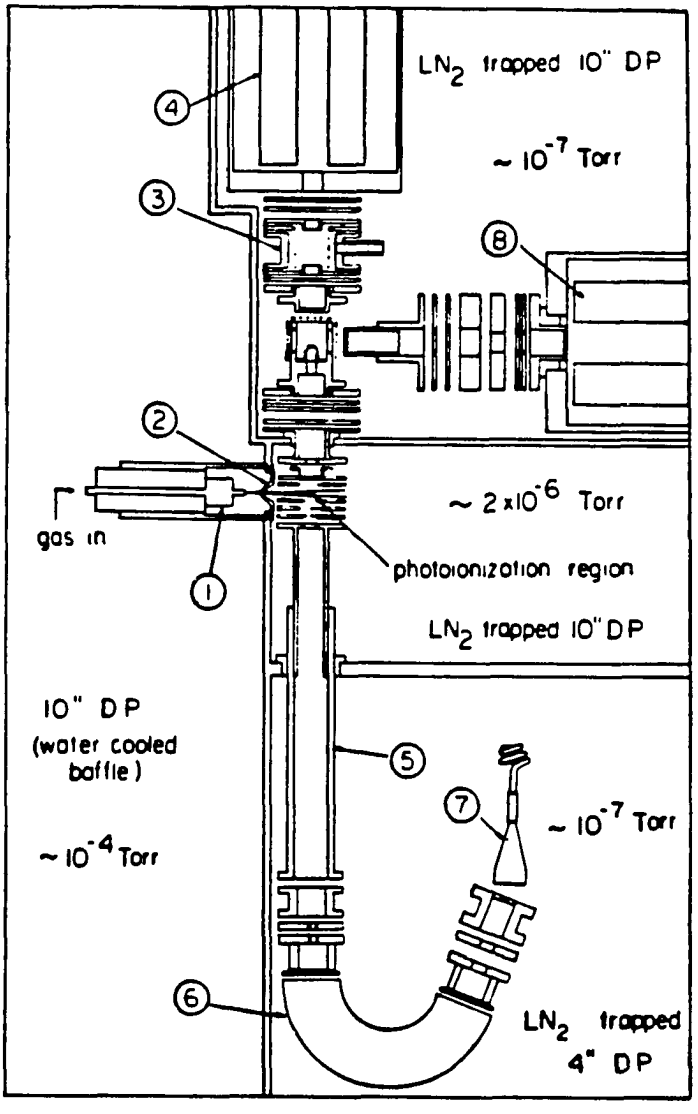

Figure 1. Cross-sectional view of the molecular beam PIPECO apparatus

(1) nozzle; (2) skimmer; (3) reaction cell; (4) vertical QMS; (5) steradiancy analyzer; (6) spherical sector electron energy analyzer (Comstock model AC-901); (7) channeltron electron detector; (8) horizontal QMS

A constant electrostatic field of ≈ 1 V/cm is applied at the photoionization region such that electrons and ions are deflected in opposite directions perpendicular to the molecular beam axis. The electrons and ions are guided towards the electron energy analyzer and the vertical QMS (4), respectively, by electrostatic lenses.

The electron energy analyzer, optimized for threshold photoelectron detection, consists of a steradiancy analyzer[12,30-32] and a spherical sector energy analyzer (Comstock Model AC-901) (6) arranged in series.[33] The electrons are detected by a channeltron electron multiplier in the pulse counting mode. In a conventional steradiancy analyzer, a long tube is connected directly to the repeller plate at the photoionization region. Thus, the long tube has the function of a drift tube which discriminates hot electrons moving in directions out of the solid angle sustained by the long tube. In this experiment, the potentials of the long tube (5) and the simple aperture lenses above and below the tube are optimized to transmit preferentially near zero kinetic energy photoelectrons. Although the potential of the long tube differs substantially from that of the repeller plate, the assembly behaves like a steradiancy analyzer. The spherical sector energy analyzer is used to cut out the hot photoelectrons ejected in the direction along the axis of the steradiancy analyzer. The electron energy analyzer is housed in a chamber maintained at a pressure of ≈ 2 x 10^{-7} Torr by a 4 in. LN_2-trapped DP. To minimize the patch contact potential effects, a thin graphite coating is applied to the inner surfaces of the long tube and spherical sector energy analyzer. The electron energy resolution can be affected by the earth and local stray magnetic field. By shielding the electron detector chamber with two layers of sheet μ-metal, the magnetic field inside the chamber is reduced to ≈ 40

milligauss. As expected, the electron energy resolution achieved depends strongly on the repeller field applied at the photoionization region. For a 1 V/cm repeller field used in this experiment, the electron energy resolution is measured to be ≈ 50 meV (FWHM). At this resolution, the threshold electron transmission of the electron energy analyzer is estimated to be ≈ 1%. The ions formed at the photoionization region pass through the collision chamber before entering the vertical QMS chamber. The collision chamber is maintained at a pressure of ≈ 5 x 10-7 Torr by a freon-trapped 10 in DP. The reactivity of photoions with neutral reactants can be investigated in the collision chamber using either the reaction gas cell (3) or a crossed ion-neutral beam arrangement. The horizontal QMS (8) is not used in the present experiment.

The vertical and horizontal QMS chambers are connected and pumped by a 4 in. LN_2-trapped DP. The pressure in the QMS chambers is kept at ≈ 2 x 10^{-8} Torr during the experiment. Due to the relatively small repeller field used at the photoionization region, the ion transmission achieved is ≈ 0.3.

One of the most common coincidence circuits uses a time-to-pulse- height converter (TAC) together with a multichannel analyzer (MCA) operated in the pulse height analysis mode.[12] Since the flight time for the electron is much shorter than that of the ion, the electronic pulse signifying the detection of an electron is used to start a voltage ramp in the TAC. The ion pulse produced by the arrival of an ion at the ion detector immediately followed the electron pulse, serves to stop the voltage ramp. After the completion of the start-stop cycle, a pulse with a height proportional to the time interval between the detections of the electron and ion is generated by the TAC and stored in the

proper channel of the MCA. When the VUV lamp is a continuous light source such as that used in our experiment, the ions which are correlated with the energy-selected electrons will appear in a narrow range of channels in the MCA corresponding to the differences in flight times of the correlated electron-ion pairs. The detection of uncorrelated ions will give rise to a uniform background because these ions arrive randomly at the ion detector at a uniform rate. The TAC arrangement is suitable for experiments with low counting rates because only one ion is detected for one start signal. As a result of false coincidences due to uncorrelated ions, the probability of observing a true coincidence after an electron start pulse is an exponentially decreasing function of time.[34] Therefore, at high count rates, the TAC circuitry is paralyzed and artificially suppress the true coincidence rate. When a TOF mass spectrometer is used in conjunction with the TAC coincidence arrangement, the paralyzed effect is to decrease signals for high mass ions which have longer flight times from the photoionization region to the ion detector. Figure 2 shows a PIPECO TOF spectrum for N_2^+ observed at the ionization threshold of N_2 (792 Å) using the TAC arrangement. At the N_2^+ ion counting rate $\approx$ 1 x 10^5 counts/s, the paralyzed effect is clearly evident. The paralyzed effect is expected to be less serious for dimer and cluster ions because the photoionization rates for dimer and cluster ions ($\leq 10^4$ ions/s) are considerably lower than that for the monomer ion. However, due to the relatively long ion flight times, we find that the PIPECO spectrum of a dimer ion at photon energies higher than the IE of the monomer obtained with the single electron start-single ion stop circuit is still strongly affected by the paralyzed effect.

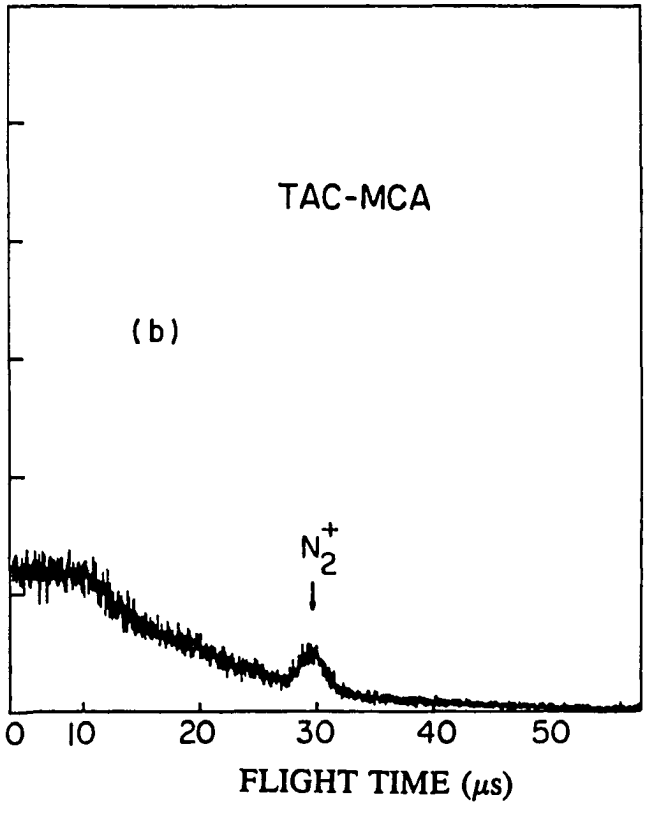

Figure 2. PIPECO TOF spectrum for N_2^+ observed at the ionization threshold of N_2^+ (792 Å) using the TAC arrangement

The timing logic used in this experiment for taking PIPECO TOF spectra is shown in Fig. 3. The electronic pulse generated by the arrival of an electron at the channeltron detector is used to trigger a multichannel scalar (MCS) which measures the TOF distribution of ions arriving at the ion detector. The active time period (τ_o) of the MCS must be longer than the flight times of the ions of interest. During the active time period of the MCS, the coincidence circuit will not accept other electron pulses. To avoid the suppression of coincidence signal at a high electron counting rate, τ_o should be shorter than the average time interval between two adjacent electron pulses which is equal to the inverse of the electron counting rate. The lower panel of Fig. 3 compares the hypothetical PIPECO TOF spectra of an ion obtained by the TAC and MCS arrangement. The false coincidence background signal observed using the MCS mode is constant over the period τ_o, while that found in the TAC mode is expected to be an exponentially decay function in time. The figure emphasizes that the true coincidence signal, represented by the net area under the ion TOF peak and above the background, is lower in the TAC mode compared to that in the MCS mode.

Fig. 4 shows a PIPECO TOF spectrum observed at 895 Å in the photoionization of an Ar/CO molecular beam at $P_o \approx 150$ Torr using the MCS arrangement. The spectrum was obtained when the QMS was operated as a radio frequency ion guide such that all ions were transmitted to the ion detector. The photon energy (13.85 eV) corresponding to 895 Å is below the IEs of CO (14.014 eV).[35] The formation of CO^+ is believed to be caused mostly by scattered light. Two minor peaks attributable to O_2^+ and Ar^+ are also discernible in the spectrum. The spectrum reveals that the intensities for

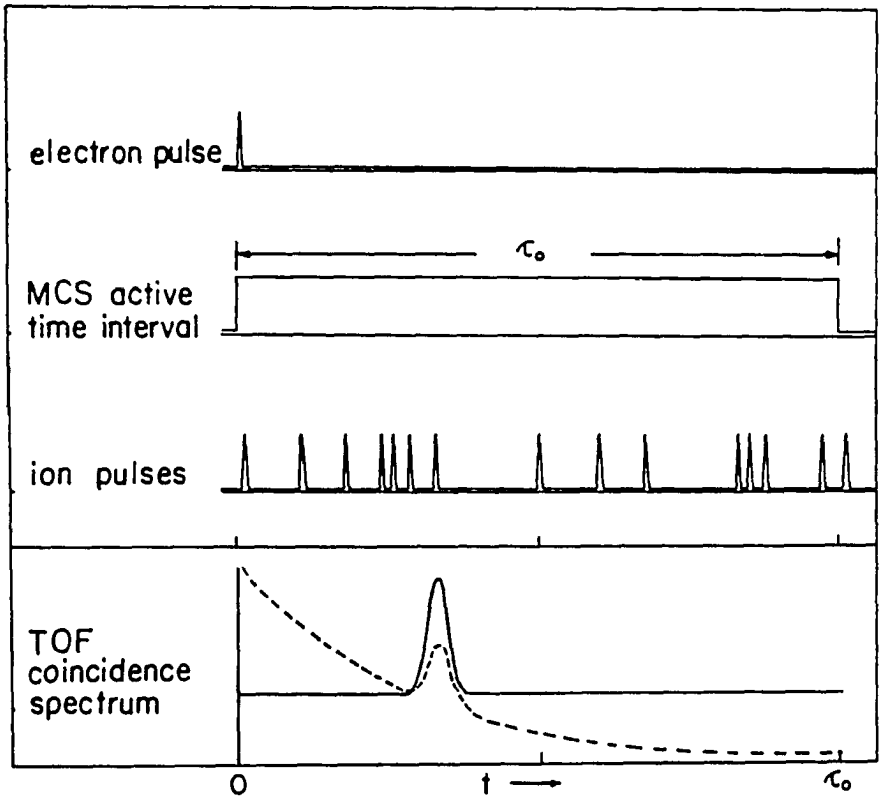

Figure 3. Timing logic of the MCS coincidence circuit

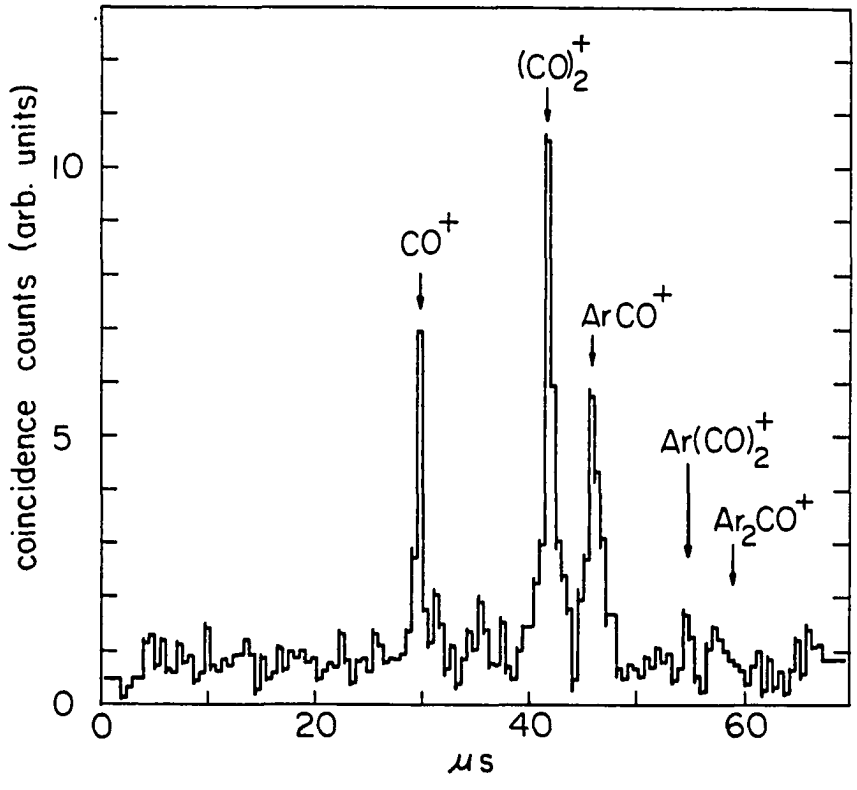

Figure 4. Coincidence TOF spectrum observed at 890 Å (P_o = 160 Torr, T = 120 K)

$(CO)_2^+$ and $ArCO^+$ dimer ions are substantially higher than those for higher cluster ions. With the exception of $Ar(CO)_2^+$, the intensities for other cluster ions are found to be within the noise level. Since the IEs for Ar dimer and cluster ions lie at higher photon energies, they are not observed in this spectrum. The difference in flight time of the correlated e^--$ArCO^+$ pair is $\approx$ 46 μs.

A PIPECO spectrum of an ion is a plot of the ratio of the measured coincidence intensity of an ion to the ionization photon intensity versus photon wavelength. The PIPECO spectra presented in this report were recorded by using the QMS to select a given ion mass.

RESULTS AND DISCUSSION

Figure 5(d) shows the PIPECO spectra for CO^+ and Ar^+ observed in the wavelength region of 610 - 910 Å. The CO molecule has the molecular orbital configuration $1\sigma^2\ 2\sigma^2\ 3\sigma^2\ 4\sigma^2\ 1\pi^4\ 5\sigma^2$.[36,37] The three electronic bands resolved in the CO^+ spectrum have been assigned to the $\tilde{X}^2\Sigma^+$, $\tilde{A}^2\Pi$, and $\tilde{B}^2\Sigma^+$ states of CO^+,[38] which arise from the removal of an electron from the 5σ, 1π, and 4σ orbital, respectively. In addition to the vibronic states observed in the HeI photoelectron spectrum (PES) of CO,[37] which are indicated by tic marks in Fig. 5(d), vibrational peaks corresponding to the formation of $CO^+(\tilde{X},v' = 3 - 7)$ via autoionization are also discernible in the PIPECO spectrum for CO^+. Two peaks due to formation of $Ar^+(^2P_{3/2})$ and $Ar^+(^2P_{1/2})$ states are found in the Ar^+ spectrum.

The PIPECO spectra for $ArCO^+$ in the wavelength region of 620 - 940 Å obtained at P_o = 92, 138, and 214 Torr are depicted in Figs. 5(a), 5(b), and 5(c), respectively, to compare with the CO^+ and Ar^+ spectra. The relative intensities of the two electronic bands observed in the $ArCO^+$ coincidence spectra are shown to depend strongly on P_o. This observation suggests that the formation of $ArCO^+$ from fragmentation of higher mixed Ar/CO cluster ions is significant at higher P_o. The $ArCO^+$ coincidence signal observed at P_o = 214 Torr is more than 8 times greater than that at P_o = 92 Torr.

Using the nozzle expansion conditions in this experiment, the $Ar(CO)_2^+$ and Ar_2CO^+ ions are found to be the major cluster species which may decompose to give $ArCO^+$. As shown in Fig. 4, the intensity of $Ar(CO)_2^+$ is higher than that of Ar_2CO^+ at lower P_o.

Figure 5. PIPECO spectrum for $ArCO^+$ in the wavelength region of 620 - 940 Å (a) P_o = 92 Torr and T = 120 K; (b) P_o = 138 Torr and T = 120 K; (c) P_o = 214 Torr, T = 120 K, and (*) is the vibrational distribution for charge transfer product $CO^+(\tilde{X},v')$ obtained from ref. 20; (d) PIPECO spectra for CO^+ and Ar^+ in the wavelength region of 610 - 910 Å

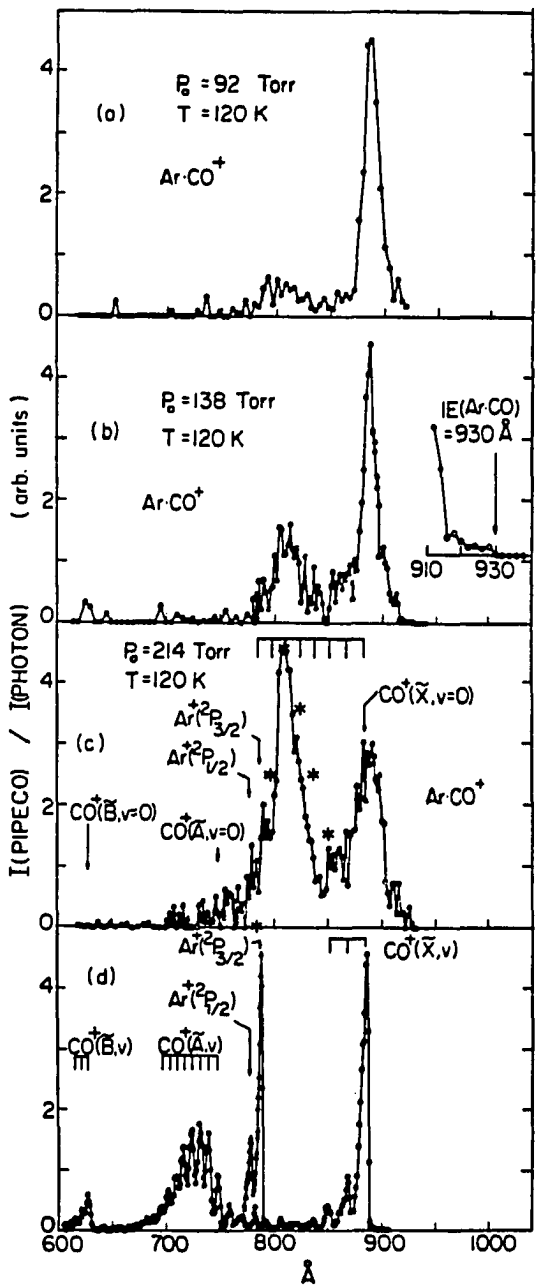
(a)
P₀ = 92 Torr
T = 120 K
Ar·CO⁺
(b)
P₀ = 138 Torr
T = 120 K
Ar·CO⁺
IE(Ar·CO) = 930 Å
910
930
(c)
P₀ = 214 Torr
T = 120 K
Ar⁺(²P3/2)
Ar⁺(²P1/2)
CO⁺(X̃,v=0)
CO⁺(B̃,v=0)
CO⁺(Ã,v=0)
Ar·CO⁺
(d)
Ar⁺(²P3/2)
Ar⁺(²P1/2)
CO⁺(X̃,v)
CO⁺(B̃,v)
CO⁺(Ã,v)
I(PIPECO) / I(PHOTON) (arb. units)
600
700
800
900
1000
Å

The mass spectrum obtained at 890 Å and P_o = 92 torr indicates that the sum of the intensities for $Ar(CO)_2^+$ and Ar_2CO^+ is ≈ 4% that of $ArCO^+$. At P_o = 214 torr, the sum, which has nearly equal contributions from $Ar(CO)_2^+$ and Ar_2CO^+ increases to ≈ 20% that of $ArCO^+$.

The first $ArCO^+$ coincidence electronic band in the wavelength region of ≈ 850 - 940 Å can be associated with the $CO^+(\tilde{X})\cdot Ar$ ground state. The width of the band observed at P_o =214 Torr is greater than those found at P_o = 92 and 138 Torr. This is likely the result of fragmentation of higher cluster ions formed at P_o = 214 Torr. The structures of the first $ArCO^+$ electronic band shown in the spectra in Figs. 5(a) and 5(b) are similar. The greater apparent width for the first band in Fig. 5(a) compared to that in Fig. 5(b) is due to the larger wavelength intervals (4 Å) used in recording the spectrum at P_o = 92 Torr. Since the intensities for $Ar(CO)_2^+$ and Ar_2CO^+ are substantially smaller than that for $ArCO^+$ at P_o = 92 Torr, the first bands of Figs. 5(a) and 5(b) can be attributed to process (1).

According to the ab initio quantum calculations,[36,39] the 5σ orbital of CO is essentially an s-like lone pair orbital localized at the carbon atom. Stemming from the nonbonding nature of the 5σ orbital, the equilibrium distance for $CO^+(\tilde{X})$ (1.115 Å) differs only slightly from that of CO(X) (1.128 Å).[40] Thus, the $CO(X,v = 0) \rightarrow CO^+(\tilde{X},v' = 0)$ Franck-Condon transition is strongly favored in photoionization as manifested by the overwhelming $CO^+(\tilde{X},v' = 0)$ photoelectron peak in the PES of CO. Upon ionization of an electron from the 5σ orbital, the resulting $CO^+(\tilde{X})$ ion has a positive charge mainly associated with the carbon atom. Therefore, the most stable geometry for $CO^+(\tilde{X})\cdot Ar$ is

likely to be linear with Ar attached to the carbon end in CO^+. The theoretical[26] and infrared absorption[27] studies show that the van der Waals ArCO molecule has a near T-shape configuration with Ar leaned slightly closer to the oxygen atom. The distance between Ar and the center-of-mass of CO is predicted to be $\approx$ 3.77 Å.[26] The near T-shape configuration is in accordance with the expectation that Ar and CO are mainly held together by long range dispersion forces. Since the most stable geometries for ArCO and $CO^+(\tilde{X})\cdot Ar$ are anticipated to be quite different, the Franck-Condon factor for process (1) near the threshold should be poor. The observation of the steep decline in the $ArCO^+$ intensity from the vertical IE at 888 Å toward the ionization threshold in Figs. 5(a) and 5(b) is consistent with this conclusion. The $CO^+(\tilde{X})\cdot Ar$ coincidence intensity near the ionization threshold is more than 150 times lower than that at 888 Å. The vertical IE for $CO^+(\tilde{X})\cdot Ar$ is only red shifted by $\approx$ 0.06 eV with respect to the IE (884 Å) for $CO^+(\tilde{X},v' = 0)$. The sharp drop in $CO^+(\tilde{X})\cdot Ar$ coincidence intensity at 884 Å is found to coincide with the IE of $CO^+(\tilde{X},v' = 0)$, indicating that $CO^+(\tilde{X},v' > 0)\cdot Ar$ is dissociative when formed at energies higher than the $Ar + CO^+(\tilde{X},v' = 0)$ asymptote.

It has been pointed out by Ng[1] that the appearance energies for the dissociative photoionization processes of higher van der Waals clusters such as

$$Ar(CO)_2 \text{ (or } Ar_2CO) + h\nu \rightarrow CO^+(\tilde{X})\cdot Ar + CO \text{ (or Ar)} + e^- \qquad (4)$$

should be higher than the ionization threshold of process (1), i.e., the IE for $CO^+(\tilde{X})\cdot Ar$. Therefore, the IE measurement for $CO^+(\tilde{X})\cdot Ar$ should not be affected by the fragmentation of higher cluster ions initially formed by photoionization. This expectation is confirmed by the finding that the values for the IE for $CO^+(\tilde{X})\cdot Ar$ determined in the

spectra measured at P_o = 138 and 214 torr (Figs. 5(b) and 5(c)) are identical. The value of 13.33 ± 0.06 eV (930 ± 4 Å) for the adiabatic IE for $CO^+(\tilde{X})\cdot Ar$ obtained by the PIPECO measurements is in excellent agreement with that determined from the PIE spectra of $ArCO^+$ recorded at P_o = 76 and 280 torr (Figs. 6(a) and 6(b)). Using the IEs for $CO^+(\tilde{X})\cdot Ar$ and $CO^+(\tilde{X})$ and the estimated binding energy (0.017 eV)[26] for Ar·CO, we calculate a value of 0.70 ± 0.06 eV for the dissociation energy of $CO^+(\tilde{X})\cdot Ar$. This value is substantially lower than the dissociation energies for Ar_2^+ (1.33 eV)[41] and $(CO)_2^+$ (> 1.29 eV).[15] Recently, Gislason[42] has performed an ab initio calculation on the $[Ar\cdot CO]^+$ system using a method similar to that of Archirel and Levy.[43] Their calculation predicts a value of 0.82 eV for the binding energy of $CO^+(\tilde{X})\cdot Ar$ in the linear Ar-C-O structure. This value is slightly higher than the experimental value reported here.

An ab initio investigation of $CO^+\cdot N_2$ has also been reported recently by Baker and Buckingham.[44] The fact that the IEs of N_2 and Ar are nearly the same makes the comparison of the bonding in $CO^+\cdot Ar$ and $CO^+\cdot N_2$ interesting. The most stable structure for $CO^+\cdot N_2$ is predicted to have a C_s symmetry with the carbon atom of CO^+ attached to a nitrogen atom along the N-N bond direction and an NCO angle of ≈ 135°. The theoretical study gives a binding energy between CO^+ and N_2 of 0.97 eV, a value approximately 30% higher than that for $CO^+(\tilde{X})\cdot Ar$ determined in this experiment. Surprisingly, the calculation shows that most of the binding between N_2 and CO^+ can be accounted for by the long range electrostatic and induction energies and there is little evidence for the formation of an incipient "chemical bond". The strong long range

Figure 6. PIE spectra for CO^+, Ar_2^+, and $ArCO^+$

(a) PIE curve for $ArCO^+$ in the wavelength region of 600 - 950 Å obtained at P_o = 280 Torr and T = 120 K; (b) PIE curve for $ArCO^+$ in the wavelength region of 625 - 950 Å obtained at P_o = 76 Torr and T = 120 K; (c) PIE curve for Ar_2^+ in the wavelength region of 720 - 950 Å obtained at P_o = 76 Torr and T = 120 K; (d) PIE curve for CO^+ in the wavelength region of 700 - 910 Å

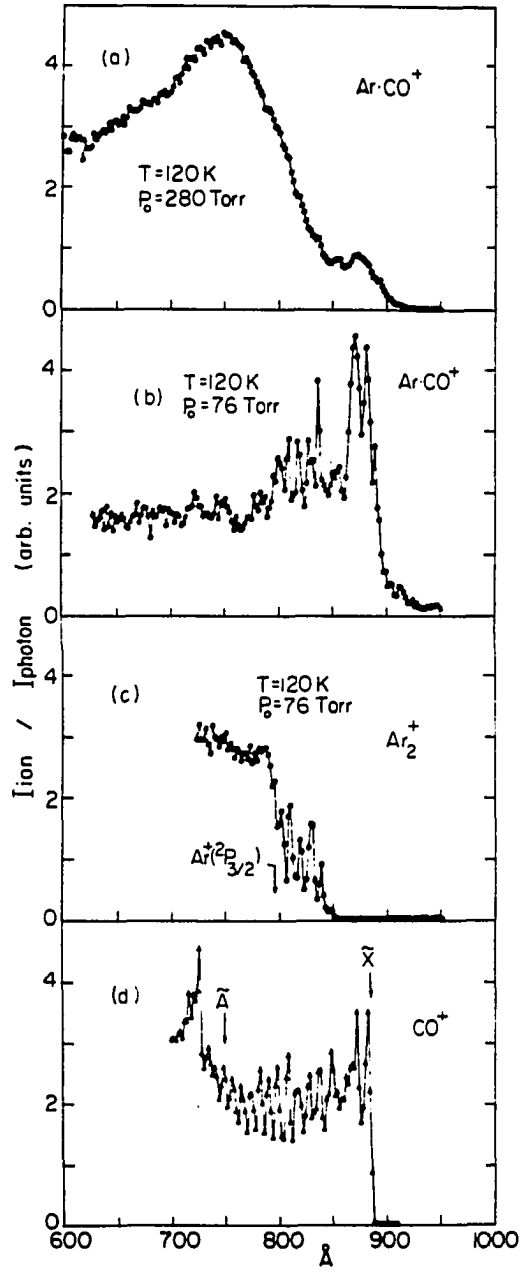
(a)
Ar·CO+
T=120K
P0=280 Torr
(b)
T=120K
P0=76 Torr
Ar·CO+
(c)
T=120K
P0=76 Torr
Ar2+
Ar+(2P3/2)
(d)
Ã
X̃
CO+
Iion / Iphoton (arb. units)
0
2
4
600
700
800
900
1000
Å

interactions are attributed to the peculiar charge distribution of $CO^+(\tilde{X})$. The center of charge of $CO^+(\tilde{X})$ is predicted to lie 0.026 Å outside of the C nucleus and the C-O bond. The peculiar charge distribution of $CO^+(\tilde{X})$ may also be responsible for the relatively strong binding in $CO^+(\tilde{X})\cdot Ar$.

The intensity of the second $ArCO^+$ coincidence electronic band in the wavelength region of $\approx$ 770 - 850 Å relative to that of the first $ArCO^+$ band diminishes rapidly as P_o is decreased from 214 to 92 Torr. It is most likely that the trend will continue when the intensities of trimer and higher clusters in the Ar/CO molecular beam are further reduced with respect to that of ArCO by lowering P_o to less than 92 Torr. As shown in the spectrum in Fig. 5(c), the $ArCO^+$ coincidence intensity is found to decrease sharply at the IE (787 Å) for $Ar^+(^2P_{3/2})$. A minor drop in the $ArCO^+$ coincidence intensity at the IE (778 Å) for $Ar^+(^2P_{1/2})$ also seems to be evident in the spectrum. These observations suggest that the second $ArCO^+$ coincidence electronic band originates mostly from the formation of an $Ar^+(^2P_{3/2})$ ion by photoionization in a cluster ion and that $Ar^+(^2P_j)\cdot CO$ dimer ions formed by process (2) are dissociative in a time scale shorter than the flight time ($\approx$ 46 μs) of $ArCO^+$.

The results of the rate constant measurement for the Ar^+ + CO charge transfer reaction[16] at low collision energies, which suggest a long-lived collision complex mechanism for the reaction, can be taken as a support that $Ar^+(^2P_{3/2})$ and CO interact attractively. The valence bond arguments presented by Hamilton et al.[20] also favor a bound $Ar^+(^2P_{3/2})\cdot CO$ intermediate. The ab initio calculation of Gislason[42] obtained a binding energy of 0.75 eV for $Ar^+(^2P_{3/2})\cdot CO$ in a T-shape structure. Figure 7

shows the energy level diagram of the $Ar^+(^2P_{3/2})$ + CO(X,v = 0), $Ar^+(^2P_{1/2})$ + CO(X,v = 0), $CO^+(\tilde{X},v'= 0 - 7)$ + Ar, and $CO^+(\tilde{A},v'= 0,1)$ + Ar states in the asymptotic limits. The formation of Ar + $CO^+(\tilde{X},v' = 0)$ from $Ar^+(^2P_{3/2})$ + CO(X,v = 0) is exothermic by 1.74 eV. If the $Ar^+(^2P_{3/2})\cdot CO$ dimer ion is bound by $\approx$ 0.8 eV as predicted, energy selected $Ar^+(^2P_{3/2})\cdot CO$ ions can be prepared in the wavelength region of $\approx$ 770 - 840 Å by the PIPECO method to match the $CO^+(\tilde{X},v' = 3 - 7)$ + Ar asymptote states. The positions of the $CO^+(\tilde{X},v' = 0 - 7)$ + Ar asymptote states are indicated by tic marks in Fig. 5(c).

The rapid dissociation of $Ar^+(^2P_J)\cdot CO(X,v = 0)$ initially formed by process (2) may be rationalized by a stepwise mechanism:

$$Ar^+(^2P_J)\cdot CO\ (X,v = 0) \rightarrow CO^+(\tilde{X},v' = 3 - 7)\cdot Ar \qquad (5a)$$

$$\rightarrow Ar + CO^+(\tilde{X},v') \qquad (5b)$$

The first step (5a) is a near resonance intramolecular charge transfer process which produces a vibrationally excited complex, $CO^+(\tilde{X},v' = 2 - 7)\cdot Ar$. This vibrationally excited dimer ion is expected to fall apart efficiently via a vibrational predissociation process (5b) because its internal energy content is greater than the dissociation energy of $CO^+(\tilde{X},v' = 0)\cdot Ar$. The flight time of $ArCO^+$ (46 μs) can be assigned as an upper bound for the dissociation lifetime of $Ar^+(^2P_J)\cdot CO(X,v = 0)$. A more ideal experiment to investigate the intramolecular charge transfer process is to measure the PIPECO intensity for $CO^+(\tilde{X},v')$ produced by processes (5a) and (5b) in the second $ArCO^+$ electronic band. Due to overwhelming background CO^+ formed by the photoionization of CO we have not been able to obtain a PIPECO spectra for CO^+ produced in the

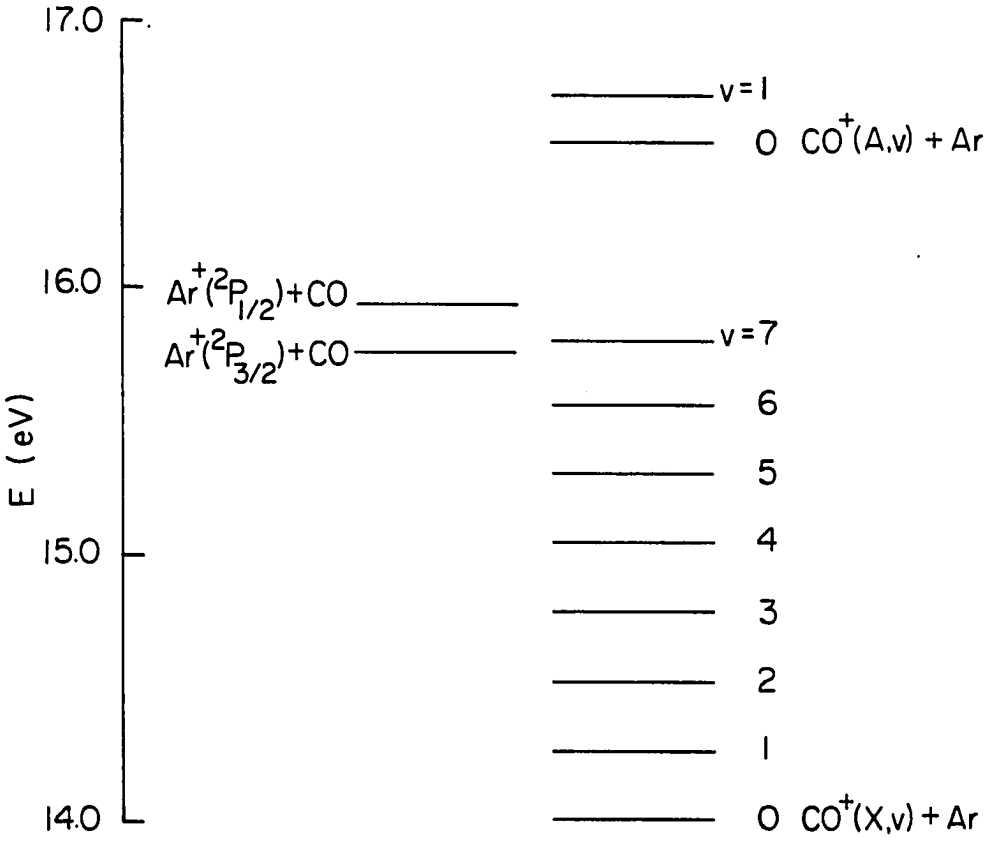

Figure 7. Energy level diagram of the $Ar^+(^2P_{3/2})$ + CO(X,v = 0), $Ar^+(^2P_{1/2})$ + CO(X,v = 0), $CO^+(\tilde{X},v' = 0 - 7)$ + Ar, and $CO^+(\tilde{A},v' = 0,1)$ + Ar states in the asymptotic limits

photoionization of ArCO in the wavelength region of 770-850 Å.

The $CO^+(\tilde{A})\cdot Ar$ and $CO^+(\tilde{B})\cdot Ar$ produced by process (3) cannot be seen in the spectra shown in Figs. 5(a)-5(c). The $CO^+(\tilde{A})\cdot Ar$ and $CO^+(\tilde{B})\cdot Ar$ coincidence electronic bands are also absent in the $ArCO^+$ PIPECO spectrum obtained at 350 Torr which is not shown here. The absence of the $CO^+(\tilde{A})\cdot Ar$ and $CO^+(\tilde{B})\cdot Ar$ coincidence electronic bands clearly shows the dissociative nature of the electronically excited dimer ions. The $CO^+(\tilde{A},\tilde{B})\cdot Ar$ complexes may decompose via a stepwise charge transfer mechanism similar to that summarized in process (5). In the theoretical calculations of the Ar + CO^+ and Ar + N_2^+ reactions, the Ar + $CO^+(\tilde{A})$ (or $N_2^+(\tilde{A})$) state is shown to couple directly with the Ar + $CO^+(\tilde{X})$ (or $N_2^+(\tilde{X})$) state. Thus the intramolecular quenching process,

$$CO^+(\tilde{A},v')\cdot Ar \rightarrow CO^+(\tilde{X},v')\cdot Ar \qquad (6)$$

may proceed to give a highly vibrationally excited $CO^+(\tilde{X},v')\cdot Ar$ complex prior to the vibrational predissociation process (5b). The rapid dissociation of the $CO^+(\tilde{A})\cdot Ar$ is also consistent with the theoretical calculation[42] showing that the potential for $CO^+(\tilde{A})\cdot Ar$ in a T-shape structure is essentially repulsive and has only a well of 0.05 eV. The $CO^+(\tilde{A})\cdot Ar$ and $CO^+(\tilde{B})\cdot Ar$ complexes can be stabilized by radiative decay. If we assume the radiative lifetimes of $CO^+(\tilde{A}$ or $\tilde{B})$ and $CO^+(\tilde{A}$ or $\tilde{B})\cdot Ar$ to be identical, the absence of the $CO^+(\tilde{A},\tilde{B})\cdot Ar$ coincidence bands is in accordance with the conclusion that the dissociation lifetimes for $CO^+(\tilde{A})\cdot Ar$ and $CO^+(\tilde{B})\cdot Ar$ are shorter than the radiative lifetimes of $CO^+(\tilde{A})$ ($\approx$ 4 μs)[45,46] and $CO^+(\tilde{B})$ ($\approx$ 50 ns),[47] respectively.

Evidence for the involvement of the Rydberg states of CO and Ar in the formation $ArCO^+$ can be found in the PIE spectrum for $ArCO^+$ plotted in Fig. 6(b). The spectrum is obtained at P_o = 76 Torr, a nozzle pressure at which negligible intensities for $Ar(CO)_2^+$ and Ar_2CO^+ are observed. The PIE spectra for Ar_2^+ and CO^+ are shown in Figs. 6(c) and 6(d), respectively. The Ar_2^+ spectrum is in good agreement with that measured previously[48,a] using a similar wavelength resolution. The autoionization peaks resolved in the Ar_2^+ spectrum are found to correlate with the $3p^5ns$ ($n \geq 6$) and $3p^5nd$ ($n \geq 4$) Rydberg states of Ar. The comparison of the spectra in Figs. 6(b) - 6(d) clearly illustrates that the two strong peaks at $\approx$ 870 and 880 Å appearing in the $ArCO^+$ PIE spectrum in Fig. 6(b) stem from the Rydberg states of CO[32,b] and the autoionization peaks of $ArCO^+$ in the wavelength region of 787 - 850 Å are due to the excitation of the Ar Rydberg states. The weak $ArCO^+$ coincidence intensities observed in the wavelength region of 860-880 Å in Fig. 5(a) indicates that autoionization of excited $CO^*\cdot Ar$ dimers at $\approx$ 870 and 880 Å produces energetic electrons together with the formation of $CO^+(\tilde{X})\cdot Ar$ ions. It is interesting to note that with the exception of the Rydberg states at $\approx$ 870 and 880 Å, autoionization structures correlating to other CO Rydberg states appear to be very weak in the PIE spectrum for $ArCO^+$ shown in Fig. 6(b). The autoionization of excited Rydberg $Ar^*\cdot CO$ dimers in the wavelength region of $\approx$ 790 - 845 Å may produce

---

[a]The autoionization states for Ar_2 in a similar wavelength region have been studied with a higher resolution by Dehmer and Poliakoff[49].

[b]The high resolution PIE spectrum for CO^+ in the wavelength region of $\approx$ 870 - 880 Å reveals many autoionization states which have not yet been assigned in detail.

$Ar^+(^2P_J)\cdot CO$ as well as $CO^+(\tilde{X})\cdot Ar$, accompanying a slow and a fast group of electrons, respectively.

As P_o is increased from 76 Torr, the autoionization peaks found in Fig. 6(b) merge into broader structures and the photoion yields of $ArCO^+$ at wavelengths < 845 Å rise rapidly relative to those in the wavelength region of 845 - 930 Å. The PIE spectrum for $ArCO^+$ measured at P_o = 280 Torr (Fig. 6(a)), a typical spectrum observed at a higher P_o, essentially consists of two gradual steps. Considering the PIE spectrum to be the integral curve of the corresponding PES, we find that the relative heights of the steps are in accord with the relative peak intensities of the first and second $ArCO^+$ coincidence electronic bands measured at the same P_o. The PIE measurements show that autoionization of trimers and clusters in excited Rydberg states also contributes to the observed $ArCO^+$ intensities.

If the measured relative intensities of cluster ions represent a fair estimate of the distribution of neutral clusters formed in the Ar/CO molecular beam, we can conclude that $ArCO^+$ fragments mostly originate from the photoionization of $Ar(CO)_2$ and Ar_2CO. The higher $ArCO^+$ coincidence intensities in the wavelength region of 850 - 884 Å observed at P_o = 214 Torr compared to those at P_o = 92 and 138 Torr may involve the production of stable $CO^+(\tilde{X},v' = 0)\cdot Ar$ ions from vibrationally excited $CO^+(\tilde{X},v' > 0)\cdot(ArCO)$ formed by photoionization of $Ar(CO)_2$ at energies above that of the Ar + $CO^+(\tilde{X},v' = 0)$ asymptote state. A plausible mechanism for $CO^+(\tilde{X},v' = 0)\cdot Ar$ formation from $Ar(CO)_2$ is summarized by processes (7a), (7b), and (8).

$$\begin{matrix} CO\cdots CO \\ \cdot\ \cdot\ \cdot \\ \cdot Ar \end{matrix} + h\nu \rightarrow \begin{matrix} CO^+(\tilde{X},v' > 0)\cdots CO \\ \cdot\ \cdot\ \cdot \\ \cdot Ar \cdot \end{matrix} + e^- \qquad (7a)$$

$$\rightarrow \begin{matrix} CO(X,v > 0)\cdots CO^+(\tilde{X},v' = 0) \\ \cdot\ \cdot\ \cdot \\ \cdot Ar \cdot \end{matrix} + e^-, \qquad (7b)$$

$$\begin{matrix} CO(X,v > 0)\cdots CO^+(\tilde{X},v' = 0) \\ \cdot\ \cdot\ \cdot \\ \cdot Ar \cdot \end{matrix} + e^- \rightarrow CO(X,v > 0) + CO^+(\tilde{X},v' = 0)\cdot Ar \qquad (8)$$

The size of Ar (covalent radius $\approx$ 1.74 Å) is considerably larger than the equilibrium bond distance of CO. In order to maximize the long range attractive forces, each CO molecule in $Ar(CO)_2$ will interact with Ar to maintain a T-shape structure, similar to that in ArCO, such that both the carbon and oxygen atoms are in the proximity of Ar. For the same reason, the two CO molecules may prefer to be close to each other. Therefore, $Ar(CO)_2$ is expected to have a triangular geometry. Since photoionization involves a vertical transition, the vibrationally excited $CO^+(\tilde{X},v' > 0)\cdot(ArCO)$ ion formed by the photoionization of one of the CO molecules in $Ar(CO)_2$ (process (7a)), will retain a triangular structure. Process (7b), a near resonance intramolecular charge transfer reaction, should be highly efficient because the vibrational quanta for $CO^+(\tilde{X})$ and CO(X) are nearly the same. The efficient deactivation of vibrationally excited $CO^+(\tilde{X})$ by CO via the charge transfer route has been demonstrated in the LIF experiment.[20] The results of the experiment imply that the complete relaxation of a vibrationally excited CO^+ ion is likely to result in a single deactivation event. From the energetic consideration, both the

$CO^+(\tilde{X},v' > 0)\cdot(ArCO)$ and $CO^+(\tilde{X},v' = 0)\cdot(Ar\cdot CO(X,v > 0))$ complexes may decompose. The vibrational predissociation of $CO^+(\tilde{X}$ $,v' = 0)\cdot(Ar\cdot CO(X,v > 0))$ according to process (8) leads to the formation of a stable $CO^+(v' = 0)\cdot Ar$.

The second $ArCO^+$ coincidence electronic band observed here necessarily originates from the photoionization of an Ar atom in a cluster. The formation of a stable $CO^+(\tilde{X},v' = 0)\cdot Ar$ ion from the excited $Ar^+(^2P_J)\cdot(CO)_2$ trimer ion produced by photoionization (process (9a)) can also be rationalized by a similar stepwise mechanism as described above,

$$\begin{matrix} CO\cdots CO \\ \cdot\ \cdot \\ \ \ Ar \end{matrix} + h\nu \rightarrow \begin{matrix} CO\cdots CO \\ \cdot\ \cdot \\ \ \ Ar^+(^2P_J) \end{matrix} + e^- \qquad (9a)$$

$$\rightarrow \begin{matrix} CO\cdots CO^+(\tilde{X},v' = 2 - 7) \\ \cdot\ \cdot\ \cdot \\ \ \ \ \ Ar \end{matrix} + e^-. \qquad (9b)$$

Step 9(b) converts the excited $Ar^+(^2P_J)\cdot(CO)_2$ trimer ion into a vibrationally excited $CO^+(\tilde{X},v')\cdot(ArCO)$ complex by a near resonance intramolecular charge transfer process between $Ar^+(^2P_J)$ and a CO molecule in the trimer ion. The production of $CO^+(\tilde{X},v'=0)\cdot Ar$ from the vibrationally excited $CO^+(\tilde{X},v')\cdot(ArCO)$ complex may proceed via processes (7b) and (8).

The previous measurements of the energetics of weakly bound cluster ions[50-52] show that the stabilization energy of a cluster ion has the dominant contribution from that of the dimer ion interaction in the cluster ion. That is, an excited trimer ion such as

$Ar^+(^2P_{3/2})\cdot(CO)_2$, which may be represented as $((Ar^+(^2P_{3/2})\cdot CO)\cdot CO$, is expected to have a stabilization energy only slightly greater than the binding energy of $Ar^+(^2P_{3/2})\cdot CO$. Based on the PIPECO spectra shown in Figs. 5(a) - 5(c), the ionization threshold for the second electronic band is estimated to lie in the range of 830-842 Å. Although the proposed mechanism for the formation of $CO^+(\tilde{X},v' = 0)\cdot Ar$ from $Ar^+(^2P_J)\cdot(CO)_2$ is a reasonable one, we cannot exclude the formation of $ArCO^+$ from $Ar^+(^2P_J)\cdot(ArCO)$. Since the latter trimer ion may be viewed as a CO molecule attached to the Ar_2^+ dimer ion, the IE for $(Ar^+(^2P_{3/2})\cdot Ar)\cdot CO$ should be close to that for Ar_2^+. The IE for Ar_2^+ is well known and has a value of 14.501 eV (855 $\pm$ 1.5 Å).[49] The ionization threshold of 842 Å for the second electronic band determined in Fig. 5(c) may be affected by the fragmentation of $(Ar^+(^2P_{3/2})\cdot Ar)\cdot CO$. In view of the fact that the observed intensity for $Ar(CO)_2^+$ is substantially high compared to that of Ar_2CO^+ at P_o = 92 Torr, the threshold value of 830 Å, obtained by the spectrum in Fig. 5(a), may be a better estimate of the IE for $Ar^+(^2P_{3/2})\cdot(CO)_2$. Assigning the IE for $Ar^+(^2P_{3/2})\cdot(CO)_2$ to lie in the range of 830-842 Å and using the estimated binding energy (0.054 eV)[c] for $Ar(CO)_2$, we estimate the dissociation energy for $Ar^+(^2P_{3/2})\cdot(CO)_2$ with respect to the $Ar^+(^2P_{3/2})$ + 2CO asymptote to have a value in the range of 0.86 - 1.07 eV. The observation of the second $ArCO^+$ coincidence electronic band can be taken as a strong evidence that $Ar^+(^2P_{3/2})\cdot CO$ is bound. Based on the previous measurements on the energetics of similar cluster ion

---

[c]The binding for $Ar(CO)_2$ is estimated to be twice that for the ArCO dimer.

systems,[d] the interaction energy for $Ar^+(^2P_{3/2})\cdot CO + CO$ is likely to be $\approx$ 0.1-0.2 eV. Taking into account the estimated binding energy between $Ar^+(^2P_{3/2})\cdot CO$ and CO, the dissociation energy for $Ar^+(^2P_{3/2})\cdot CO$ is expected to fall in the range of 0.66-0.97 eV. The latter estimate is in agreement with the theoretical value of 0.75 eV obtained by Gislason.[42]

The rate constants for the relaxation of $CO^+(\tilde{X},v' = 1 \text{ and } 4)$ by CO via the charge transfer route[20] are found to be equal within the experimental uncertainties, suggesting that process (7b) may only be weakly dependent on v'. The vibrational predissociation process (8) may take place in a time scale ($\approx 10^{-9}$ sec)[54] much shorter than the ion flight time ($> 10^{-5}$ sec). Assuming process (7b) to be independent of v' and the rapid dissociation of $CO(X,v > 0)\cdot(CO^+(\tilde{X},v = 0)\cdot Ar)$ according to process (8), the profile for the second $ArCO^+$ coincidence electron band observed in Figs. 5(a) - 5(c) should reflect the relative probabilities for the formation of $CO^+(\tilde{X},v')\cdot(ArCO)$ in v' = 2 - 7 from $Ar(CO)_2$, i.e., the combined relative cross sections of processes (9a) and (9b). The cross section for process (7a) has the contributions from direct ionization and autoionization. The energy dependence of the relative cross section for direct photoionization of $Ar(CO)_2$, governed by the Franck-Condon envelope for process (9a), should have a profile similar to that of the $CO^+(\tilde{X})\cdot Ar$ coincidence electronic band and peaked close to the IE for $Ar^+(^2P_{3/2})$. Autoionization of $Ar^*\cdot(CO)_2$ to form

---

[d]Since the polarizabilities for Ar and CO are similar, the binding energy for $Ar^+\cdot CO + CO$ should be close to that for $Ar_2^+ + Ar$. The binding energy between Ar_2^+ and Ar is determinded to be 0.18 eV by Dehmer and Pratt,[52] and Turner and Conway.[53]

$Ar^+(^2P_{3/2})\cdot(CO)_2$ is expected to render strength to the ionization cross sections at energies near the ionization threshold and smooth the energy dependence of the ionization cross section for process (9a). As shown in Fig. 5(c), the second $ArCO^+$ coincidence band is found to peak sharply at 810 Å implying the formation of $CO^+(\tilde{X},v' = 5)\cdot(ArCO)$. This observation is consistent with the finding of the LIF experiment[20] showing that the vibration distribution of $CO^+(\tilde{X},v')$ formed by the $Ar^+(^2P_{3/2})$ + CO charge transfer reaction at near thermal energies has a maximum at v' = 5. The position of the maximum in the distribution may be a measure of the crossing region of the $Ar^+(^2P_{3/2})$ + CO and Ar + $CO^+(\tilde{X})$ potential surfaces. The vibrational distribution of product $CO^+(\tilde{X},v')$ obtained in the LIF experiment is compared to the distribution for $ArCO^+$ formation in the second band in Fig. 5(c). The maxima of the two distributions have been normalized to the same value. The lower relative $ArCO^+$ coincidence intensities compared to the relative vibrational populations for product $CO^+(\tilde{X},v' = 2 - 4)$ observed in the wavelength region of ≈ 820 - 850 Å can be attributed to the low Franck-Condon factors for process (9a) near the ionization threshold. The overall good agreement of the two distributions can be viewed as a support for the involvement of the near resonance intramolecular charge transfer process (9b).

The vibrationally excited trimer ion $CO^+(\tilde{X},v' = 2 - 7)\cdot(ArCO)$ formed in process (9b) may decompose according to the process,

$$\begin{matrix} CO\cdots CO(X,v' = 2 - 7) \\ \quad\quad\quad\ \ Ar \end{matrix} \rightarrow CO^+(\tilde{X},v')\cdot CO + Ar. \qquad (10)$$

The PIPECO spectrum for $(CO)_2^+$ in the wavelength region of 700 - 940 Å obtained using a mixed Ar/CO molecular beam at P_o = 214 Torr is shown in Fig. 8(a) and compared with the $ArCO^+$ coincidence spectrum measured at the same P_o in Fig. 8(b). The $(CO)_2^+$ coincidence electronic bands observed in the wavelength regions of ≈ 850 - 940 and ≈ 700 - 760 Å have been assigned to the $CO^+(\tilde{X})\cdot CO$ and $CO^+(\tilde{A})\cdot CO$ electronic bands, respectively, arising from the photoionization of $(CO)_2$.[15] The $(CO)_2^+$ coincidence electronic band centered at 810 Å is not found in the PIPECO spectrum for $(CO)_2^+$ obtained using a pure CO molecular beam. The close resemblance of the second electronic bands resolved in Figs. 5(c) and 8(b) as illustrated in Fig. 8(b) suggests that $(CO)_2^+$ and $ArCO^+$ observed in the second electronic band are fragments from similar cluster ions. We note that the width of the $(CO)_2^+$ band is greater than that of the $ArCO^+$ band. The comparison of the second $ArCO^+$ and $(CO)_2^+$ coincidence electronic bands also brings out the steplike structures on the second band which seem to correlate well with the positions of the $CO^+(\tilde{X},v' = 2 - 7)$ + Ar asymptotic states.

The PIE spectrum for $(CO)_2^+$ recorded at P_o = 214 Torr (Fig. 9(a)) also resembles that for $ArCO^+$ observed at the same P_o. The PIE spectra for $(CO)_2^+$ plotted in Figs. 8(a) and 8(b) show that the PIEs for $(CO)_2^+$ in the wavelength region of 750 - 850 Å decrease as P_o is reduced, an observation similar to that found in the PIE measurement for $ArCO^+$. The comparison of the PIE spectra obtained using a mixed Ar/CO (Fig. 9(b)) and a pure CO (Fig. 9(c)) molecular beam clearly shows the effect of fragmentation from mixed Ar/CO clusters such as $Ar^+(^2P_{3/2})\cdot(CO)_2$, giving higher photoion yields for $(CO)_2^+$ in the wavelength region of 750-850 Å in the PIE spectrum shown in Fig. 9(b).

Figure 8. PIPECO spectra for $ArCO^+$ and $(CO)_2^+$

(a) PIPECO spectrum for $(CO)_2^+$ in the wavelength region of 700 - 940 Å obtained at P_o = 214 Torr and T = 120 K; (b) the comparison of the PIPECO spectra for $ArCO^+$ (o) and $(CO)_2^+$ (Δ) obtained at P_o = 214 Torr and T = 120 K

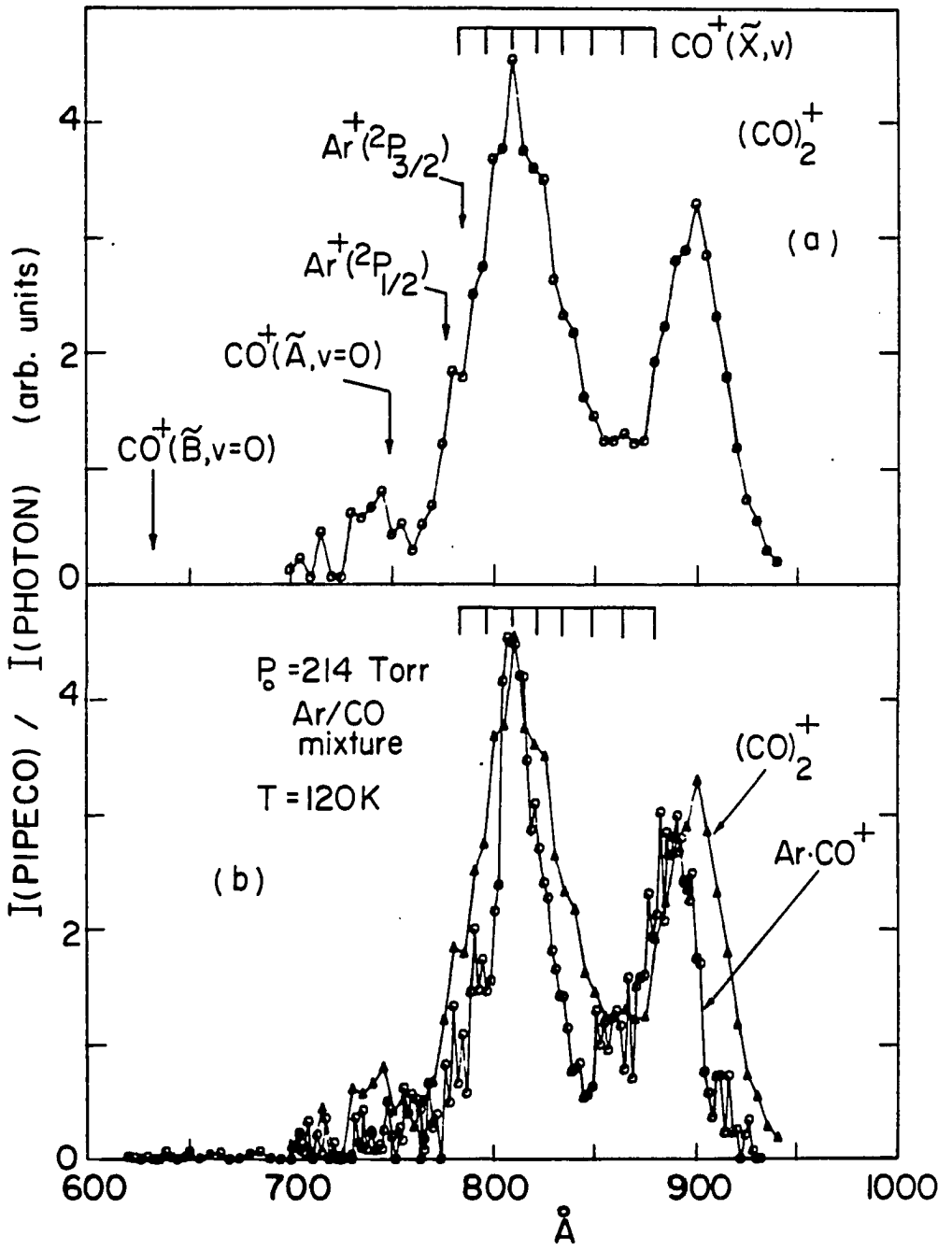
CO+(X̃,v)
Ar+(2P3/2)
Ar+(2P1/2)
(CO)2+
(a)
CO+(Ã,v=0)
CO+(B̃,v=0)
I(PIPECO) / I(PHOTON) (arb. units)
P° =214 Torr
Ar/CO
mixture
T = 120K
(b)
(CO)2+
Ar·CO+
0
2
4
600
700
800
900
1000
Å

Figure 9. PIE spectra for $(CO)_2^+$ in the wavelength region of 650 - 970 Å

(a) P_o = 214 Torr (Ar/CO mixture) and T = 120 K; (b) P_o = 138 Torr (Ar/CO mixture) and T = 120 K; (c) P_o = 200 Torr (pure CO) and T = 120 K

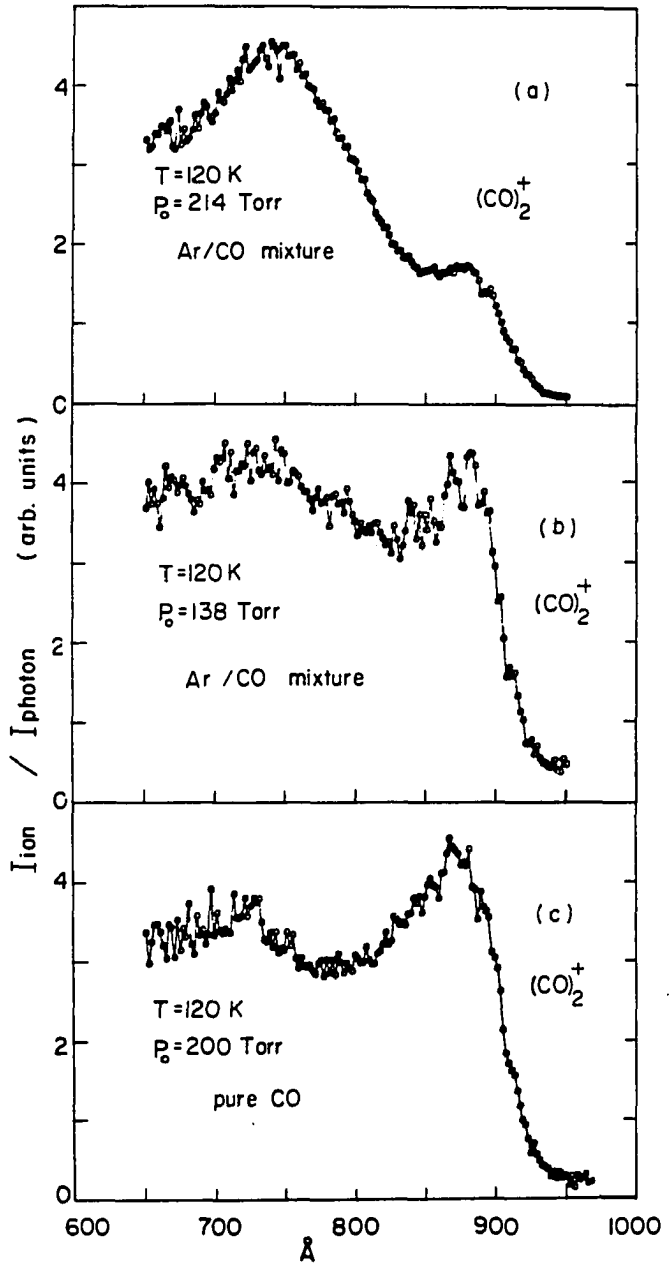
(a)
T=120 K
P₀=214 Torr
Ar/CO mixture
(CO)₂⁺
(b)
T=120 K
P₀=138 Torr
Ar /CO mixture
(CO)₂⁺
(c)
T=120 K
P₀=200 Torr
pure CO
(CO)₂⁺
I ion / I photon (arb. units)
Å
600
700
800
900
1000
0
2
4

In order for $CO^+(\tilde{X},v')\cdot CO$ to be detected in this experiment, it has to be a stable or a metastable dimer ion which lives longer than 42 μs, the flight time of $(CO)_2^+$. The formation of a stable $CO^+(\tilde{X},v')\cdot CO$ ion in process (10) requires the conversion of a substantial amount ($\approx$ 0.5 - 1.7 eV) of internal vibrational energy into the translation energies of Ar and $CO^+(\tilde{X},v')\cdot CO$. The decay of $CO^+(\tilde{X},v' = 2 - 7)\cdot(ArCO)$ according to process (10) is likely to produce $CO^+(\tilde{X},v')\cdot CO$ with a distribution of internal energy. The fraction of $CO^+(\tilde{X},v')\cdot CO$ with internal energies lower than that of the $CO^+(\tilde{X},v = 0)$ + CO asymptote state will be stable. If the fraction of stable $CO^+(\tilde{X},v')\cdot CO$ formed is not strongly dependent on the internal energy content of $CO^+(\tilde{X},v' = 2 - 7)\cdot(ArCO)$, the profile of the second PIPECO electronic band for $(CO)_2^+$ should be governed mainly by the relative probabilities for the formation of $CO^+(\tilde{X},v' = 2 - 7)\cdot(ArCO)$ in v' = 2 - 7. This suggestion is supported by the good agreement found between the second $ArCO^+$ and $(CO)_2^+$ coincidence bands.

As pointed out above, we cannot rule out the production of $ArCO^+$ from Ar_2CO at high P_o. The observation indicating the possible formation of $(CO)_2^+$ from $Ar^+(^2P_{3/2})\cdot(CO)_2$ suggests that stable $ArCO^+$ ions may also be produced by the following processes:

$$\begin{matrix} Ar\cdots Ar \\ \diagdown\ \diagup \\ CO \end{matrix} + h\nu \rightarrow \begin{matrix} Ar^+(^2P_{3/2})\cdots Ar \\ \diagdown\ \diagup \\ CO \end{matrix} + e^- \qquad (11a)$$

$$\rightarrow \begin{matrix} Ar\cdots Ar \\ \diagdown\ \diagup \\ CO^+(\tilde{X},v' = 2 - 7), \end{matrix} + e^- \qquad (11b)$$

$$\underset{\cdot\,\cdot\,\cdot\,\cdot}{Ar\cdots Ar} + h\nu \rightarrow CO^+(\tilde{X},v')\cdot Ar + Ar. \qquad (12)$$

$$\cdot\,\cdot\,\cdot\,\cdot$$

$$CO^+(\tilde{X},v' = 2 - 7)$$

Again, if the fraction of stable $CO^+(\tilde{X},v')\cdot Ar$ ions formed in process (12) is only weakly dependent on the internal energy of $CO^+(\tilde{X},v'=2 - 7)\cdot Ar_2$, the profile for the second $ArCO^+$ coincidence electronic band arisen from processes (11a), (11b), and (12) should be similar to that observed in Figs. 5(a)-5(c).

CONCLUSIONS

A molecular beam PIPECO apparatus is described. Using a new MCS coincidence circuit, we have overcome the paralyzed effect at high false coincidence rates encountered in using a single-electron-start-single- (or multi) ion-stop coincidence circuitry. The MCS coincidence arrangement allows the measurement of the PES of a size-selected cluster at a concentration less than 1% that of the monomer. In the case when the TOF peaks for various cluster ions are well resolved in the coincidence TOF spectrum, the PIPECO spectra for individual cluster ions can be measured simultaneously.

The PIPECO spectra for $ArCO^+$ in the wavelength range of 620 - 940 Å have been recorded at different nozzle expansion conditions. The excited $Ar^+(^2P_j)\cdot CO$ and $CO^+(\tilde{A},\tilde{B})\cdot Ar$ dimer ions prepared by processes (2) and (3) are found to be dissociative in a time scale much shorter than the flight time (46 μs) of $ArCO^+$. A stepwise mechanism invoking near resonance intramolecular charge transfer and vibrational predissociation is used to rationalize the observation. If the radiative lifetimes for $CO^+(\tilde{A},\tilde{B})$ is assumed to be identical to those for $CO^+(\tilde{A},\tilde{B})\cdot Ar$, the dissociation lifetimes for $CO^+(\tilde{A})\cdot Ar$ and $CO^+(\tilde{B})\cdot Ar$ are estimated to be shorter than 4 μs and 50 ns, respectively. The IE for $CO^+(\tilde{X})\cdot Ar$ is determined to be 13.33 $\pm$ 0.06 eV. This value makes possible the calculation of a value of 0.70 $\pm$ 0.06 eV for the binding energy of $CO^+(\tilde{X})\cdot Ar$ which is in fair agreement with the theoretical value of 0.82 eV obtained by Gislason.[42] The absence of the $CO^+(\tilde{A})\cdot Ar$ coincidence electronic band is

also consistent with the theoretical prediction that the potential surface for $CO^+(\tilde{A})$ + Ar in a T-shape structure is nearly repulsive. The formation of $ArCO^+$ from fragmentation of cluster ions are shown to be significant. Since the observed intensities for $Ar(CO)_2^+$ and Ar_2CO^+ are substantially higher than those for other mixed Ar/CO cluster ions in this experiment, the $ArCO^+$ fragments should be mainly produced by process (4). The observation of the second $ArCO^+$ and $(CO)_2^+$ coincidence bands indicates that $Ar^+(^2P_J)\cdot(CO)_2$ and $Ar^+(^2P_J)\cdot(ArCO)$ ions initially produced by photoionization of $Ar(CO)_2$ and Ar_2CO are the precursor ions for $ArCO^+$ and $(CO)_2^+$ detected in the wavelength region of $\approx$ 770 - 750 Å. A charge transfer mechanism similar to that used to explain the rapid dissociation of excited $Ar^+(^2P_J)\cdot CO$ dimer ions is proposed to rationalize the formation of stable $ArCO^+$ ions from the excited $Ar^+(^2P_J)\cdot(CO)_2$ parent ions. The good agreement found in the comparison of the vibrational distribution of $CO^+(\tilde{X},v')$ formed in the $Ar^+(^2P_{3/2})$ + CO charge transfer reaction and the profiles of the second $ArCO^+$ and $(CO)_2^+$ coincidence electronic band supports the involvement of the near resonance intramolecular charge transfer process (9b). The IE for $Ar^+(^2P_{3/2})\cdot(CO)_2$ is estimated to be in the range of $\approx$ 14.73 - 16.85 eV, suggesting that the value for the dissociation energy of $Ar^+(^2P_{3/2})\cdot(CO)_2$ with respect to the $Ar^+(^2P_{3/2})$ + 2CO asymptote state lies in the range of 0.86-1.07 eV. Taking into account the estimated binding energy between $Ar^+(^2P_{3/2})\cdot CO$ and CO, the dissociation energy for $Ar^+(^2P_{3/2})\cdot CO$ is expected to fall in the range of 0.66 - 0.97 eV, in agreement with the theoretical prediction.

REFERENCES

1. C. Y. Ng, Adv. Chem. Phys. 52, 263 (1983).

2. Y. Ono and C. Y. Ng, J. Chem. Phys. 77, 2947 (1982).

3. W.-B. Tzeng, Y. Ono, S. H. Linn, and C. Y. Ng, J. Chem. Phys. 83, 2803 (1985).

4. W.-B. Tzeng, Y. Ono, S. H. Linn, and C. Y. Ng, J. Chem. Phys. 83, 2813 (1985).

5. Y. Ono, S. H. Linn, W.-B. Tzeng, and C. Y. Ng, J. Chem. Phys. 80, 1482 (1984).

6. Y. Ono and C. Y. Ng, J. Am. Chem. Soc. 104, 4752 (1982).

7. Y. Ono, S. H. Linn, H. F. Prest, M. E. Gress, and C. Y. Ng. J. Chem. Phys. 74, 1125 (1981).

8. B. Brehm and E. von Puttkamer, Z. Naturforsch. A22, 8 (1967).

9. J. H. D. Eland, Int. J. Mass Spectrom. Ion Phys. 8, 143 (1972).

10. R. Stockbauer, J. Chem. Phys. 58, 3800 (1973).

11. M. E. Gellender and A. D. Baker, in "Electron Spectroscopy", Eds., C. R. Brundle and A. D.Baker (Academic Press, New York, 1977), Vol. 1, p. 435.

12. T. Baer, in "Gas Phase Ion Chemistry", Ed., M. T. Bowers (Academic Press, New York, 1979), Vol. 1, p. 153.

13. E. D. Poliakoff, P. M. Dehmer, J. L. Dehmer, and R. Stockbauer, J. Chem. Phys. 75, 5214 (1982).

14. L. Cordis, G. Ganteför, J. Besslich, and A. Ding, Z. Phys. D3, 323 (1986).

15. K. Norwood, J.-H. Guo, G. Luo, and C. Y. Ng, J. Chem. Phys. 88, 4098 (1988); K. Norwood, J.-H. Guo, G. Luo, and C. Y. Ng, J. Chem. Phys. 90, 6026 (1989).

16. I. Dotan and W. Lindinger, J. Chem. Phys. 76, 4972 (1982).

17. R. Marx, G. Mauclaire, and R. Derai, Int. J. Mass Spectrom. Ion Phys. 47, 155 (1983).

18. R. Marx, in "Ionic Processes in the Gas Phase", Ed. M. A. Almoster Ferreira (Reidel, Boston, 1984), p. 67.

19. C.-H. Lin, J. Mair, and S. R. Leone, J. Chem. Phys. 82, 5527 (1985).

20. C. E. Hamilton, V. M. Bierbaum, and S. R. Leone, J. Chem. Phys. 83, 2284 (1985).

21. J. Danon and R. Marx, Chem. Phys. 68, 255 (1982).

22. T. Kato, K. Tanaka, and I. Koyano, J. Chem. Phys. 77, 337 (1982).

23. E. A. Gislason, G. Parlant, P. Archirel, and M. Sizun, Faraday Dis. of Chem. Sci. (in press).

24. M. R. Spalburg and E. A. Gislason, Chem. Phys. 94, 339 (1985).

25. G. Parlant and E. A. Gislason, Chem. Phys. 101, 227 (1986).

26. G. A. Parker and R. T. Pack, J. Chem. Phys. 69, 3268 (1978).

27. S. J. Buelow, Chemistry Graduate Student, Harvard University, Cambridge, Massachusetts (private communication).

28. Y. Ono, S. H. Linn, H. F. Prest, M. E. Gress, and C. Y. Ng, J. Chem. Phys. 73, 2523 (1980).

29. C.-L. Liao, J.-D. Shao, R. Xu, G. D. Flesch, Y.-G. Li, and C. Y. Ng, J. Chem. Phys. 85, 3874 (1986).

30. T. Baer, W. B. Peatman, and E. W. Schlag, Chem. Phys. Lett. 4, 243 (1969).

31. R. Spohr, P. M. Guyon, W. A. Chupka, and J. Berkowitz, Rev. Sci. Instrum. 42, 1872 (1971).

32. J. Berkowitz, "Photoabsorption, Photoionization, and Photoelectron Spectroscopy" (Academic Press, New York, 1979).

33. R. Stockbauer, J. Chem. Phys. 58, 3800 (1973).

34. C. Holzapfel, Rev. Sci. Instrum. 45, 894 (1974).

35. J. H. Fock, P. Gürtler, and E. E. Koch, Chem. Phys. 47, 87 (1980).

36. W. M. Huo, J. Chem. Phys. 43, 624 (1965).

37. P. H. Krupenie, "The Bond Spectrum of Carbon Monoxide", Natl. Bur. Stand. 5 (U.S. Govt. Printing Office, Washington, DC, 1966).

38. D. W. Turner, C. Baker, A. D. Baker, and C. R. Brundle, "Molecular Photoelectron Spectroscopy" (Wiley, New York, 1970).

39. J. T. Blair, J. C. Weisshaar, J. E. Carpenter, and Frank Weinhold, J. Chem. Phys. 87, 392 (1987).

40. G. Herzberg, "Molecular Spectra and Molecular Structure I. Spectra of Diatomic Molecules" (Van Nostrand Reinhold Co., New York, 1950).

41. J. T. Moseley, R. P. Saxon, B. A. Huber, P. C. Cosby, R. Abouaf, and M. Tadjeddine, J. Chem. Phys. 67, 1659 (1977).

42. E. A. Gislason, Professor of Physical Chemistry, University of Illinois at Chicago, Chicago, Illinois (private communication).

43. P. Archirel and B. Levy, Chem. Phys. 106, 51 (1986).

44. J. Baker and A. D. Buckingham, J. Chem. Soc. Faraday Trans. II, 83, 1609 (1987).

45. J. Danon, G. Mauclaire, T. R. Gover, and R. Marx, J. Chem. Phys. 76, 1255 (1982).

46. V. E. Bondybey and T. A. Miller, J. Chem. Phys. 69, 3597 (1978).

47. M. Bloch and D. W. Turner, Chem. Phys. Lett. 30, 344 (1975).

48. C. Y. Ng, D. J. Trevor, B. H. Mahan, and C. Y. Ng, J. Chem. Phys. 66, 446 (1977).

49. P. M. Dehmer and E. D. Poliakoff, Chem. Phys. Letters 77, 326 (1981).

50. H. Haberland, Surf. Sci. 156, 305 (1985).

51. F. Carnovale, J. B. Peel, and R. G. Rothwell, J. Chem. Phys. 88, 642 (1988).

52. P. M. Dehmer and S. T. Pratt, J. Chem. Phys. 76, 843 (1982).

53. D. L. Turner and D. C. Conway, J. Chem. Phys. 71, 1899 (1979).

54. E. E. Ferguson, J. Phys. Chem. 90, 731 (1986).

PART II.

PHOTOION-PHOTOELECTRON COINCIDENCE SPECTROSCOPY OF THE TRANSIENT MOLECULES SO AND S_2O

INTRODUCTION

Photoelectron spectroscopic measurements have provided most of the energetic information available today on molecular cations in their ground and excited states.[1,2] Combined with high level quantum calculations, photoelectron spectroscopic studies also yield structural information on molecular ions. Due to the difficulty in the preparation of radicals, the photoelectron spectroscopic study of radicals remains in its infancy. The reactive nature of radicals usually prevents the production of radicals with high purity. However, many radicals can be produced readily in electrical discharge, photodissociation, and thermal pyrolysis sources, coexisting with their precursors and products resulting from secondary reactions. In order to measure unambiguously the photoelectron spectrum (PES) of a specific radical formed in such a source, an experimental method capable of identifying the origins of photoelectrons, must be used. The photoion-photoelectron coincidence (PIPECO) techniques measure the time-correlated electron-ion pairs formed in photoionization and are most suitable for measuring PESs of radicals coexisting with other molecular species. To our knowledge, the application of PIPECO techniques to the study of transient species[a] has not been made previously.

In an effort to provide thermochemical data for radicals and transient molecules relevant to combustion chemistry, we have developed a pulsed PIPECO method for

---

[a]A transient molecule is defined to have a lifetime less than a few minutes in the pressure range of 0.1 - 1.0 Torr encountered in its production.[3]

radical studies. In this communication, we present preliminary results on the PIPECO study of SO and S_2O. Both SO and S_2O are products of the combustion of sulfur at low oxygen pressures.[4]

EXPERIMENTAL

The experimental arrangement of the PIPECO apparatus has been described previously.[5-7] Briefly, the apparatus consists of a 3 m near normal incidence vacuum ultraviolet (VUV) monochromator, a capillary discharge lamp, a VUV light detector, a microwave discharge source for radical production, a quadrupole mass spectrometer (QMS) for ion detection, and an electron energy analyzer for threshold photoelectron (TPE) detection.

The transient molecules SO and S_2O, together with other gaseous species, are produced by a low pressure microwave discharge of pure SO_2 in a quartz tube. The gaseous mixture formed by the discharge flows into a buffer chamber which is evacuated by a 6" liquid-nitrogen-trapped diffusion pump system. A small fraction of the gases enters the photoionization region as an effusive beam through a 3mm x 1.5mm slit between the buffer and photoionization chambers. During the experiment, the buffer and photoionization chambers are maintained at 2×10^{-4} and 2.5×10^{-5} Torr, respectively. Photoionization efficiency (PIE) measurements show that SO_2, SO, S_2O, S_3, S_2, S, O, O_2, and SO_3 are major constituents of the effusive beam. The intensity of SO_2^+ is greater than those of other ions by at least a factor of five.

The energy resolution of the detection of TPEs depends strongly on the electrostatic field at the photoionization region. In this experiment, the photoionization region is kept nearly field free. The coincidence detection is initiated by an electronic pulse signifying

the arrival of a TPE at the electron detector. The electronic pulse triggers two identical extraction pulses, which have a width (Δt) of 100 ns and a height of 300 V, to extract photoions toward the ion detector. The QMS is used to select the ion of interest for detection. The first and second extraction pulses are delayed by 0 and 40 μs, respectively, with respect to the electronic pulse. Since the electron flight time from the photoionization region to the electron detector is $\lesssim$ 0.1 μs, in such a short time the correlated photoion is expected to remain in the photoionization region. Thus, the first extraction pulse serves to extract the correlated photoion as well as background ions formed within Δt. The second extraction pulse draws out only background ions formed within the the temporal range of 100 ns. The ions arriving at the ion detector are recorded by a multichannel scaler (MCS). The difference of the ion intensities detected due to the first and second extraction pulse represents the true coincidence signal. The coincidence detection cycle is completed in a period of 100 μs. The electron detector will not accept another TPE until the end of the coincidence period.

Figure 1(a) shows the PIPECO spectrum for NO^+ in the wavelength region of 1200 - 1345 Å obtained using the pulsed PIPECO method. The counting time for each data point is 12 s. The NO^+ PIPECO spectrum is in excellent agreement with the TPE spectrum for NO (Fig. 1(b)) except that the electron background present in the TPE spectrum is not discernible in the PIPECO spectrum. The structureless electron background, which increases gradually as the photon energy is increased, is believed to arise from photoelectrons ejected from the exit slit of the monochromator. The NO^+ spectra show that the electron energy resolution achieved is $\approx$ 30 meV (FWHM) for a

Figure 1. PIPECO and TPE spectrum for NO^+ in the wavelength region 1200 - 1345 Å obtained using a wavelength resolution = 1.4 Å (FWHM) and an electron energy resolution of ~ 30 meV (FWHM)

(a) PIPECO spectrum for NO^+; (b) TPE spectrum for NO^+

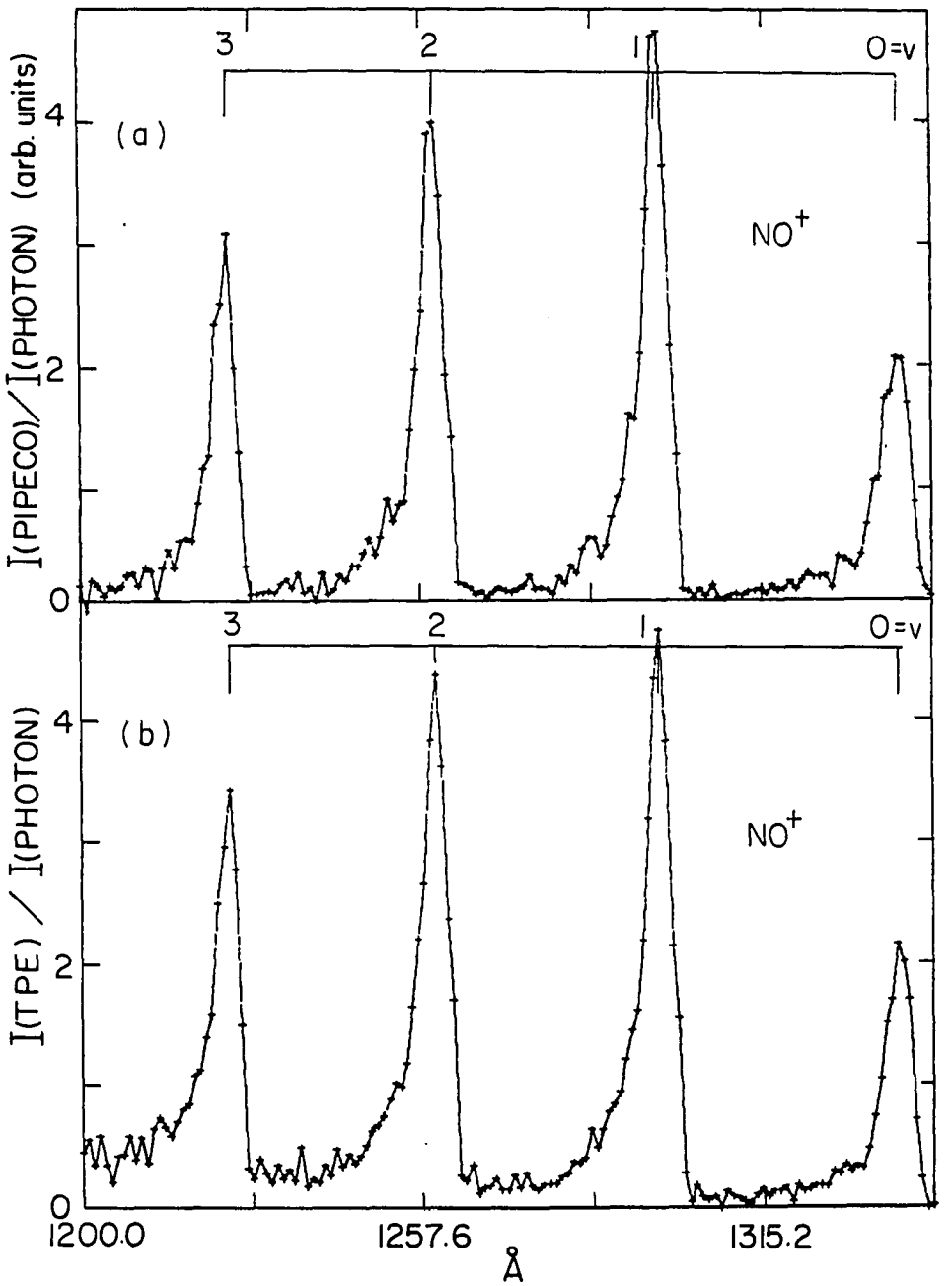
3
2
1
0=v
(a)
NO+
I(PIPECO)/I(PHOTON) (arb. units)
4
2
0
3
2
1
0=v
(b)
NO+
I(TPE) / I(PHOTON)
4
2
0
1200.0
1257.6
1315.2
Å

wavelength resolution of 1.4 Å (FWHM). The electron energy resolution is expected to be better when a higher wavelength resolution is used.

The pulsed PIPECO method is found to be superior in both sensitivity and resolution compared to the continuous MCS PIPECO scheme[5-7] partly because the electron energy resolution and ion collection efficiency can be optimized in the pulsed PIPECO experiment. The greatest improvement in sensitivity of the pulsed PIPECO method stems from the substantial reduction of false coincidences as a result of the smaller 100 ns temporal window used here compared to the 5 - 10 μs window determined by the width of the ion time-of-flight peak in the MCS PIPECO experiments. The detailed comparison of the signal-to-noise ratios achieved in the pulsed and MCS PIPECO schemes will be presented in a future publication.

RESULTS

Figure 2 shows the TPE spectrum in the wavelength region of 1030 - 1210 Å for the gas mixture produced in the discharge of pure SO_2.

In this wavelength range, the TPEs result from photoionization of SO, S_2O, S_3, S_2, S, and $O_2(^1\Delta_g)$, etc. The PIE and PIPECO spectra for SO^+ are depicted in Figs. 3(a) and 3(b) and those for S_2O^+ are compared in Figs. 4(a) and 4(b), respectively. The accumulation time for each of the SO^+ and S_2O^+ PIPECO spectra is $\approx$ 4 hours. The spectra shown in Figs. 2 and 3(b) have been smoothed using a three-point averaging routine. Because of the involvement of autoionization, the PIPECO spectra for SO^+ and S_2O^+ are different from the HeI PESs of SO[8-10] and S_2O[11,12]. The PIE spectrum for S_2O shown in Fig. 4(a) is consistent with that reported previously.[13]

Figure 2. TPE spectrum for the gas mixture ($SO + S_2O + S_3 + S_2 + S + ...$) produced in the microwave discharge of SO_2 in the wavelength region of 1025 - 1210 Å and obtained using a wavelength resolution = 1.4 Å (FWHM) and an electron energy resolution ~ 30 meV (FWHM)

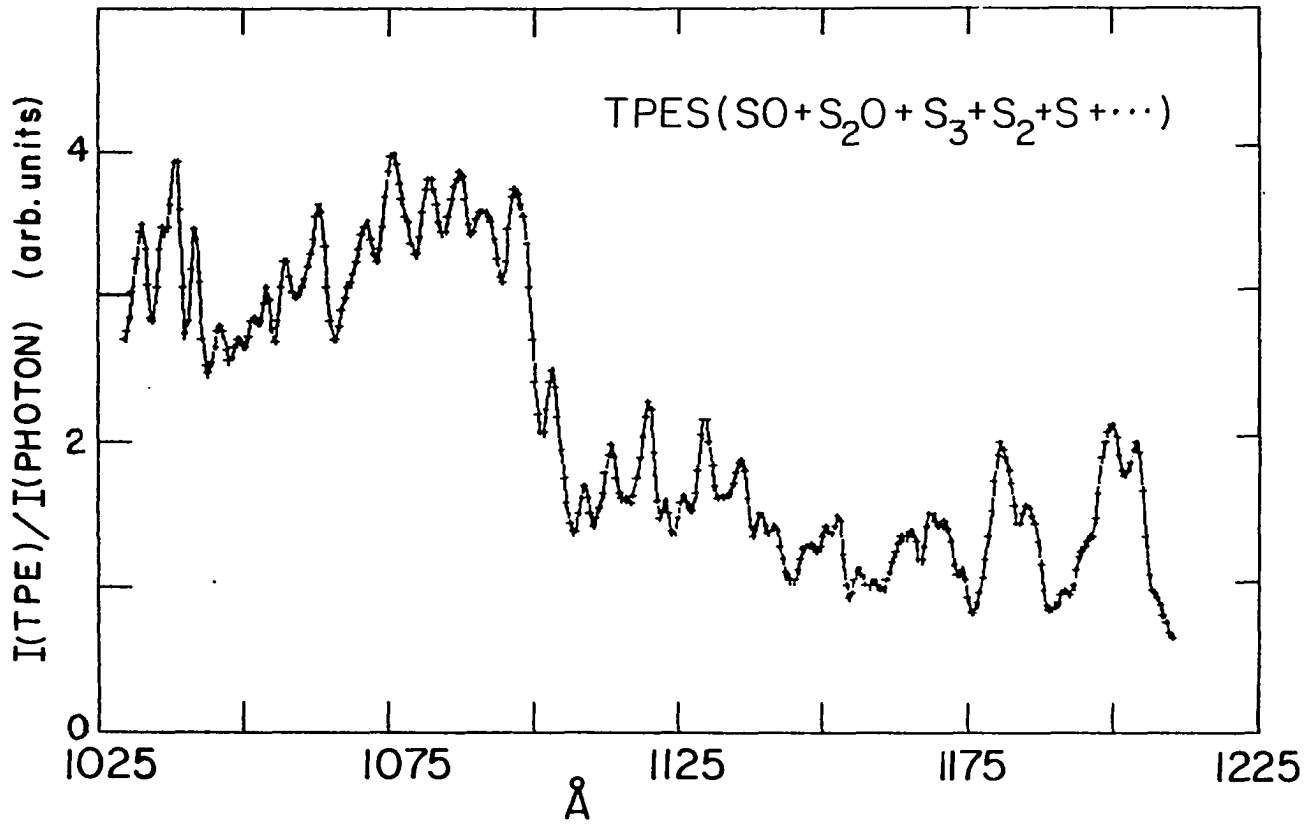
TPES(SO+S2O+S3+S2+S+···)
I(TPE)/I(PHOTON) (arb.units)
0
2
4
1025
1075
1125
1175
1225
Å

Figure 3. PIPECO and PIE spectrum for SO^+ in the wavelength region of 1025 - 1210 Å obtained using a wavelength resolution = 1.4 Å (FWHM) and an electron energy resolution ~ 30 meV (FWHM)

(a) PIE spectrum for SO^+; (b) PIPECO spectrum for SO^+

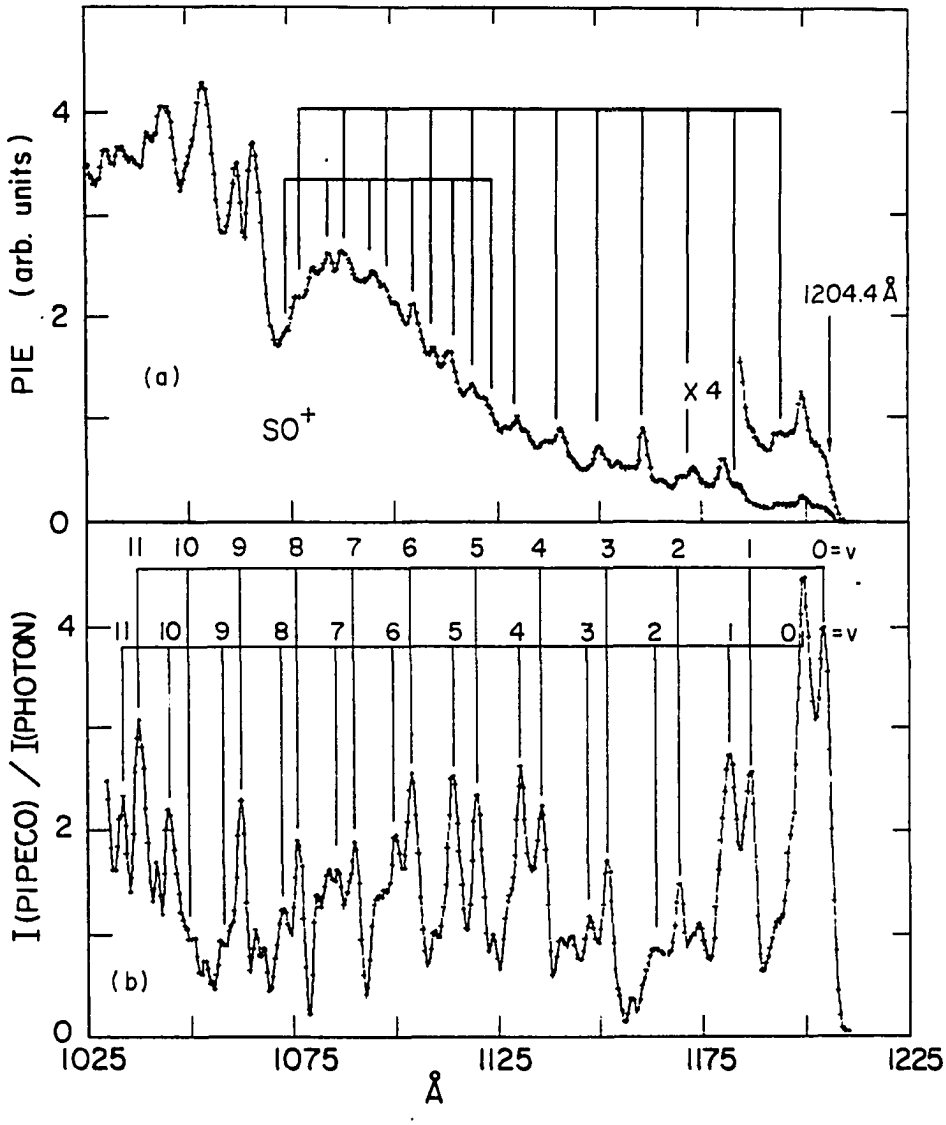
PIE (arb. units)
(a)
SO+
X 4
1204.4 Å
11 10 9 8 7 6 5 4 3 2 1 0=v
I(PIPECO) / I(PHOTON)
(b)
1025
1075
1125
1175
1225
Å

Figure 4. PIPECO and PIE spectra for S_2O^+ in the wavelength region of 1025 - 1180 Å obtained using a wavelength resolution = 1.4 Å (FWHM) and an electron energy resolution ~ 30 meV (FWHM)

(a) PIE spectrum for S_2O^+; (b) PIPECO spectrum for S_2O^+

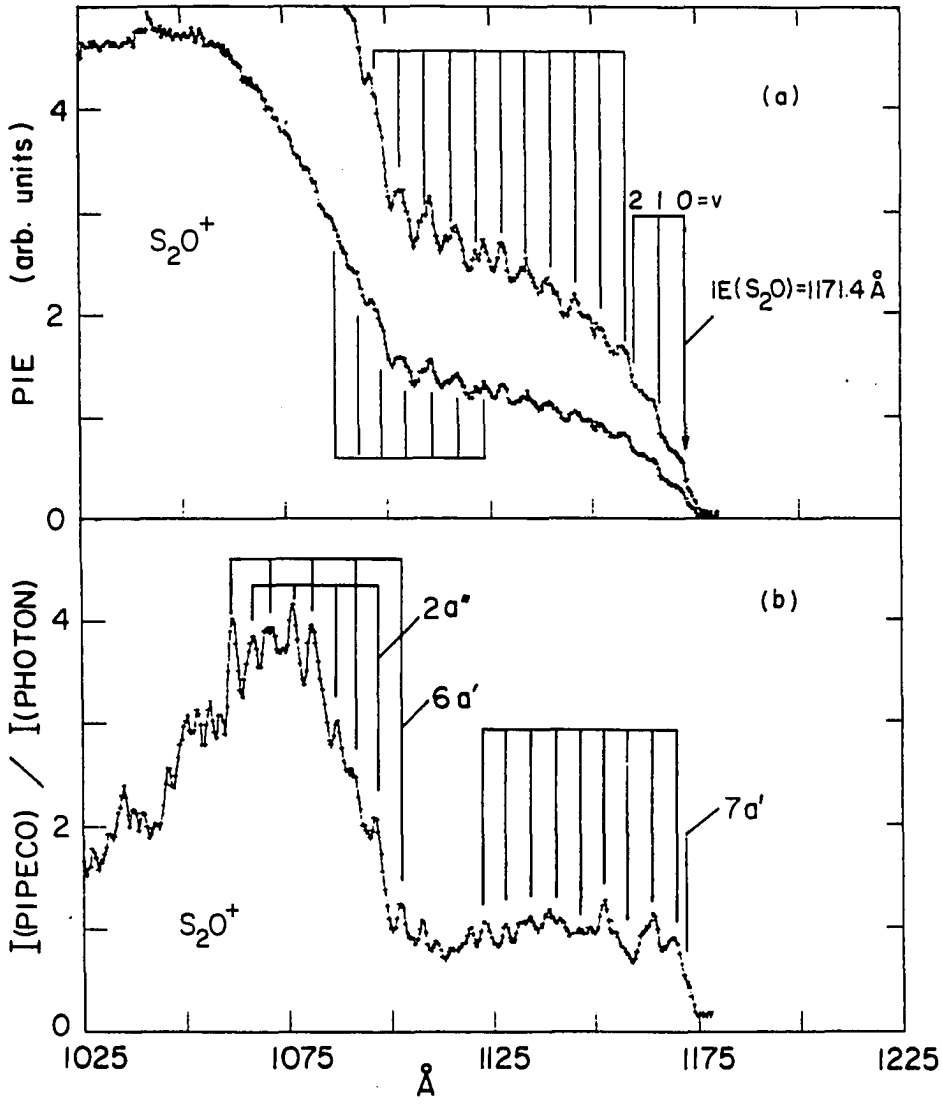
(a)
PIE (arb. units)
S_2O^+
2 1 0=v
IE(S_2O)=1171.4 Å
0
2
4
(b)
I(PIPECO) / I(PHOTON)
2a"
6a'
7a'
S_2O^+
0
2
4
1025
1075
1125
1175
1225
Å

DISCUSSION

The adiabatic ionization energy (IE) for SO to $SO^+(\tilde{X}^2\Pi_{3/2})$ determined by the SO^+ PIE spectrum is 10.294 ± 0.004 eV (1204.4 ± 0.5 Å),[b] in agreement with values obtained from the HeI PES of SO.[9,10] The PIE spectrum for SO^+ exhibits complex autoionization features. It appears that most of these features can be grouped into two progressions of vibrational bands with vibrational spacings ($\Delta\tilde{\nu}$) of 800 cm^{-1} as indicated by tic marks in Fig. 3(a). The $\tilde{a}^4\Pi$ electronic band observed in the HeI PES of SO consists of a long vibrational progression with an average $\Delta\tilde{\nu}$ value of 750 - 800 cm^{-1}.[9-10] It is most likely that the progressions resolved in the SO^+ PIE spectrum are due to Rydberg states converging to $SO^+(\tilde{a}^4\Pi)$.

The vertical IE for SO observed in the SO^+ PIPECO spectrum is 10.305 eV. The two peaks in the PIPECO spectrum at wavelengths > 1176 Å are similar to those observed in the HeI PES of SO. The doublet structures of the two peaks have been assigned to the formation of $SO^+(\tilde{X}^2\Pi_{3/2,1/2}, v = 2 - 11)$. The assignments summarized in Table I indicate that the spin-orbit splitting ($\Delta\tilde{\nu}_{sp}$) for the $\tilde{X}^2\Pi$ state is 371 ± 20 cm^{-1}. The uncertainty for this value is mainly contributed by the finite wavelength interval used in the experiment. The ($\Delta\tilde{\nu}_{sp}$) value determined here is in agreement with previous

---

[b]This value is determined from a PIE spectrum measured using a wavelength resolution of 0.28 Å (FWHM).

Table I. Progressions of vibrational bands for $SO^+(^2\Pi_{3/2,1/2}, v = 0 - 11)$

v	$\tilde{X}(^2\Pi_{3/2})$		$^2\Pi_{1/2}$		
	$\tilde{\nu}(cm^{-1})^a$	$\Delta\tilde{\nu}(cm^{-1})^b$	$\tilde{\nu}(cm^{-1})^a$	$\Delta\tilde{\nu}(cm^{-1})^b$	$\Delta\tilde{\nu}_{sp}(cm^{-1})^c$
0	83119	1262	83500	1260	381
1	84381	1265	84760	1254	379
2	85646	1265	86014	1277	368
3	86911	1226	87291	1236	380
4	88137	1260	88527	1232	390
5	89397	1257	89759	1266	362
6	90654	1207	91025	1217	371
7	91861	1197	92242	1164	381
8	93058	1184	93406	1192	348

[a]Peak positions of vibrational bands. Estimated uncertainty = $\pm$ 20 cm^{-1}.

[b]Vibrational spacings.

[c]Spin-orbit splitting for $SO^+(\tilde{X}^2\Pi)$.

Table I (Continued)

v	$\tilde{X}(^2\Pi_{3/2})$		$^2\Pi_{1/2}$		
	$\tilde{\nu}$(cm^{-1})[a]	$\Delta\tilde{\nu}$(cm^{-1})[b]	$\tilde{\nu}$(cm^{-1})[a]	$\Delta\tilde{\nu}$(cm^{-1})[b]	$\Delta\tilde{\nu}_{sp}$(cm^{-1})[c]
9	94242	1169	94598[d]	1178	356
10	95411	1151	95776	1161	365
11	96562		96937		375
		$\Delta\tilde{\nu}_{ave}$=1222[e]		$\Delta\tilde{\nu}_{ave}$=1222[e]	$\Delta\tilde{\nu}_{sp}$=371±20[f]

[d]Estimated value.

[e]Average value for $\Delta\tilde{\nu}$.

[f]Average value for $\Delta\tilde{\nu}_{sp}$.

measurements[9,10] and the predicted value of 360 cm^{-1}.[10,14,15] Combining the values for the adiabatic IE for SO to $SO^+(\tilde{X}^2\Pi_{3/2})$ and $\Delta\tilde{\nu}_{sp}$, we calculated a value of 10.340 ± 0.005 eV for the adiabatic IE for SO to $SO^+(\tilde{X}^2\Pi_{1/2})$.

The vibrational bands observed for $SO^+(\tilde{X}^2\Pi_{3/2,1/2}, v = 3 - 11)$ are the results of autoionization. Based on the observation of the $SO^+(\tilde{X}^2\Pi_{3/2,1/2}, v = 0 - 3)$ PIPECO bands, the average value for $\Delta\tilde{\nu}$ is 1264 cm^{-1} which is nearly 100 cm^{-1} lower than that reported by Dyke et al.[9] Nevertheless, the average $\Delta\tilde{\nu}$ value of 1270 ± 20 cm^{-1} observed by Lee[10] is in excellent agreement with the result of this study. The $\Delta\tilde{\nu}$ value decreases from ≈ 1270 to 1150 cm^{-1} as v increases in the range of 0 - 11. The observed trend of

$\Delta\tilde{\nu}$ is consistent with a value of 5.5 cm^{-1} for the anharmonicity constant.

S_2O

The value of 10.584 ± 0.005 eV (1171.4 ± 0.5 Å) (see footnote b) for the adiabatic IE of S_2O to $S_2O^+(\tilde{X}^2A')$ determined by the S_2O^+ PIE spectrum agrees with that obtained in the previous PIE study[13]. However, this value is higher than those found in the HeI photoelectron spectroscopic measurements.[11,12] The S_2O^+ PIE spectrum shows two vibrational steps at the onset. The spacings of these steps are equal to the average $\Delta\tilde{\nu}$ value of 480 cm^{-1} observed in the first electronic band of the HeI PES of S_2O. In the wavelength region of 1090 - 1157 Å, the S_2O^+ PIE spectrum displays quite regular autoionization features. Some of these features are found to split into doublets in a higher resolution PIE spectrum. The two progressions of autoionization vibrational bands, with spacings of ≈ 480 cm^{-1} indicated in Fig. 4(a), are consistent with the higher resolution PIE measurement.

The three peaks at wavelengths > 1160 Å found in the S_2O^+ PIPECO spectrum, which correspond to the three steps observed in the PIE spectrum, are similar to those in the HeI PES of S_2O.[12,12] These features have been assigned to the formation of $S_2O^+(\tilde{X}^2A')$ in the ν_3 = 0,1, and 2 vibrational states. The ν_3 vibrational mode corresponds mainly to S-S stretch. The S_2O^+ PIE and PIPECO spectra rise markedly in the wavelength region of ≈ 1075 - 1100 Å, indicating the existence of a new electronic

band. According to the HeI photoelectron spectroscopic study of Frost et al., the IEs for S_2O to the first $S_2O^+(^2A')$ and second $S_2O^+(^2A'')$ excited states are 11.25 and 11.31 eV and the ν_1 vibrational frequencies of 930 and 940 cm^{-1}, respectively. Using these values, we have assigned the vibronic bands observed in the wavelength region of 1060 - 1105 Å in Fig. 4(b) to the formation of $S_2O^+(^2A', v_1 = 0 - 3)$ and the $S_2O^+(^2A'', v_1 = 0 - 3)$. Table 2 summarizes the assignments of the observed vibrational bands for the ground $\tilde{X}^2A'$ and the first ($^2A'$) and second ($^2A''$) excited states of S_2O^+. The $\Delta\tilde{\nu}$ values for these states determined here and from the HeI PES of S_2O are in agreement.

Table II. Progressions of vibrational bands for $S_2O^+(7a'^{-1}, 6a'^{-1}, \text{and } 2a''^{-1})$

v	$\tilde{X}(7a'^{-1})$		$(6a'^{-1})$		$(2a''^{-1})$	
	$\tilde{\nu}(cm^{-1})^a$	$\Delta\tilde{\nu}(cm^{-1})$	$\tilde{\nu}(cm^{-1})^a$	$\Delta\tilde{\nu}(cm^{-1})$	$\tilde{\nu}(cm^{-1})^a$	$\Delta\tilde{\nu}(cm^{-1})$
0	85426	485	91091	922	91558	915
1	85911	487	92013	924	92473	915
2	86386		92937		93388	
	$\Delta\tilde{\nu}_{avc}=480^b$		$\Delta\tilde{\nu}_{avc}=923^b$		$\Delta\tilde{\nu}_{avc}=915^b$	

[a]Estimated uncertainties = ± 20 cm^{-1}.

[b]Average value for $\Delta\tilde{\nu}$.

CONCLUSIONS

Using the pulsed PIPECO method described in this report, we have measured the PIPECO spectra for SO and S_2O formed in a discharge of SO_2 in the wavelength region of 1025 - 1210 Å. The PIE and PIPECO spectra for SO and S_2O have provided accurate energetic and spectroscopic data for these ions. Experiments to extend the PIPECO measurements of S_2O and SO to higher photon energies and to other transient molecules are in progress. This experiment has demonstrated that the pulsed PIPECO scheme provides good sensitivity and resolution and is a promising method for the study of radicals coexisting with other molecular species.

REFERENCES

1. D. W. Turner, C. Baker, A. D. Baker, and C. R. Brundle, "Molecular Photoelectron Spectroscopy" (Wiley, New York, 1970).

2. K. Kimura, S. Katsumata, Y. Achiba, T. Yamazaki and S. Iwata, "Handbook of HeI Photoelectron Spectra of Fundamental Organic Molecules" (Halsted Press, New York, 1981).

3. J. M. Dyke, N. Jonathan and A. Morris, "Electron Spectroscopy, Theory, Techniques, and Applications" (Academic Press, New York, 1979), Vol. 3, p. 189.

4. P. W. Schenik, Z. Anorg. Allg. Chem. 211, 150 (1933).

5. K. Norwood, J. - H. Guo, G. Luo, and C. Y. Ng, J. Chem. Phys. 88, 4098 (1988).

6. K. Norwood, J. - H. Guo, G. Luo, and C. Y. Ng, Chem. Phys. 129, 109 (1989).

7. K. Norwood, J. - H. Guo and C. Y. Ng, J. Chem. Phys. 90, 2995 (1989).

8. N. Jonathan, K. J. Ross and D. J. Smith, Chem. Phys. Letters 9, 217 (1971).

9. J. M. Dyke, L. Golob, N. Jonathan, A. Morris, M. Okuda and D. J. Smith, J. Chem. Soc. Faraday Trans. II 70, 1818 (1974).

10. S. T. Lee, Ph.D. Thesis, The University of British Columbia (1974).

11. D. C. Frost, S. T. Lee, and C. A. McDowell, Chem. Phys. Letters 22, 243 (1974).

12. H. Bock, B. Soluki, P. Rosmus and R. Steudel, Angew. Chem. 85, 987 (1973).

13. J. Berkowitz, J. H. D. Eland and E. H. Appelman, J. Chem. Phys. 66, 2183 (1977).

14. S. Leach, Acta Phys. Polon. 34, 705 (1968).

15. F. A. Grimm, J. Electron Spectry. 2, 475 (1973).

GENERAL CONCLUSIONS

The PIPECO spectra of Ar_n^+(n =2 - 4), Kr_2^+, Xe_2^+, $(CO)_{2,3}^+$, and $(Ar_n \cdot CO_m$, n+m = 2,3)$^+$ van der Waals clusters was successfully obtained. These studies were the first PIPECO spectra of van der Waals clusters reported for energies higher than the corresponding monomer IE. Results from these PIPECO studies provide valuable information on ionization energies (IEs) of ground and excited states of these van der Waals dimer and trimer clusters. Upper bounds for dissociative lifetimes of many superexcited cluster ions were estimated. The only cluster ions studied which had superexcited states that were non-dissociative, within the flight time from the photoionization region to the ion detector, were Ar_2^+ and Ar_3^+. A radiative model was suggested to explain the dissociative nature of the $Kr_2^+[\Pi(1/2)_u]$ and $Xe_2^+[\Pi(1/2)_u]$ states, and the non-dissociative (metastable) $Ar_2^+[\Pi(1/2)_u]$ state observed in these experiments. Theoretical calculations for the radiative lifetimes of Rg_2^+ $\Pi(1/2)_u \rightarrow I(1/2)_g$ (Rg = Ar, Kr, Xe) support this model.

PIPECO spectra of all cluster systems studies show that fragmentation of larger clusters into dimer and trimer cluster ions is an efficient means of disposing of energy in excess of the dissociation limit. A mechanism was suggested to explain the extreme efficiency of such processes. The visual similarities in structure observed for the high pressure dimer PIPECO spectra and the respective monomer spectra are consistent with the perturbed monomer ion model for photoionization of van der Waals clusters. These

spectra also support the interpretation that the monomer ion, within the cluster, initially formed by photoionization experiences mostly the influence of the dimer ion potential.

The study of mixed Ar/CO dimer and trimer ions provides information on the Ar^+ + CO charge transfer reaction, which is presumed to proceed via complex formation. Good agreement is found between the measured vibrational distribution of $CO^+(\tilde{X},v')$ produced in the $Ar^+(^2P_{3/2})$ + CO charge transfer reaction and the profile for the $ArCO^+$ coincidence electronic band arising from dissociation of $Ar(^2P_{3/2})\cdot(ArCO)$ and $Ar(^2P_{3/2})\cdot(CO)_2$. This agreement is rationalized by a near-resonant intramolecular charge transfer between $Ar^+(^2P_{3/2})$ and a CO molecule in the trimer ions prior to their decomposition.

The PIPECO studies on the SO and S_2O transient molecules were successful in providing mass-selected TPE spectra. Information on vibrational frequencies, adiabatic and vertical IEs, and energy separations of spin orbit states were obtained. These values are in agreement with available data from HeI PES experiments.

In future experiments, the PIPECO technique described for the study of cluster ions can be used for studying energy (or state)-selected intracluster reactions. Preliminary experiments on the energy selected intracluster reaction

$$[(H_2O)_2^+]^* \rightarrow H_3O^+ + OH$$

were carried out for energies less than the IE for H_2O. Secondary reactions of state selected H_2O monomers present interference at energies higher than the IE for H_2O. By careful choice of molecular beam conditions (nozzle diameter, skimmer diameter, nozzle skimmer distance, stagnation temperature and pressure) it may be possible to eliminate

these secondary reactions and thus study the intracluster reaction for electronic excited states as well as the ground state. Studies of this type are of great chemical significance but no reports of energy (or state)-selected intracluster reactions have been reported in the literature.

REFERENCES

1. C. Y. Ng, Adv. Chem. Phys. 52, 263 (1983).

2. T. D. Märk and A. W. Castleman, Jr., Adv. At. Mol. Phys. 20, 65 (1985).

3. J. T. Moseley, R. P. Saxon, B. A. Huber, P. C. Cosby, R. Abouaf, and M. Tadjeddine, J. Chem. Phys. 67, 1659 (1977).

4. R. Abouaf, B. A. Huber, P. C. Cosby, R. P. Saxon, and J. T. Moseley, J. Chem. Phys. 68, 2406 (1978).

5. C. R. Albertoni, R. Kuhn, H. W. Sarkas, and A. W. Castlemann, J. Chem. Phys. 87, 5043 (1987).

6. N. E. Levinger, D. Ray, K. K. Murray, A. S. Mullin, C. P. Schultz, and W. C. Lineberger, J. Chem. Phys. 89, 71 (1988).

7. C. A. Woodward, J. E. Upham, A. J. Stace, and J. N. Murrell, J. Chem. Phys. 91, 7612, (1989).

8. S. C. Ostrander, L. Sanders, J. C. Weisshaar, J. Chem. Phys. 84, 529 (1986).

9. A. J. Illies, M. F. Jarrold, W. Wagner-Redeker, and M. T. Bowers, J. Phys. Chem. 88, 5204 (1984).

10. M. F. Jarrold, A. J. Illies, and M. T. Bowers, J. Chem. Phys. 81, 214 (1984).

11. P. M. Dehmer and J. L. Dehmer, J. Chem. Phys. 68, 3462 (1978).

12. P. M. Dehmer and J. L. Dehmer, J. Chem. Phys. 69, 125 (1978).

13. A. van Deursen and J. Reuss, Int. J. Mass Spectrom. Ion Phys. 23, 109 (1977).

14. P. M. Dehmer, S. T. Pratt, and J. L. Dehmer, J. Phys. Chem. 91, 2593 (1987).

15. B. Brehm and E. von Puttkamer, Z. Naturforsch. Teil A 22, 8 (1967).

16. T. Baer, "Gas Phase Ion Chemistry", Ed., M. T. Bowers (Academic Press, New York, 1979), Vol. 1, p. 153.

17. L. Cordis, G. Ganteför, J. Besslich and A. Ding, Z. Physik D 3, 323 (1986).

18. E. D. Poliakoff, P. M. Dehmer, J. L. Dehmer, and R. Stockbauer, J. Chem. Phys. 75, 5214 (1982).